AD-A055 397 JOHNS HOPKINS UNIV LAUREL MD APPLIED PHYSICS LAB F/G 17/9
ANALYSIS OF SINGLE AND MULTIPLE WAVELENGTH RADAR SYSTEMS FOR ES--ETC(U)
MAR 78 J GOLDHIRSH MIPR-FY7620-77-00026
UNCLASSIFIED APL/JHU-S1R77U-036 RADC-TR-78-60 NL

1 OF 2
ADA
055397

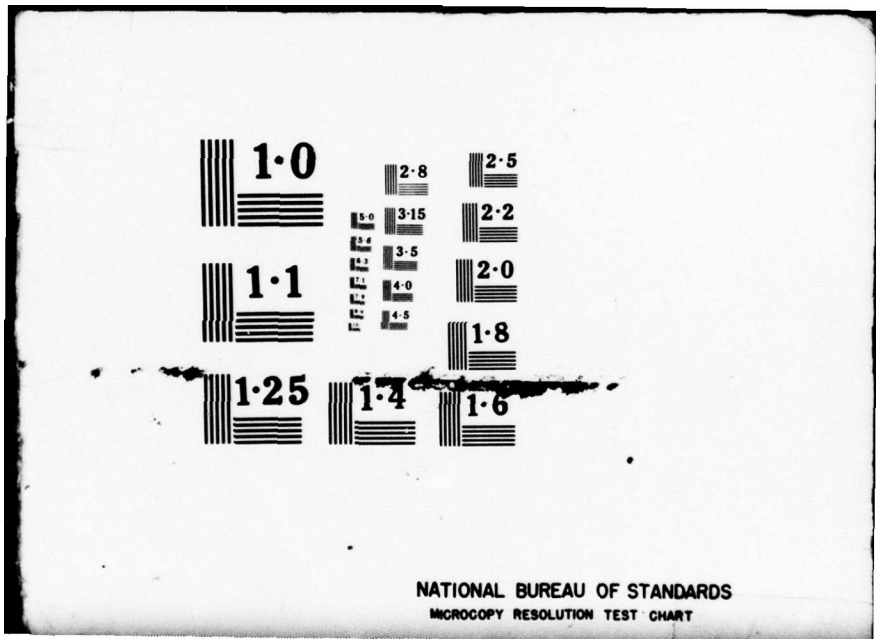
1·0
1·1
1·25
2·8
3·15
3·5
4·0
4·5
1·4
2·5
2·2
2·0
1·8
1·6
NATIONAL BUREAU OF STANDARDS
MICROCOPY RESOLUTION TEST CHART

RADC-TR-78-60
Final Report
March 1978

ANALYSIS OF SINGLE AND MULTIPLE WAVELENGTH RADAR SYSTEMS FOR ESTIMATING SLANT PATH ATTENUATION THROUGH RAIN AND CLOUD AT FREQUENCIES GREATER THAN 10 GHz

Applied Physics Laboratory
The Johns Hopkins University
Laurel, Maryland 20810

Approved for public release:
distribution unlimited.

ROME AIR DEVELOPMENT CENTER
AIR FORCE SYSTEMS COMMAND
GRIFFISS AIR FORCE BASE NEW YORK 13441

This report has been reviewed and is approved for publication.

APPROVED:

Uve H. W. Lammers

UVE H. W. LAMMERS
Contract Monitor
Propagation Branch
Electromagnetic Sciences Division

APPROVED:

Terence J. Elkins

TERENCE J. ELKINS, Acting Chief
Propagation Branch
Electromagnetic Sciences Division

APPROVED:

Allan C. Schell

ALLAN C. SCHELL, Acting Chief
Electromagnetic Sciences Division

John P. Kuss

Do not return this copy. Retain or destroy.

UNCLASSIFIED

SECURITY CLASSIFICATION OF THIS PAGE (When Data Entered)

REPORT DOCUMENTATION PAGE	READ INSTRUCTIONS BEFORE COMPLETING FORM
1. REPORT NUMBER: RADC-TR-78-60	2. GOVT ACCESSION NO.
	3. RECIPIENT'S CATALOG NUMBER
4. TITLE (and Subtitle): ANALYSIS OF SINGLE AND MULTIPLE WAVELENGTH RADAR SYSTEMS FOR ESTIMATING SLANT PATH ATTENUATION THROUGH RAIN AND CLOUD AT FREQUENCIES GREATER THAN 10 GHz.	5. TYPE OF REPORT & PERIOD COVERED: Final rept. 1 Dec 76 - 30 Sep 77
	6. PERFORMING ORG. REPORT NUMBER: S1R77U-036
7. AUTHOR(s): Julius Goldhirsh	8. CONTRACT OR GRANT NUMBER(s): MIPR-FY7620-77-00026
9. PERFORMING ORGANIZATION NAME AND ADDRESS: Applied Physics Laboratory, The Johns Hopkins University, Johns Hopkins Road, Laurel, Maryland 20810	10. PROGRAM ELEMENT, PROJECT, TASK AREA & WORK UNIT NUMBERS: 61102F, 2305J427, 2305
11. CONTROLLING OFFICE NAME AND ADDRESS: Deputy for Electronic Technology (RADC), Hanscom AFB, Massachusetts 01731, Monitor/Uve Lammers/EEP	12. REPORT DATE: March 1978; 13. NUMBER OF PAGES: 125
14. MONITORING AGENCY NAME & ADDRESS (if different from Controlling Office)	15. SECURITY CLASS. (of this report): Unclassified
	15a. DECLASSIFICATION/DOWNGRADING SCHEDULE

16. DISTRIBUTION STATEMENT (of this Report)

Approved for public release; distribution unlimited

17. DISTRIBUTION STATEMENT (of the abstract entered in Block 20, if different from Report)

18. SUPPLEMENTARY NOTES

19. KEY WORDS (Continue on reverse side if necessary and identify by block number)

Rain Attenuation, Dual Wavelength Radar, Radar Prediction of Attenuation, Cloud Attenuation, Slant Path Attenuation, Radar Parameter Design, Error Analysis, Drop Size Distribution, Cloud Liquid Water Content

K sub u

20. ABSTRACT (Continue on reverse side if necessary and identify by block number)

The feasibility of using various types of radars including dual wavelength configurations for arriving at slant path attenuations through rain and cloud at frequencies up to 100 GHz has been analyzed. Optimum performance parameters of systems which best perform these functions are established. The configurations examined include single S-band (f = 3 GHz) and K_u-band (f = 15.7 GHz) systems as well as dual wavelength systems operating at K_a-S (35-3 GHz) and K_u-S (15.7-3 GHz) bands.

(continued)

DD FORM 1 JAN 73 1473 EDITION OF 1 NOV 65 IS OBSOLETE

UNCLASSIFIED

SECURITY CLASSIFICATION OF THIS PAGE (When Data Entered)

K sub a

20. ABSTRACT (continued)

The following conclusions have been arrived at from the analysis of the above systems: (1) Of the various systems examined, the most straightforward is an S-Band system monitoring the path reflectivity profiles. (2) The use of a single attenuating wavelength radar (e.g., one operating at 15.7 GHz) for measuring rain path attenuation leads to unacceptably high errors and should be avoided. (3) A radar system operating at 15.7 GHz is suitable for estimating cloud liquid water content from which cloud path attenuation may be determined at frequencies above 10 GHz. (4) A dual wavelength system involving K_a and S-band (35-3 GHz) radar system is feasible for establishing drop size distributions aloft from which appropriate empirical relations at higher frequencies may be generated. (5) A K_u-S band (15.7-3 GHz) dual wavelength system may give rise to unacceptably large errors and its use should be avoided.

K sub a

K sub u

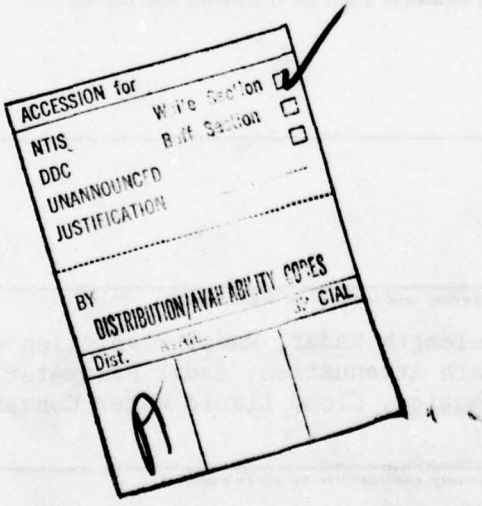

EVALUATION

MIPR FY7620-77-00026

1. The Propagation Branch (EEP) is conducting research in several areas of tropospheric microwave propagation which are affected by hydrometeors aloft. A remote, quantitative measurement of condensed water in the form of rain, snow, hail, water cloud and ice cloud is of importance in the interpretation of radiometric sky temperature, slant path attenuation, wave depolarization and related parameters.

2. One objective of this investigation was to determine the potential of existing Ku band scatter equipment, if it was modified to perform quantitative measurements on hydrometeors aloft. If satisfactory performance could not be established, another objective was to define a single, more suitable frequency or a combination of frequencies to perform the task.

3. Subject report presents a comprehensive study of the radar measurement of rain and water cloud parameters in order to calculate path attenuation at arbitrary frequencies. The author reviews the current state of meteorological radar theory and compiles from the literature or derives the necessary meteorological or radar parameters required for a quantitative interpretation of measurements. The conclusion is drawn that a quantitative interpretation of radar signals in terms of meteorological parameters and in turn path attenuation is possible only if the radar signals have not experienced significant path attenuation themselves. This restricts the use of Ku band equipment on long paths

to cloud measurements. Rain drop spectra can be determined on short paths using two widespaced frequencies, but Ka band is preferred here to Ku band.

Uve H. W. Lammers

UVE. H. W. LAMMERS
Contract Monitor
Propagation Branch
Electromagnetic Sciences Division

2

TABLE OF CONTENTS

TABLE OF CONTENTS (continued)

LIST OF TABLES

LIST OF TABLES (continued)

LIST OF FIGURES

LIST OF FIGURES (continued)

LIST OF FIGURES (continued)

LIST OF FIGURES (continued)

ANALYSIS OF SINGLE AND MULTIPLE WAVELENGTH RADAR SYSTEMS FOR ESTIMATING SLANT PATH ATTENUATION THROUGH RAIN AND CLOUD AT FREQUENCIES GREATER THAN 10 GHz

1.0 SUMMARY AND CONCLUSIONS

The aim of this report is to analyze the feasibility of using various types of radars including dual wavelength configurations for arriving at slant path attenuation through rain and cloud at frequencies up to 100 GHz, and to establish optimum performance parameters for a given system which will best perform this function. The results associated with this aim may be used in developing a radar system capable of estimating path attenuation through rain or cloud where the path may link a ground station and an aircraft at arbitrary elevation angles and azimuths.

Knowledge of the path attenuation both on a case by case as well as statistical basis is extremely useful in establishing the transmitter power and receiver sensitivity requirements for any airplane-ground link system (or earth-satellite system). It may also establish the need to utilize space diversity systems.

Although the radar systems described in this report operate at single or dual wavelengths, resulting path attenuations may be deduced from these radar data at variable frequencies above 10 GHz where the attenuation due to rain and possibly cloud may become sizeable.

The major analytical topics dealt with in this report are:

(1) Parameters associated with an S-band radar to measure the rain reflectivity profile along a path and the conversion of such profiles to path attenuations (Section 2.0).

(2) The feasibility of using a single attenuating wavelength radar operating at 15.7 GHz (K_u-band) for establishing rain path attenuation at arbitrary frequencies above 10 GHz (Section 3.0).

(3) The feasibility of using a K_u-band radar for establishing path attenuation through cloud at arbitrary frequencies (Section 4.0).

(4) Multiple wavelength radar systems such as K_a-S band (35-3 GHz) or K_u-S band (15.7-3 GHz) for establishing path attenuation at arbitrary frequencies (Section 5.0).

The following conclusions have been arrived at from the analysis of the above topics:

(1) Of the various systems examined, the most straightforward is an S-band system monitoring the path reflectivity profiles. The conversion to path attenuation is achieved using empirical relations based on a measured or assumed drop size distribution.

(2) The use of a single attenuating wavelength radar (e.g., one operating at 15.7 GHz) for measuring rain path attenuation leads to unacceptably high errors and should be avoided.

(3) A radar system operating at 15.7 GHz is suitable for estimating cloud liquid water content from which cloud path attenuation may be determined at frequencies above 10 GHz.

(4) A dual wavelength system involving a K_a and S-band (35-3 GHz) radar system is feasible for establishing drop size distributions aloft from which appropriate empirical relations at higher frequencies may be generated. These empirical relations may subsequently be used in a single wavelength (S-band) system as described by (1).

(5) A K_u-S band (15.7-3 GHz) dual wavelength system may give rise to unacceptably large errors and its use should be avoided.

In arriving at the above conclusions, error analyses were performed where they were deemed necessary and use was made of a typical reflectivity profile as measured at Wallops Island, Virginia, with a high resolution S-band radar.

This report is useful as a reference for future work in the aforementioned areas. It contains many derived as well as referenced

tables and curves and the formulations are either systematically derived or referenced.

2.0 S-BAND RADAR PARAMETER INVESTIGATION FOR ESTIMATING ATTENUATION DUE TO RAIN

We examine here various design criteria for developing an optimum S-band radar for the measurement of rain parameters from which slant path reflectivity profiles are obtained. In addition, the methods by which path reflectivity profiles are converted to integrated path attenuation are examined.

2.1 The Radar Equation at S-Band

We start with the expression for the received power scattered from rain assumed uniformly distributed throughout the pulse volume (Probert-Jones [1962]),

$$P_r = \frac{c}{1024\,\pi^2\,\ell n 2}\left[P_t\,\tau\,\lambda^2\,G^2(\Delta\theta_e)(\Delta\theta_h)\,L_t\,L_r\,\frac{\eta}{r^2}\right] 10^{-0.2\int_0^r (k_g + k_p + k_c)\,dr} \qquad (2.1)$$

where

- c = velocity of light (3×10^3 m/sec)
- P_t = transmitted power (watts)
- τ = pulsewidth (sec)
- λ = wavelength (m)
- G = antenna gain
- $\Delta\theta_e, \Delta\theta_h$ = vertical and horizontal beamwidths (radians)
- L_t = transmitter loss factor (≤ 1.0). (Corresponds to losses from transmitter power measurement point through to gain measurement point.)
- L_r = Receiver Loss factor (≤ 1.0). (Corresponds to losses from receiver calibration point to antenna gain measurement point.)
- η = rain reflectivity (m^{-1})
- r = range (m)
- k_g, k_p, k_c = attenuation coefficients due to atmospheric gas, precipitation, and clouds, respectively (dB/km).

Since we are scattering from rain drops which, in general, have drop diameters, D, given by,

$$D < .5 \text{ cm} \tag{2.2}$$

and the radar wavelength assumed is,

$$\lambda = 10 \text{ cm} \tag{2.3}$$

hence,

$$\frac{D}{\lambda} < \frac{1}{20} \tag{2.4}$$

and Rayleigh scattering is applicable. Hence, the reflectivity, η, is given by (Battan [1973]),

$$\eta = \frac{\pi^5}{\lambda^4} |K_o|^2 Z \qquad (m^{-1}) \tag{2.5}$$

where

$$|K_o|^2 = \frac{m^2 - 1}{m^2 + 2} \tag{2.6}$$

and where m is the complex refractive index. The parameter $|K_o|^2$ has been tabulated for various frequencies and temperatures by Gunn and East [1954].

For rain at $\lambda = 10$ cm for temperatures ranging from 0° to 20°C,

$$|K_o|^2 \simeq 0.93 \tag{2.7}$$

The quantity, Z, is called the reflectivity factor and is theoretically given by,

$$Z = \int_0^\infty N(D)\, D^6\, dD \tag{2.8}$$

where D is the drop diameter and N(D)dD is the number of drops per unit volume with diameters between D and D+dD (i.e., the drop size distribution). It is convenient to express D in mm and the unit volume associated with N(D)dD in m^{-3}. Hence, (2.5) becomes,

$$\eta = \frac{\pi^5}{\lambda^4} |K_o|^2 Z \times 10^{-18} \qquad [m^{-1}] \tag{2.9}$$

where $[Z] = (mm)^6/m^3$ and $[\lambda] = m$.

Substituting (2.7) and (2.9) into (2.1),

$$P_r = 1.22 \times 10^{-14} \left[P_t \tau G^2 \Delta\theta_e \Delta\theta_h L_t L_r\right] \frac{Z}{r^2 \lambda^2} \times 10^{-0.2 \int_o^r (k_g + k_p + k_c)dr} \tag{2.10}$$

where the units of the radar parameters are given in the mks system except for Z which has the units mm^6/m^3. Also, r, both in the denominator and exponent, is given in km and k in the exponent is in dB/km. The resulting received power, P_r, is expressed here in milliwatts.

2.2 Attenuation Contributions from Atmospheric Gases, Precipitation, and Cloud at S-Band

It is convenient to examine k_g, k_p, and k_c at λ = 10 cm as well as the respective integrated attenuations as a function of range.

In Fig. 1 are given plots of the two way atmospheric gas absorption at f = 3 GHz for various elevation angles. These curves were obtained from Blake [1969, 1970] assuming a CRPL exponential reference atmosphere (N_s = 313) where the absorption is due to O_2 and H_2O collision broadening. We note that at low elevation angles the atmospheric absorption should be accounted for in the radar equation as two way attenuations as much as 1 to 3 dB may result at the larger ranges.

In Fig. 2 is the attenuation coefficient versus rain rate at f = 3 GHz assuming the Laws and Parsons drop size distribution (Medhurst [1965]), and in Fig. 3 are plotted the corresponding two way path attenuations at variable elevation angles assuming a uniform rain rate up to an altitude of 4 km where a 4/3 earth radius is assumed here to account for

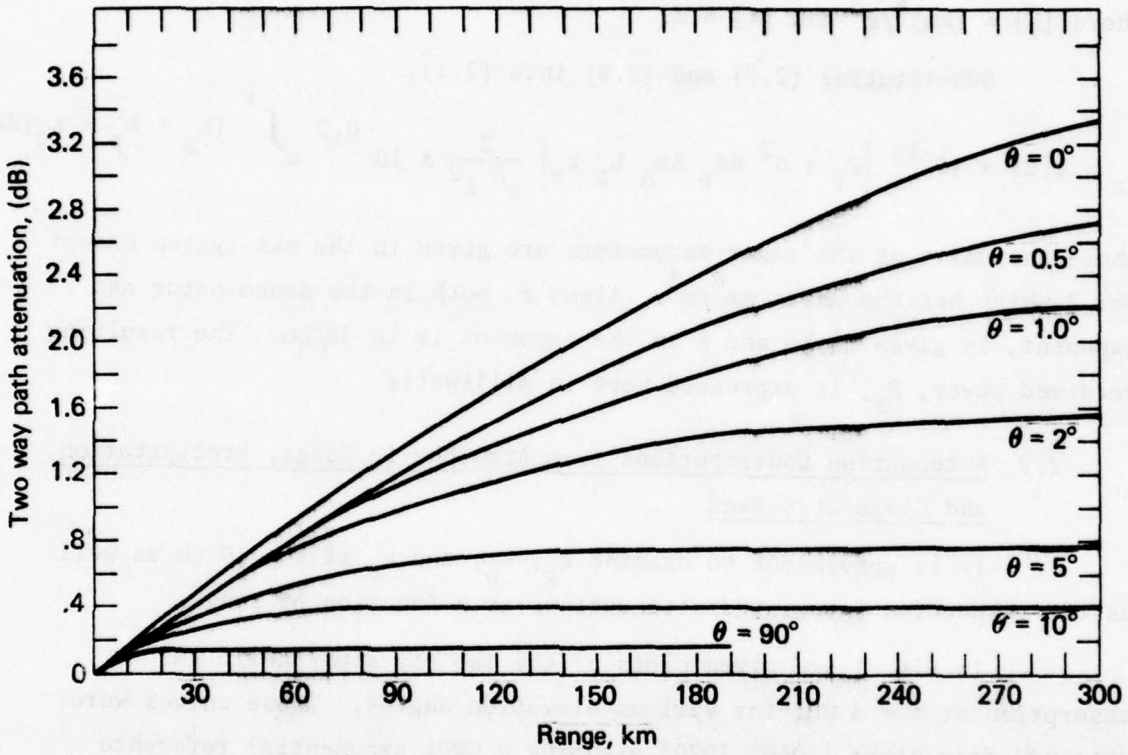

Figure 1. Two way attenuation due to atmospheric absorption at f = 3 GHz for various elevation angles. CRPL exponential reference atmosphere assumed (N_s = 313). Absorption due to 0_2 and H_20 collision broadening. Normalized to 7.5 gm/m^3 at zero altitude (Blake [1969,1970], Skolnik [1970]).

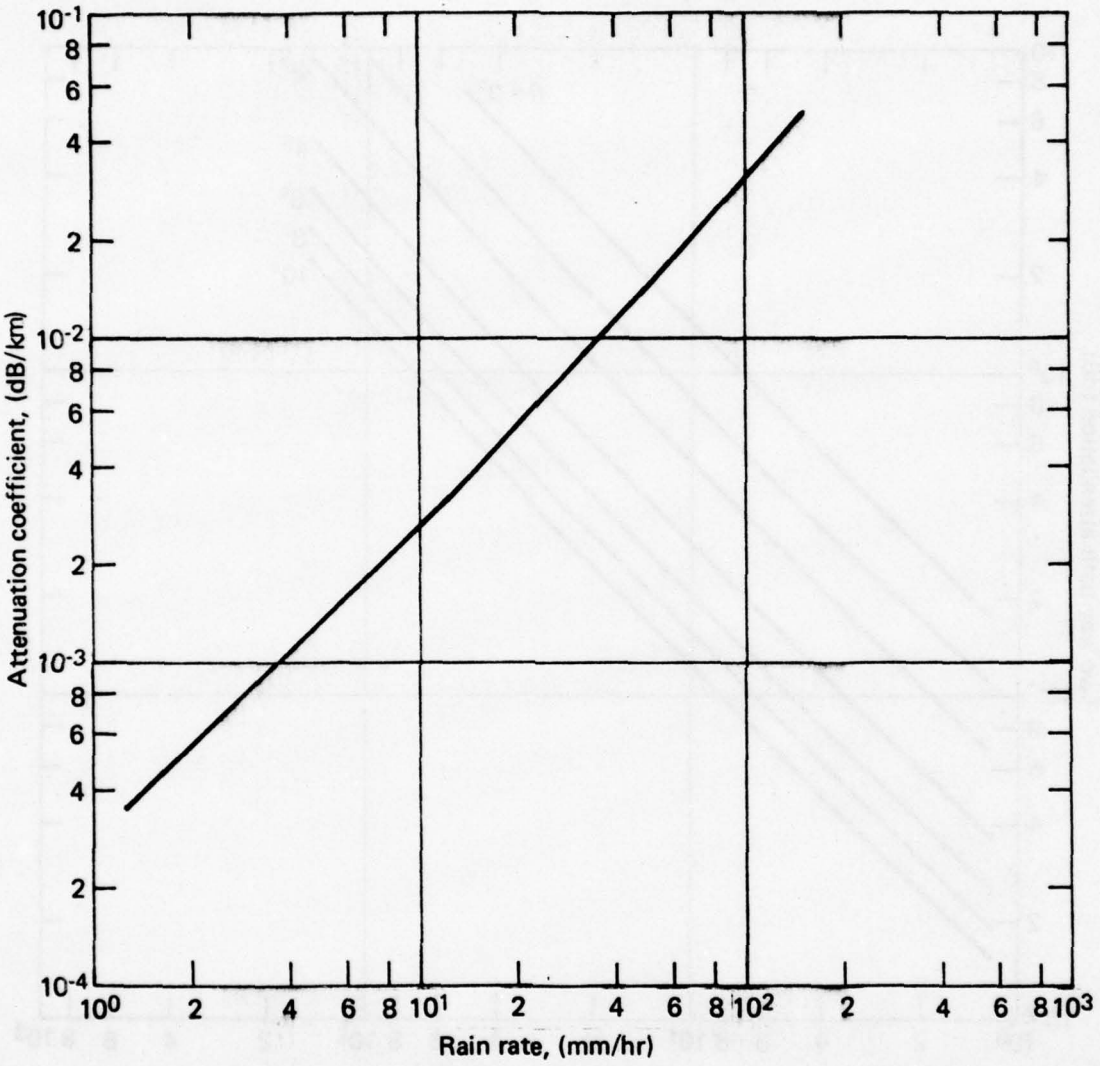

Figure 2. Attenuation coefficient versus rain rate at f = 3 GHz assuming the Laws and Parsons drop size distribution (Medhurst [1965]).

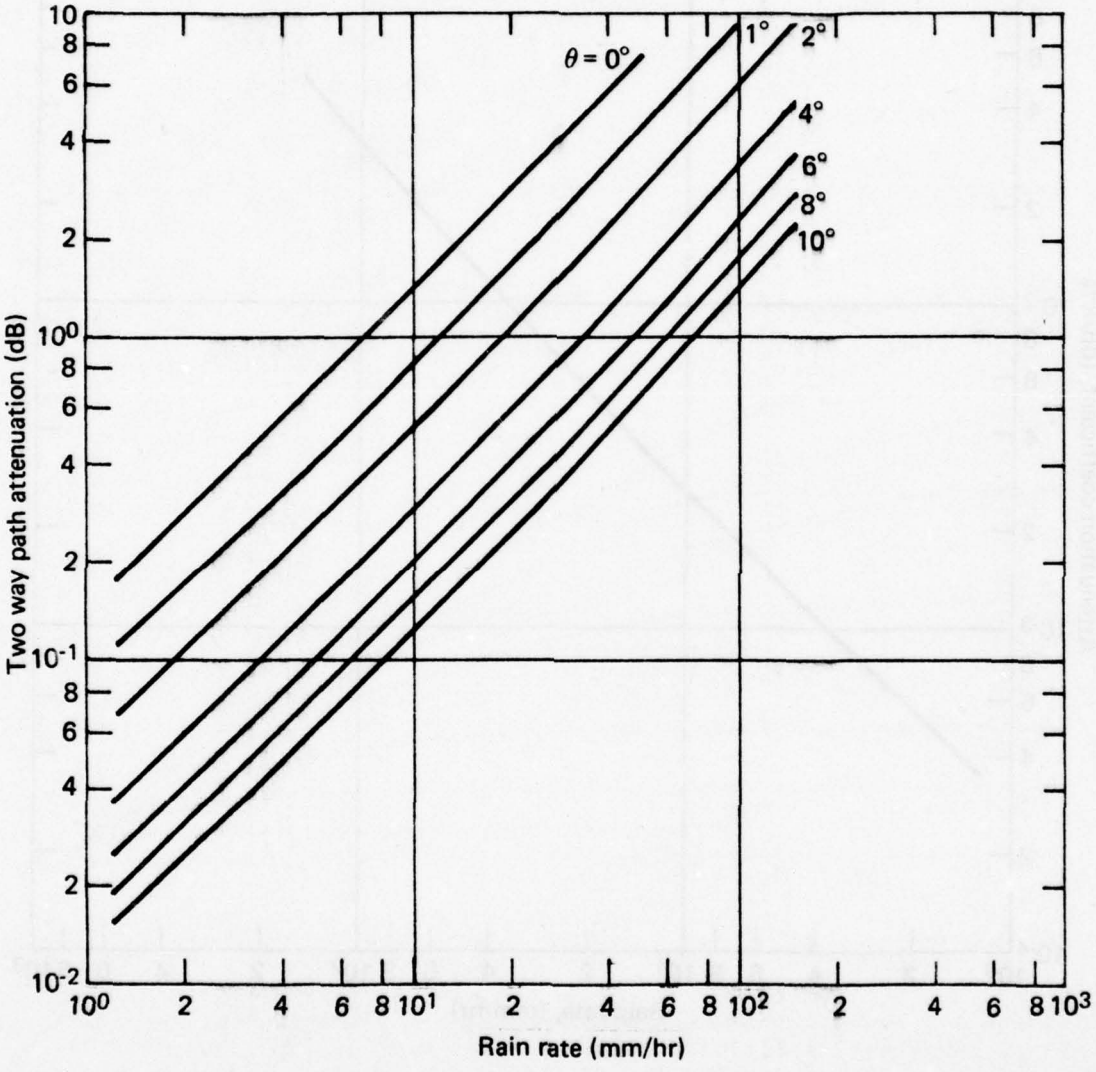

Figure 3. Two way path attenuation versus rain rate at f = 3 GHz at variable elevation angles assuming a uniform rain with height of 4 km and a 4/3 earth radius.

refraction. It is apparent that at low elevations (0° to 2°) the two way path attenuation could exceed 1 dB for rain rates greater than 7 to 20 mm/hr along the entire path. However, since these rain rates over such long ranges are unlikely to occur even for widespread rain conditions, we neglect the attenuation contribution due to rain at f = 3 GHz.

The attenuation contribution due to water cloud at λ = 10 cm is given in Table 2.1. Assuming the worst case situation of 0° elevation, the path length interval in a widespread cloud extending from 3 to 5 km in altitude (assuming a 4/3 earth radius model) is 65.7 km. This gives rise to a 0.5 dB two way path attenuation assuming $k/M = 0.9 \times 10^{-2}$ and $M = 0.5$ gm/m^3. Since this attenuation is minimal and the parameters selected are extreme for the widespread cloud conditions, we neglect the cloud attenuation at S-band.

Hence, neglecting k_p and k_c in (2.10), we obtain for λ = 10 cm,

$$P_r = 1.22 \times 10^{-12} \left[P_t \tau G^2 \Delta\theta_e \Delta\theta_h L_t L_r \right] \frac{Z}{r^2} L_g \qquad (2.11)$$

where the attenuation contribution due to atmospheric gas, L_g, is given by,

$$L_g = 10^{-0.2 \int_o^r k_g \, dr} \qquad (2.12)$$

2.3 Dynamic Range Requirements

Since reflectivity factors as high as 10^7 mm^6/m^3 (i.e., 70 dBZ) have been measured with radar (Donaldson and Tear [1963], Katz [1976]), the radar dynamic range should be large enough to measure these high reflectivity targets close in as well as smaller levels (e.g., 20-30 dBZ) at greater distances.

Considering (2.11) at ranges r_1 and r_2, we arrive at the dB ratio,

$$10 \, \mathrm{Log}_{10} \frac{P_r(r_1)}{P_r(r_2)} \simeq 10 \, \mathrm{Log}_{10} \left\{ \frac{Z(r_1)}{Z(r_2)} \left(\frac{r_2}{r_1} \right)^2 \right\} \qquad (2.13)$$

Table 2.1

THE ATTENUATION DUE TO CLOUD AT λ = 10 cm FOR VARIOUS TEMPERATURES
$[k_c]$ = dB/km, $[M_c]$ = gm/m^3 (GUNN AND EAST [1954])

Temperature °C	k_c/M_c [dB/km/gm/m^3]
20	0.39×10^{-2}
10	0.56×10^{-2}
0	0.90×10^{-2}

where we have neglected the effect of gas absorption in (2.13). We may define the left hand side of (2.13) as the required dynamic range of the receiver where $Z(r_1)$ and $Z(r_2)$ represent the largest and smallest reflectivities measured at the shortest range, r_1, and largest range, r_2, respectively.

In Fig. 4 is plotted the required receiver dynamic range as a function of the range ratio, r_2/r_1, where $Z(r_1)$ and $Z(r_2)$ are assumed to be 10^7 and 10^2 mm^6/m^3, respectively. Hence, if r_1 = 5 km, the required dynamic ranges at 50 and 200 km are 70 and 82 dBZ, respectively.

The above results suggests the use of a logarithmic receiver, ideally having a dynamic range of the order of 90 dB.

2.4 Integration Requirements

In arriving at the integration requirements associated with the backscattered signals from rain, two essential features of rain must be recognized. They are:

(1) Rain represents a distributed target in a pulse volume, where the particles backscatter randomly in phase. As such, in order to arrive at a reliable estimate of the backscattered reflectivity a number of independent samples must be averaged for each pulse volume, Δv (i.e., $\Delta v = (\frac{c\tau}{2})(r\Delta\theta_e)(r\Delta\theta_h)$).

(2) Because the rain particles are in motion due to fall velocity and turbulence, it takes a defined time interval for the particles to achieve new spatial positions such that the scattering phases have been sufficiently altered for causing a decorrelated or independent signal to be backscattered.

With regard to the first statement, Marshall and Hitschfeld [1953] examined the question dealing with the required number of independent samples, k, to achieve a reliable estimate of the mean backscattered power.

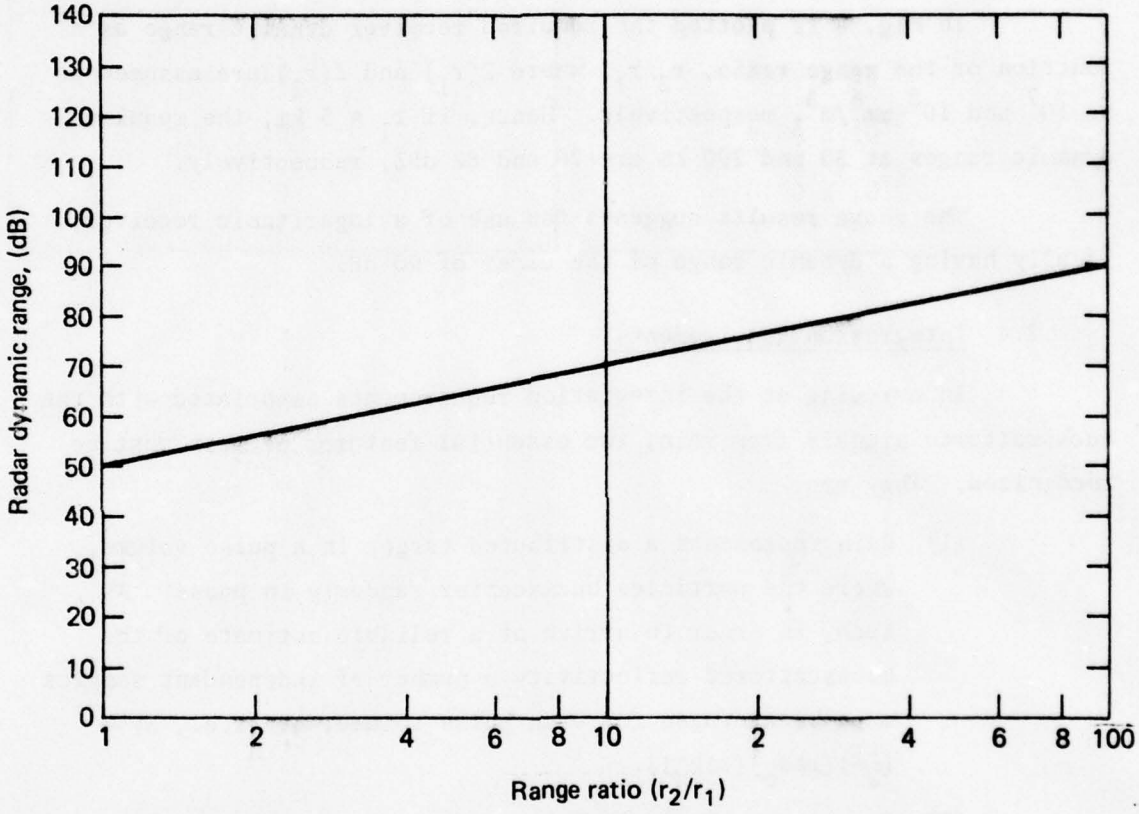

Figure 4. Radar dynamic range given by (2.13) as a function of range ratio r_2/r_1; r_1 and r_2 are closest and furthest ranges, respectively, and $Z(r_1)/Z(r_2) = 10^5$.

Smith [1966] clarified and extended some details of this work and demonstrated that the mean power can be arrived at by selecting only the maximum signal from a sample size of k independent samples. He showed this method to be more accurate for k up to 10; however, for larger values of k this method was found to be less accurate than the straightforward averaging method.

The basic results of Marshall and Hitschfeld are given in Figs. 5 and 6. Fig. 5 contains the probability density function, $P(J_k)$, of the measured average signal intensity, J_K, where

$$J_k = \frac{1}{k} \sum_{1}^{k} A_k^2 \tag{2.14}$$

and A_k^2 represents the measured k^{th} sample of the intensity (power). The horizontal scale represents the measured value of the power, J_k. We note that as the number of samples averaged reach 100 the likelihood increases significantly that the measured value of the averaged power will equal the true average. Although these curves were arrived at analytically for A^2, Marshall and Hitschfeld show that the results for Log A^2 to be approximately the same.

Fig. 6 (derived from Fig. 5) shows the dB errors in estimating the power (or log power) plotted as a function of sample size for a family of confidence levels. We note, for example, that an error of 10 Log A^2 within $\pm$ 0.5 dB results 90% of the time for a sample size of 100. For a sample size of 20, a 90% confidence level gives rise to an error between +1 and -1.6 dB.

With regard to the time to decorrelation, theoretical studies have led to the expression (Battan [1973], Altas [1964]),

$$\Delta\tau = 1.71\ \lambda \times 10^{-3} \text{ sec} \tag{2.15}$$

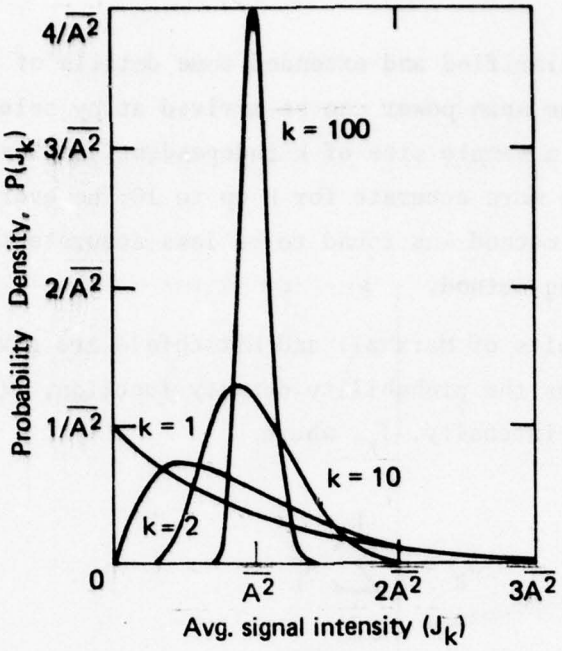

Figure 5. Probability density function, $P(J_k)$ of the measured average signal, J_k, for averages comprised of different sample sizes, k.

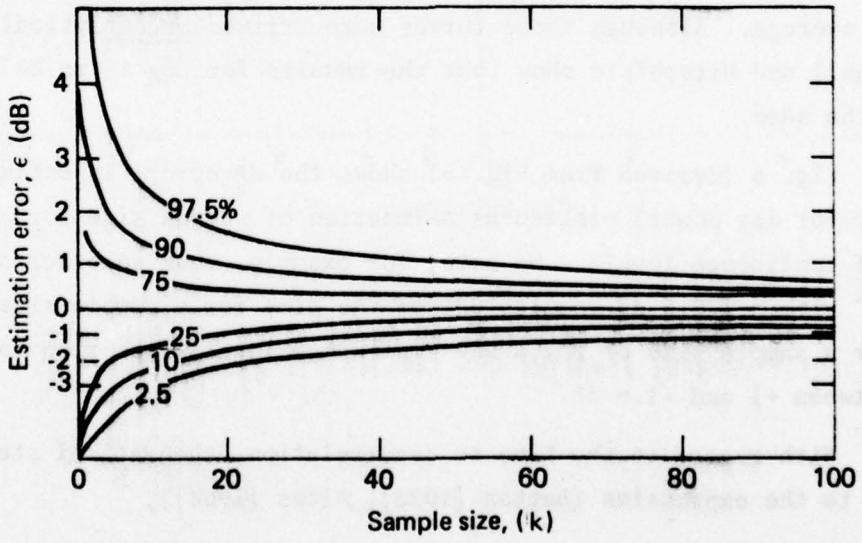

Figure 6. Statistical errors, ε, as a function of sample size, k, for different confidence levels.

where $\Delta\tau$ is the time required for the autocorrelation function to fall to 0.01 and λ is the radar wavelength in cm. Hence, for a 10 cm radar, it takes about 20 milliseconds after which the backscattered echoes may be said to be decorrelated. Assuming a sample size of 100, an integration time of 2 seconds is therefore required if straightforward methods are used in achieving a reliable estimate.

2.5 Resolution Requirements

2.5.1 Beam Shape Errors

In measuring a nonuniform reflectivity factor with a radar, a given inherent smoothing error exists as the received echoes correspond to the integrated effects of the true reflectivity integrated throughout the entire attenna pattern including sidelobes. Donaldson and Tear [1963] and Donaldson [1964a,b] investigated this problem and examined errors which may arise in both the estimation of the reflectivities of rain cell structures as well as errors in corresponding cell heights.

As an illustration of the magnitude of the beam shape errors, we show a family of curves in Fig. 7 deduced from the results of Donaldson [1964b] for a quadratic circular cell model defined by,

$$10 \text{ Log } Z = 50 - 9.57 \times 10^{-1} \rho^2 \qquad (2.16)$$

where ρ is the radial distance in kilometers from the storm center where ρ is confined to the plane orthogonal to the radar antenna beam axis. Although the original calculations were made for model antenna patterns depicting the CPS-9 radar having 1° beamwidth, the results here have been extrapolated to antennas with arbitrary beamwidths but having the same general pattern as used by Donaldson. The cell model given by (2.16) has a peak value of 50 dBZ and has been scaled from the original 70 dBZ used.

The dashed curve of Fig. 7 represents the true reflectivity values as a function of the distance from the cell center. The other curves denote the measured reflectivity variations for the range-beamwidth

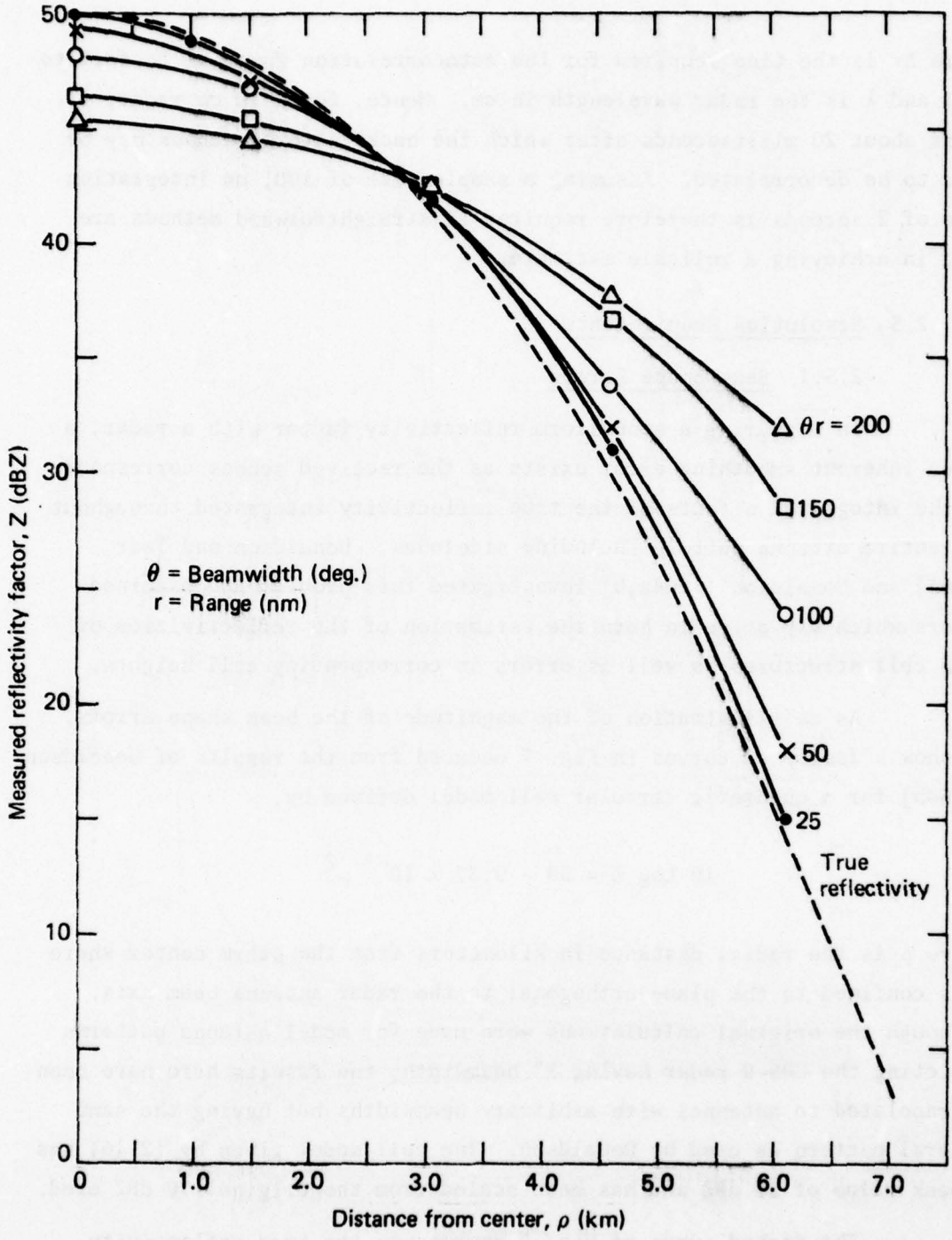

Figure 7. Measured reflectivity factor versus distance from rain cell center for indicated ranges assuming true cell reflectivity variation shown (dashed curve).

products indicated. We note that for a beamwidth of 1° and a range of 50 nm, a 3 dB error may exist 6 km from the cell center. This error is mitigated by the fact that the reflectivity factors here are small (i.e., smaller than 20 dBZ). We, however, note that at the larger ranges and at the steeper gradient locations, serious beam shape errors may arise. These results emphasize the need to utilize small beamwidths in the design of antenna systems used for rain reflectivity measurements. It also demonstrates the limitation of making measurements at extended ranges.

2.5.2 Reflectivity Gradient Errors

For the case in which the pulse volume contains gradients in the reflectivity factor and in addition a log receiver is used, the probability density functions depicted in Fig. 5 and statistical errors denoted in Fig. 6 are altered. Both the variance and the mean change depending upon the reflectivity gradient as well as the beam resolution. In Figs. 8(a) and (b) are given the results of Rogers [1971] which describe the deviations from the uniform reflectivity case as a function of Z_2/Z_1, the ratio of the power received from the strongest reflecting region in the pulse volume (proportional to the reflectivity factor, Z_2) to the power received from the weakest portion (proportional to Z_1).

The ordinate parameters in Figs. 8(a) and (b) are defined as,

$\langle J \rangle$ = the estimates of $\overline{\text{Log } A^2}$ when a reflectivity gradient is present.

J = the estimate of $\overline{\text{Log } A^2}$ for a uniform reflectivity in pulse volume. This is equal to an average across the gradient.

$\sum_j^2$ = the variance of the $\overline{\text{Log } A^2}$ when a reflectivity gradient is present.

σ_j^2 = the variance of the $\overline{\text{Log } A^2}$ for a uniform reflectivity in the pulse volume.

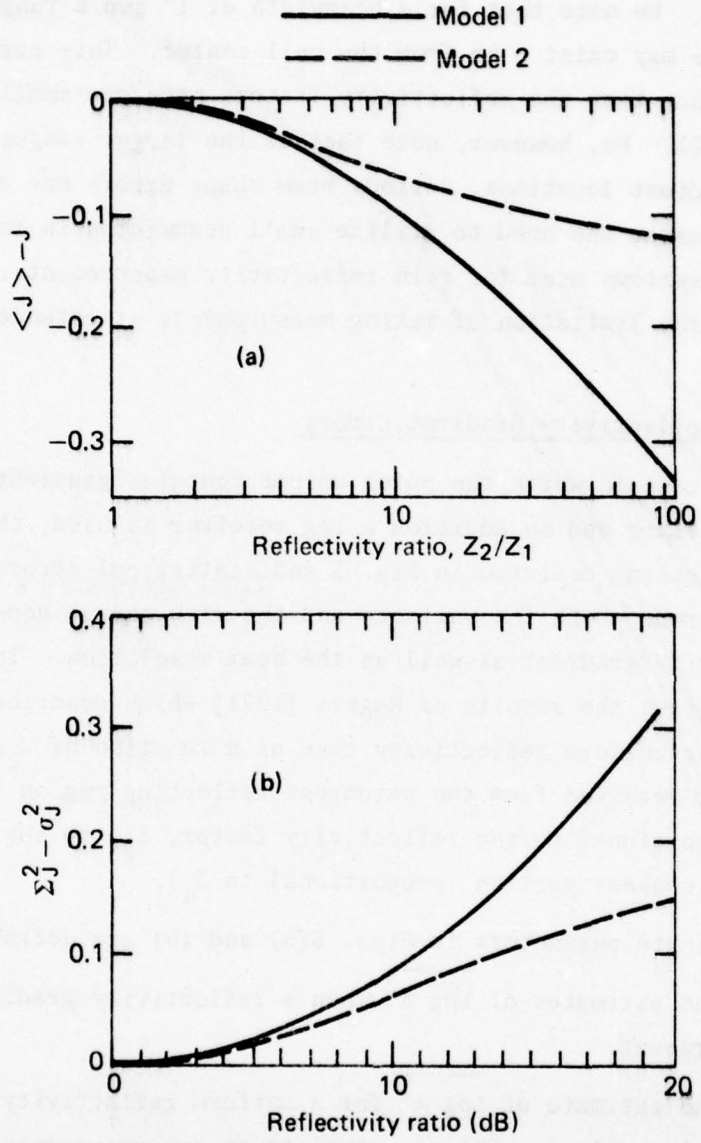

Figure 8. Deviations of (a) intensity levels (i.e., $\overline{\text{Log } A^2}$) and (b) variances of intensity levels from the uniform reflectivity case as a function of the ratio of largest (Z_2) to smallest (Z_1) reflectivity in pulse volume. The solid and dashed curves represent models pertaining to a linear variation of Log Z and Z, respectively, across the beam.

The solid and dashed curves represent models pertaining to a linear variation in log Z and Z, respectively; the former being considered as a more realistic model.

We again note the desirability of utilizing a narrow beamwidth as it is accompanied by a reduction in the ratio of Z_2/Z_1 within the pulse volume. As an illustration, it may be observed that for a pulse beam resolution of 1 km and gradients of reflectivity of 10 and 20 dB/km, the reflectivity will be underestimated by 1.0 and 3 dB, respectively (ten times the value shown). We also note that the additional variances (Fig. 8(b) for these gradients are 0.1 and 0.33 $(\text{bels})^2$ which correspond to standard deviations of 3.2 and 5.7 dB.

2.5.3 Resolution Errors Due to Scanning

We assume here the radar receiver integrator does not register a reflectivity value until a defined integration time, Δt_i, has elapsed. If the radar antenna is scanning, the resolution previously defined in part by the beamwidth alters since the beam is sweeping during the integration time. The effective resolution may be defined in terms of an effective beamwidth, $\Delta\theta_{ef}$, related to the true beamwidth, $\Delta\theta_o$, and scan rate α[°/sec] by the equation,

$$\Delta\theta_{ef} = \Delta\theta_o + \alpha\Delta t_i \tag{2.17}$$

The error arising due to reflectivity gradients in the effective pulse volume may be obtained from Fig. 8 where the effective pulse volume is defined in terms of the effective pulsewidth, $\Delta\theta_{ef}$, given by (2.17).

2.6 Correction Due to Log Averaging and Processor Quantization

A receiver having a logarithmic response produces an output power proportional to the logarithm of the input power (i.e., Log A^2). If the logarithm of the output power is sampled and averaged, the resulting quantity is the average of the logarithm of the power (i.e., Log $\overline{A^2}$) rather than the desired logarithm of the average power (i.e., Log $\overline{A^2}$). Austin and Shaffner [1970] have demonstrated that

$$10 \text{ Log } \overline{A^2} = 10 \overline{\text{Log } A^2} + 2.5 + \frac{Q.I.}{2} \tag{2.18}$$

where Q.I. represents the quantization interval of the output processor which converts the analog to digital data. In the event the data is averaged in analog form the measured level underestimates the true logarithm of the power simply by 2.5 dB. If a processor is used which digitizes the data, Q.I. is given by,

$$Q.I. = \frac{\text{dB Dynamic Range}}{2^N - 1} \tag{2.19}$$

where N is the word length in terms of the number of bits used for analog to digital conversion. Hence, a 6-bit word covering a 90 dB dynamic range results in a quantization interval, $Q.I. = \frac{90}{2^6 - 1} = 1.4$ dB.

2.7 Receiver Power Levels from Rain Scattering

We shall here examine typical expected received power levels for various conditions of rain assuming specific radar parameters in the bracketed factor of (2.11). The resulting curves generated are applicable however to arbitrary parameters by multiplying by an appropriate factor (to be defined) so as to adjust the radar constant.

Taking 10 Log_{10} of both sides of (2.11) we obtain the expression

$$10 \text{ Log}_{10} P_r = dBZ + 10 \text{ Log}_{10} K - 20 \text{ Log } r + 10 \text{ Log}_{10} L_g \tag{2.20}$$

where K (or $10 \text{ Log}_{10} K$) is the effective radar constant given by,

$$K = 1.22 \times 10^{-12} [P_t \tau G^2 \Delta\theta_e \Delta\theta_r L_t L_r] \tag{2.21}$$

and where,

$dBZ = 10 \text{ Log}_{10} Z$; $[Z] = mm^6/m^3$

$10 \text{ Log}_{10} P_r$ = receiver power in dBm

r = range in km

$10 \text{ Log}_{10}(L_g)$ = attenuation due to atmospheric gas (dB)

As an example we inject the following radar parameters into (2.21):

$P_t = 10^6$ watts

$\tau = 10^{-6}$ secs

$\Delta\theta_e = \Delta\theta_h = 1.75 \times 10^{-2}$ rad (1.0°)

$G = 2.35 \times 10^4$ (43.7 dB)

$L_t = L_r = 0.707$ (1.5 dB)

Hence,

$$K = 1.03 \times 10^{-7} \tag{2.22}$$

or

$$10 \text{ Log } K = -69.9 \text{ dB}$$

The gain given above is derived from the beamwidth assuming a 50% aperture efficiency, e, and the relations,

$$\Delta\theta = 1.2 \frac{\lambda}{D_o} \tag{2.23}$$

$$G = e\left(\frac{\pi D_o}{\lambda}\right)^2 \tag{2.24}$$

A beamwidth of 1° at λ = 10 cm hence corresponds to an antenna diameter, $D_o \simeq 7$ m.

In Fig. 9 are plotted curves describing the received power given by (2.20) as a function of range for a family of reflectivity levels, Z. The contribution due to atmospheric gas being at most several dB is here neglected. Although these curves correspond to the above example parameters, the power levels may be converted to other system parameters through the relation,

$$P_r(\text{dBm}) = P_{ro}(\text{dBm}) + 69.9 + 10 \text{ Log}_{10} K \tag{2.25}$$

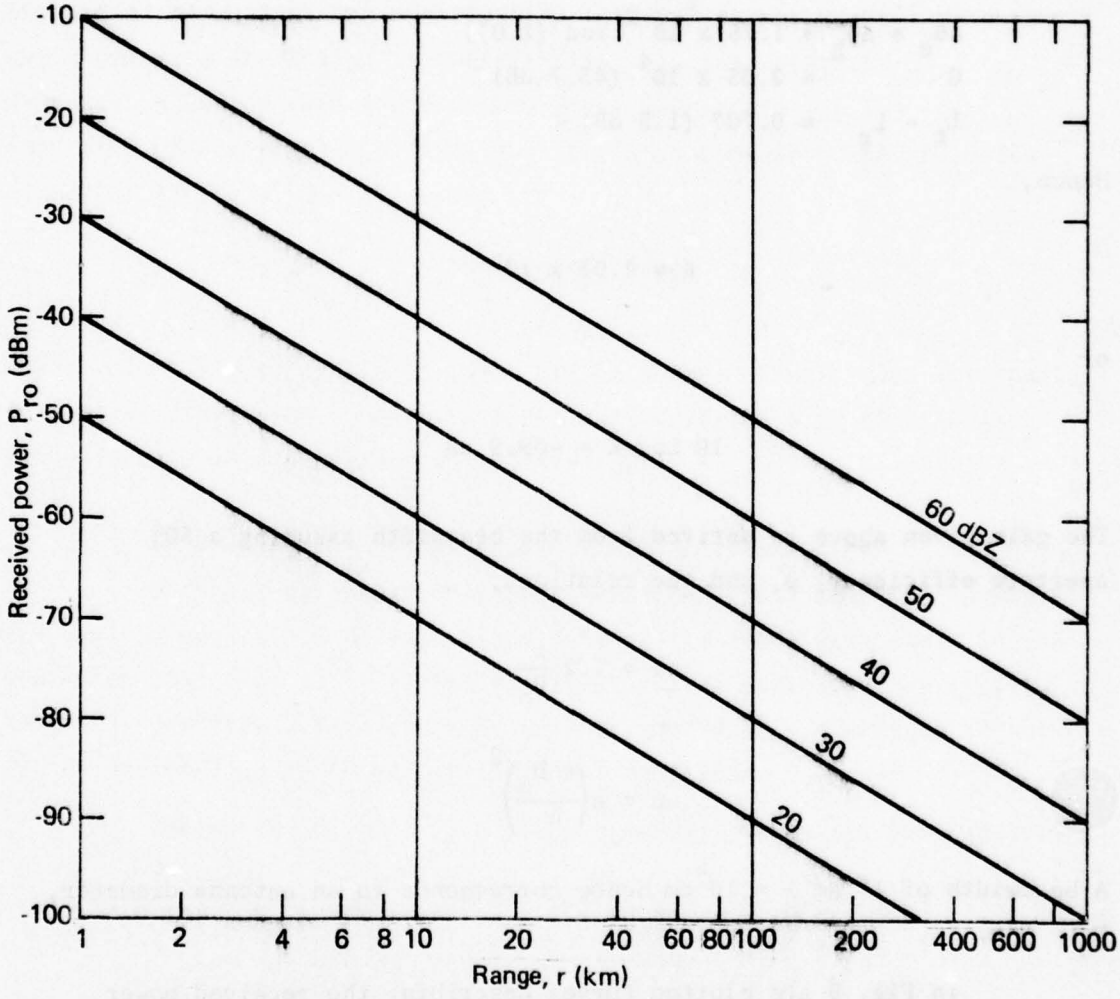

Figure 9. Received power (for example radar system) as a function of range at various rain reflectivity levels. To convert to other radar system power levels use (2.25).

where P_{ro} is the received power in dBm for the given parameters and K and P_r are the revised radar constant and received power levels, respectively, for the alternate system parameters.

In Fig. 10 are plotted curves describing the received power as a function of range for a family of effective rain rate levels, R. We use here the empirical relation [Battan, 1973],

$$Z = 200\ R^{1.6} \tag{2.26}$$

which approximately corresponds to a Laws and Parsons distribution [1943] for converting the curves of Fig. 9 to those in Fig. 10. In (2.26) Z is expressed in mm^6/m^3 and R is in mm/hr. Here again the power levels for alternate system parameters may be obtained using (2.25). We note from Fig. 10 that a receiver sensitivity down to -100 dBm would enable the detection of rain rates (>0.5 mm/hr) out to 200 km in range. The power levels in Figs. 9 and 10 may be adjusted so as to include atmospheric attenuation by subtracting the appropriate levels given in Fig. 1.

2.8 Estimation of Path Attenuation At Various Frequencies

2.8.1 Pertinent Regression Relationships

Given a defined drop size distribution, it may be demonstrated that the attenuation coefficient, k (in dB/km), may be related to the reflectivity factor, Z (in mm^6/m^3), through the empirical relation (Atlas and Ulbrich [1974]),

$$k = a\ Z^b \tag{2.27}$$

where a and b are empirical parameters dependent strongly on frequency and drop size distribution and less strongly on temperature as it influences the refractive index. Best fit parameters of a and b may be obtained through the theoretical expressions for Z and k given by,

$$Z = \int_0^\infty D^6\ N(D)dD \qquad [mm^6/m^3] \tag{2.28}$$

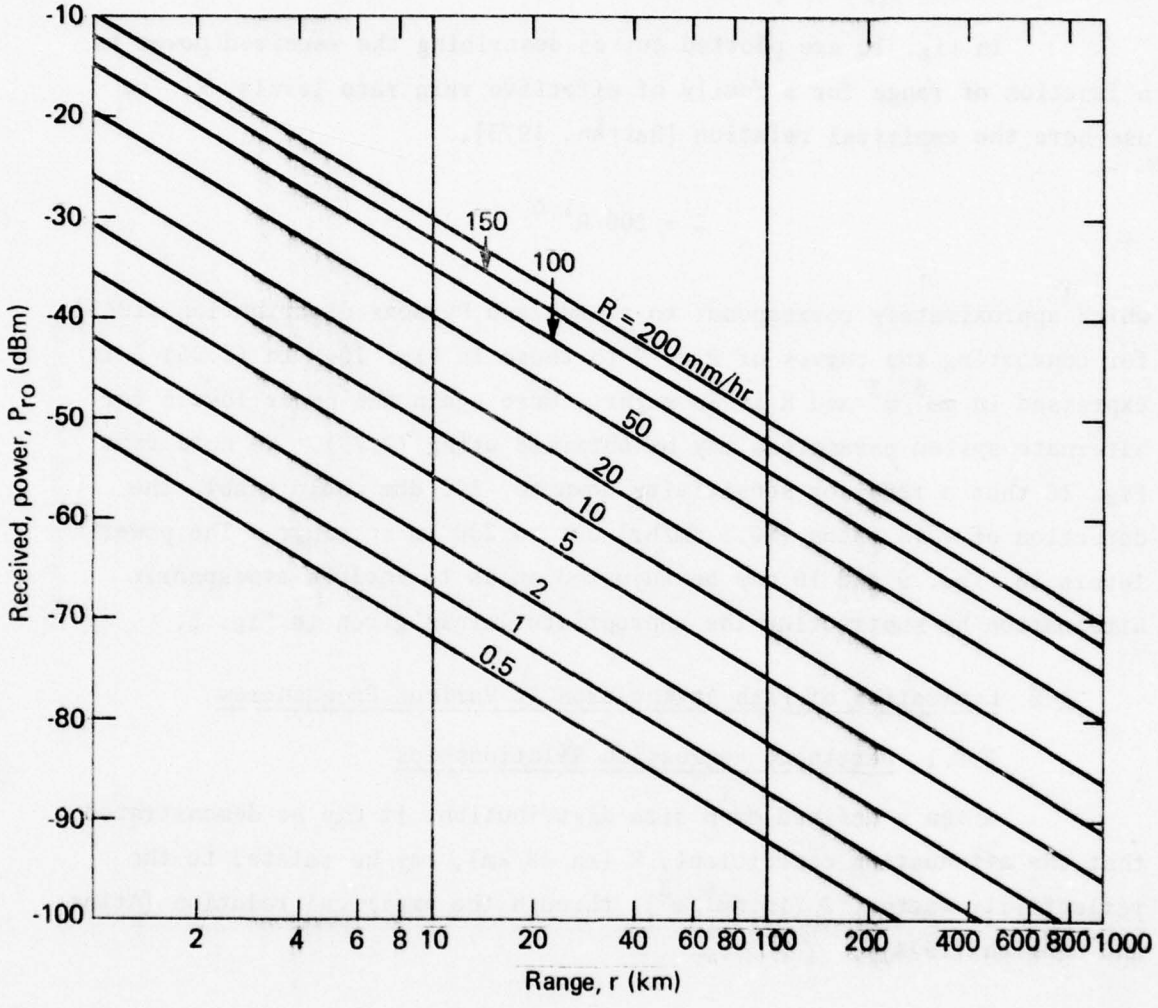

Figure 10. Received power (for example radar system) as a function of range at various rain rate levels. To convert to other radar system power levels use (2.25).

$$k = \int_0^\infty C_{ext}(D)\, N(D)dD \qquad [dB/km] \tag{2.29}$$

where Z and the drop size distribution, N(D)dD, have previously been defined and C_{ext} in (2.29) is called the extinction factor [(dB/km) x cm^3]. It is a Mie related quantity and represents a measure of the attenuation due to scattering and absorption from a drop of diameter, D, for the given frequency and refractive index. These quantities have been tabulated by several investigators for the Laws and Parsons drop size distribution (e.g., Medhurst,(1964]; Setzer [1970]).

The form (2.27) may be arrived at directly using (2.28) and (2.29) or indirectly using the rain rate formulation,

$$R = \frac{\pi}{6} \int_0^\infty D^3\, v(D)\, N(D)dD \qquad [mm/hr] \tag{2.30}$$

where v(D) is the drop terminal velocity for diameter, D. For a defined drop size distribution, empirical relations given by,

$$k = \alpha R^{\beta} \tag{2.31}$$

and

$$Z = a_o R^{b_o} \tag{2.32}$$

may also be formed by relating (2.28) and (2.29) with (2.30). The indirect method of arriving at (2.27) is to combine (2.31) and (2.32) eliminating R. The parameters in (2.32) are frequency independent and only depend on the drop size distribution whereas the parameters in (2.31) depend on frequency as well.

A number of investigators have calculated values of α and β in (2.31) for a wide range of frequencies. More recently, these parameters

have been calculated and tabulated by Rogers and Olsen [1977] and by Olsen et al. [1977] for frequencies ranging from 1 to 1000 GHz for the drop size distributions of Laws and Parsons [1943], Marshall and Palmer [1948], and Joss, Thams, and Waldvogel [1968]. The tabulations of Olsen et al. [1977] in the frequency range 10 through 100 GHz are given in Table 2.2 for the temperatures 20°C, 0°C, and -10°C (supercooled drops). The column heads have the following significance:

LP_L = Laws and Parsons distribution for rain rates less than 50 mm/hr

LP_H = Laws and Parsons distribution for rain rates between 25 and 150 mm/hr

MP = Marshall-Palmer distribution

J-T = The Joss et al. [1968] distribution for thunderstorm activity

J-D = The Joss et al. distribution for drizzle.

The parameters a_o and b_o in (2.32) have been categorized by Joss et al. [1968] for drizzle and thunderstorm and are:

$$Z = 140\ R^{1.5} \qquad \text{Drizzle} \tag{2.33}$$

$$Z = 500\ R^{1.5} \qquad \text{Thunderstorm} \tag{2.34}$$

Laws and Parsons and Marshall-Palmer distributions are often applied for widespread rain conditions and the corresponding Z-R relation is approximately,

$$Z \simeq 200\ R^{1.6} \qquad \text{Widespread} \tag{2.35}$$

If Z_i is considered to be the radar reflectivity factor at the i^{th} adjacent range bin along a radar beam (i^{th} pulse volume) the estimated path integrated attenuation, A, is given by,

$$A = \sum_{i=1}^{N} a\ Z_i^{\,b}\ \Delta r \tag{2.36}$$

Table 2.2

PARAMETER VALUES OF α AND β IN $k = \alpha R^{\beta}$. TAKEN FROM OLSEN ET AL. [1977].

T = 20°C										
FREQ. (GHz)	a					b				
	LP_L	LP_H	MP	J-T	J-D	LP_L	LP_H	MP	J-T	J-D
10	9.20×10^{-3}	1.11×10^{-2}	1.01×10^{-2}	1.90×10^{-2}	7.52×10^{-3}	1.280	1.230	1.260	1.079	1.024
11	1.27×10^{-2}	1.67×10^{-2}	1.37×10^{-2}	2.42×10^{-2}	9.67×10^{-3}	1.259	1.181	1.244	1.060	1.047
12	1.68×10^{-2}	2.33×10^{-2}	1.81×10^{-2}	3.25×10^{-2}	1.22×10^{-2}	1.236	1.142	1.223	1.022	1.067
15	3.28×10^{-2}	4.59×10^{-2}	3.57×10^{-2}	5.89×10^{-2}	2.20×10^{-2}	1.173	1.077	1.160	0.966	1.106
20	6.83×10^{-2}	8.59×10^{-2}	7.51×10^{-2}	0.103	4.57×10^{-2}	1.110	1.044	1.103	0.934	0.123
25	0.113	0.143	0.127	0.181	7.76×10^{-2}	1.075	1.007	1.064	0.868	1.119
30	0.168	0.228	0.191	0.273	0.118	1.043	0.955	1.034	0.816	1.113
35	0.235	0.337	0.269	0.360	0.167	1.008	0.904	0.999	0.782	1.107
40	0.312	0.452	0.360	0.439	0.225	0.971	0.864	0.966	0.757	1.101
50	0.484	0.648	0.572	0.610	0.368	0.900	0.816	0.900	0.708	1.082
60	0.652	0.775	0.796	0.771	0.541	0.845	0.794	0.847	0.667	1.055
70	0.802	0.850	1.01	0.814	0.735	0.802	0.785	0.807	0.663	1.020
80	0.934	0.902	1.21	0.810	0.936	0.770	0.780	0.772	0.671	0.985
90	1.03	0.938	1.39	0.876	1.14	0.749	0.777	0.744	0.656	0.952
100	1.09	0.958	1.53	0.995	1.33	0.737	0.774	0.721	0.627	0.920
T = 0°										
10	1.17×10^{-2}	1.14×10^{-2}	1.36×10^{-2}	1.69×10^{-2}	1.14×10^{-2}	1.178	1.189	1.150	1.076	0.968
11	1.50×10^{-2}	1.52×10^{-2}	1.73×10^{-2}	2.12×10^{-2}	1.41×10^{-2}	1.170	1.167	1.143	1.065	0.977
12	1.86×10^{-2}	1.96×10^{-2}	2.15×10^{-2}	2.62×10^{-2}	1.72×10^{-2}	1.162	1.150	1.136	1.052	0.985
15	3.21×10^{-2}	3.47×10^{-2}	3.68×10^{-2}	4.66×10^{-2}	2.82×10^{-2}	1.141	1.119	1.118	1.010	1.003
20	6.26×10^{-2}	7.09×10^{-2}	7.19×10^{-2}	9.83×10^{-2}	5.30×10^{-2}	1.118	1.084	1.097	0.946	1.020
25	0.105	0.132	0.121	0.173	8.61×10^{-2}	1.094	1.029	1.074	0.884	1.033
30	0.162	0.226	0.186	0.274	0.128	1.060	0.955	1.043	0.823	1.044
35	0.232	0.345	0.268	0.372	0.180	1.021	0.908	1.007	0.783	1.053
40	0.313	0.467	0.362	0.451	0.241	0.981	0.865	0.972	0.760	1.058

Table 2.2

(continued)

T = 0° (continued)										
FREQ. (GHz)	a					b				
	LP_L	LP_H	MP	J-T	J-D	LP_L	LP_H	MP	J-T	J-D
50	0.489	0.669	0.579	0.629	0.387	0.906	0.816	0.905	0.709	1.053
60	0.658	0.796	0.801	0.804	0.558	0.850	0.794	0.851	0.662	1.035
70	0.801	0.869	1.00	0.833	0.740	0.808	0.784	0.812	0.661	1.009
80	0.924	0.913	1.19	0.809	0.922	0.777	0.780	0.781	0.674	0.980
90	1.02	0.945	1.35	0.857	1.10	0.755	0.776	0.753	0.663	0.953
100	1.08	0.966	1.48	0.961	1.26	0.741	0.774	0.730	0.639	0.928
T = -10°C										
10	1.32×10^{-2}	1.13×10^{-2}	1.59×10^{-2}	1.51×10^{-2}	1.42×10^{-2}	1.125	1.171	1.092	1.087	0.932
11	1.64×10^{-2}	1.45×10^{-2}	1.97×10^{-2}	1.91×10^{-2}	1.74×10^{-2}	1.124	1.161	1.091	1.077	0.938
12	2.00×10^{-2}	1.81×10^{-2}	2.39×10^{-2}	2.37×10^{-2}	2.09×10^{-2}	1.122	1.152	1.090	1.066	0.942
15	3.31×10^{-2}	3.14×10^{-2}	3.94×10^{-2}	4.29×10^{-2}	3.34×10^{-2}	1.119	1.135	1.088	1.027	0.954
20	6.37×10^{-2}	6.68×10^{-2}	7.50×10^{-2}	9.73×10^{-2}	6.09×10^{-2}	1.111	1.098	1.082	0.951	0.971
25	0.107	0.130	0.126	0.174	9.73×10^{-2}	1.091	1.037	1.065	0.887	0.988
30	0.165	0.226	0.193	0.276	0.143	1.059	0.969	1.037	0.826	1.004
35	0.236	0.346	0.275	0.376	0.197	1.021	0.910	1.002	0.784	1.016
40	0.316	0.468	0.370	0.455	0.260	0.981	0.867	0.968	0.761	1.025
50	0.487	0.665	0.579	0.619	0.404	0.910	0.818	0.904	0.714	1.027
60	0.645	0.789	0.787	0.800	0.564	0.856	0.796	0.854	0.664	1.016
70	0.777	0.860	0.973	0.840	0.728	0.817	0.785	0.817	0.659	0.997
80	0.888	0.903	1.14	0.808	0.888	0.787	0.781	0.789	0.673	0.974
90	0.980	0.935	1.28	0.834	1.04	0.765	0.777	0.764	0.668	0.953
100	1.05	0.957	1.41	0.920	1.18	0.749	0.774	0.741	0.646	0.933

where N is the number of adjacent pulse volumes in the summation and $\Delta r = \frac{c\tau}{2}$ is the range resolution.

2.8.2 Validity of Using Radar for Attenuation Prediction

Several investigators have examined the validity of using radar for estimating the attenuations at various frequencies along a slant path applying a form similar to (2.36). McCormick [1972] and Strickland [1972, 1974] correlated their 3 GHz radar measurements with direct path measurements at f = 15.3 GHz. With receiving terminals on the ground, McCormick located the transmitter beacon on an aircraft and in Strickland's case a beacon was located on the ATS-5 satellite. Both investigators reported good general correlation between measured and predicted fade levels, although there were occasions when poor correlations were noted due to possible mixed precipitation phase conditions.

Goldhirsh [1976a] correlated his 3 GHz radar data with 13 and 18 GHz path measurements and obtained generally good results. In this latter case, 13 and 18 GHz ground transmitters operated in the uplink mode toward the ATS-6 satellite and these reflectivities along the path were monitored with a high resolution radar at Wallops Island, Virginia. At the time of this writing, radar predicted path attenuations are being compared by Goldhirsh with measured attenuations (at f = 28.5 GHz) using the COMSTAR satellite beacon and a ground receiver near the radar.

Since the melting layer and the ice above it (for a widespread rain condition) should have small influence on the real attenuation, a method was described by Goldhirsh [1976a] for culling out the false attenuation as predicted by a radar. This method essentially suggests that (2.36) be summed only up to the melting layer when the RHI signature indicates an intense layered region at the 0°C height. When the RHI shows a convective rain in the form of vertical columns through the 0°C level, the summation may be implemented through the path.

Using the form (2.36) with radar data bases of rain, several investigators employed the use of radar to establish fade statistics

(Strickland [1974], Zawadski and Rogers [1972], Rogers [1972], Inkster and Rogers [1974], Goldhirsh and Robison [1975], Goldhirsh [1975b], Goldhirsh [1976b] and Hodge [1976]). Radar has the advantage that it can measure the rain reflectivity over three-dimensional space and using modeling procedures these fade statistics may be converted to variable frequencies, path elevation angles, and path spacings (Goldhirsh [1975, 1976]). In addition, the influence of variable path azimuth and base line orientation may be examined (Goldhirsh [1976b], Hodge [1976]).

3.0 EVALUATION OF THE FEASIBILITY OF USING A SINGLE ATTENUATING WAVELENGTH RADAR FOR RAIN PARAMETER INVESTIGATION

We examine here the difficulties and ambiguities in estimating rain parameters, using a radar operating at attenuation wavelengths. As a test case, a radar operating at a frequency of 15.7 GHz is considered.

3.1 *Iteration Method*

3.1.1 Derivation of the Formulation

We derive here a method for estimating the rain rate from the scatter power returns of a radar operating at an attenuating wavelength. Although the analysis is performed in terms of rain rate, R, it could just as well be pursued in terms of the reflectivity factor, Z.

Neglecting the attenuation due to cloud and atmospheric gases, the radar equation has the form of (2.1) which may be simply expressed as,

$$P(r_j) = \frac{C_o \eta_j}{r_j^2} 10^{-0.2 \int_o^{r_j} k_p(r_j)dr} \tag{3.1}$$

where j denotes the j^{th} range bin and C_o is constant containing the multiplying parameters in (2.1). All other parameters have previously been defined. As an approximation, the Mie parameters, η and k_p, may be expressed as,

$$\eta = a' R^{b'} \qquad [m^{-1}] \tag{3.2}$$

$$k_p = \alpha R^{\beta} \qquad [dB/km] \tag{3.3}$$

where R is the effective rain rate in mm/hr and a', b', α and β are the appropriately designated parameters.

Substituting (3.2) and (3.3) into (3.1) results in,

$$\frac{P(r_j)\, r_j^2}{C_o\, a'} = [R_j]^{b'}\, 10^{-0.2 \int_o^{r_j} \alpha [R(r)]^{\beta}\, dr} \tag{3.4}$$

Considering the form (3.4) at the adjacent range bin, r_{j+1}, we obtain,

$$\frac{P(r_{j+1})\, r_{j+1}^2}{C_o\, a'} = [R_{j+1}]^{b'}\, 10^{-0.2 \int_o^{r_{j+1}} \alpha [R(r)]^{\beta}\, dr} \tag{3.5}$$

Dividing (3.4) by (3.5) and taking 10 Log_{10} of both sides of this ratio, we obtain,

$$W_{j,j+1} = U_{j,j+1} + V_{j,j+1} \tag{3.6}$$

where

$$W_{j,j+1} = 10\ \text{Log}_{10} \left\{ \frac{r_j^2\, P(r_j)}{r_{j+1}^2\, P(r_{j+1})} \right\} \tag{3.7}$$

$$U_{j,j+1} = 10\, b'\, \text{Log}_{10} \left[\frac{R_j}{R_{j+1}} \right] \tag{3.8}$$

and

$$V_{j,j+1} = 2\,\alpha \int_{r_j}^{r_{j+1}} [R(r)]^{\beta}\, dr \tag{3.9}$$

In the integrand of (3.9) it is reasonable to assume an exponential fit for rain rate between bins at r_j and r_{j+1}. That is,

$$R(r) = R_j \exp[-u(r - r_j)] \tag{3.10}$$

where,

$$u = \frac{1}{\Delta} \ell n \left\{ \frac{R(r_j)}{R(r_{j+1})} \right\} \tag{3.11}$$

and,

$$\Delta = r_{j+1} - r_j \tag{3.12}$$

Substituting (3.10) into (3.9) and performing the integration,

$$V_{j,j+1} = \frac{2\,\alpha\, R_j^{\beta}}{\beta u} \left\{ 1 - \exp[-\beta u \Delta] \right\} \tag{3.13}$$

It is clear that a knowledge of R_j and R_{j+1} allows for a computation of $U_{j,j+1}$ as given by (3.8) and $V_{j,j+1}$ as given by (3.13).

We may implement the iteration technique in the following way. Given a measurement of $W_{j,j+1}$ and a knowledge of R_j we first find R_{j+1}. Once R_{j+1} is established, we repeat the process by using the measured value of $W_{j+1,j+2}$ and arrive at R_{j+2}. In this way a rain rate profile along the radar beam is established. The iteration technique may be pursued using the following steps in conjunction with the relation (3.6).

(1) Using a range bin close to the radar, compute the corresponding rain rate from (3.4) where the attenuation may be neglected because of the short path length. For simplicity call this range bin 1. Hence from (3.4),

$$R_1 = \left\{ \frac{r_1^2 \, P(r_1)}{C_o \, a'} \right\}^{\frac{1}{b'}} \tag{3.14}$$

(2) With R_1 and $W_{1,2}$ [given by (3.14) and (3.7), respectively] obtained from the measured power, assume for the first approximation $V_{1,2} = 0$ and compute R_2 from $U_{1,2}$ as given by (3.8). Call this rain rate R_2^1 to denote the first approximation.

(3) Compute the first approximation to $V_{1,2}$ as given by (3.13) by substituting R_1 and R_2^1 into this expression. Call this first approximation $V_{1,2}^1$.

(4) Solve for the second approximation to $U_{1,2}$ by using (3.6). That is,

$$U_{1,2}^2 = W_{1,2} - V_{1,2}^1 \tag{3.15}$$

With the right hand side known, a second approximation to R_2 may be calculated using (3.8); say R_2^2.

(5) Repeat steps (3) and (4) using the value of R_2^2 and arrive at the third approximation to rain rate at r_2; namely R_2^3. This process may be continued N times until convergence; that is until,

$$R_2^N - R_2^{N-1} < \varepsilon \tag{3.16}$$

where ε is a predesignated uncertainty.

(6) After R_2 has been calculated the rain rate R_3 may be obtained using steps (2) through (5) by replacing subscripts 1 and 2 in

these steps by 2 and 3, respectively. In this manner, the entire rain rate profile may be calculated.

3.1.2 Testing the Method

As an illustration of the iteration method, we select here a segment of rain rate profile as measured at Wallops Island with an S-band radar (SPANDAR) on July 10, 1976, at 19:52:20 GMT at 60° azimuth and 20° elevation. The rain rates were computed from the measured values of Z using the empirical form,

$$Z = 200\ R^{1.6} \tag{3.17}$$

The rain rate profile over an approximate 2 km segment is shown plotted (solid line) in Fig. 11 where a level is indicated every 0.15 km which corresponds to the range resolution, Δ, of the radar (1 μsec pulsewidth).

Using the results of Haddock [1956] and assuming a Laws and Parsons distribution, we obtain for f = 15.7 GHz,

$$a' = 9.808 \times 10^{-7} \tag{3.18}$$

$$b' = 1.438 \tag{3.19}$$

From the results of Medhurst [1965],

$$\alpha = 4.343 \times 10^{-2} \tag{3.20}$$

$$\beta = 1.122 \tag{3.21}$$

The parameters given by (3.20) and (3.21) may be substituted in (3.13) where Δ = 0.15 km.

We assume the profile given in Fig. 11 (solid line) to be the true rain rates and compute the values of $W_{j,j+1}$ that would be measured

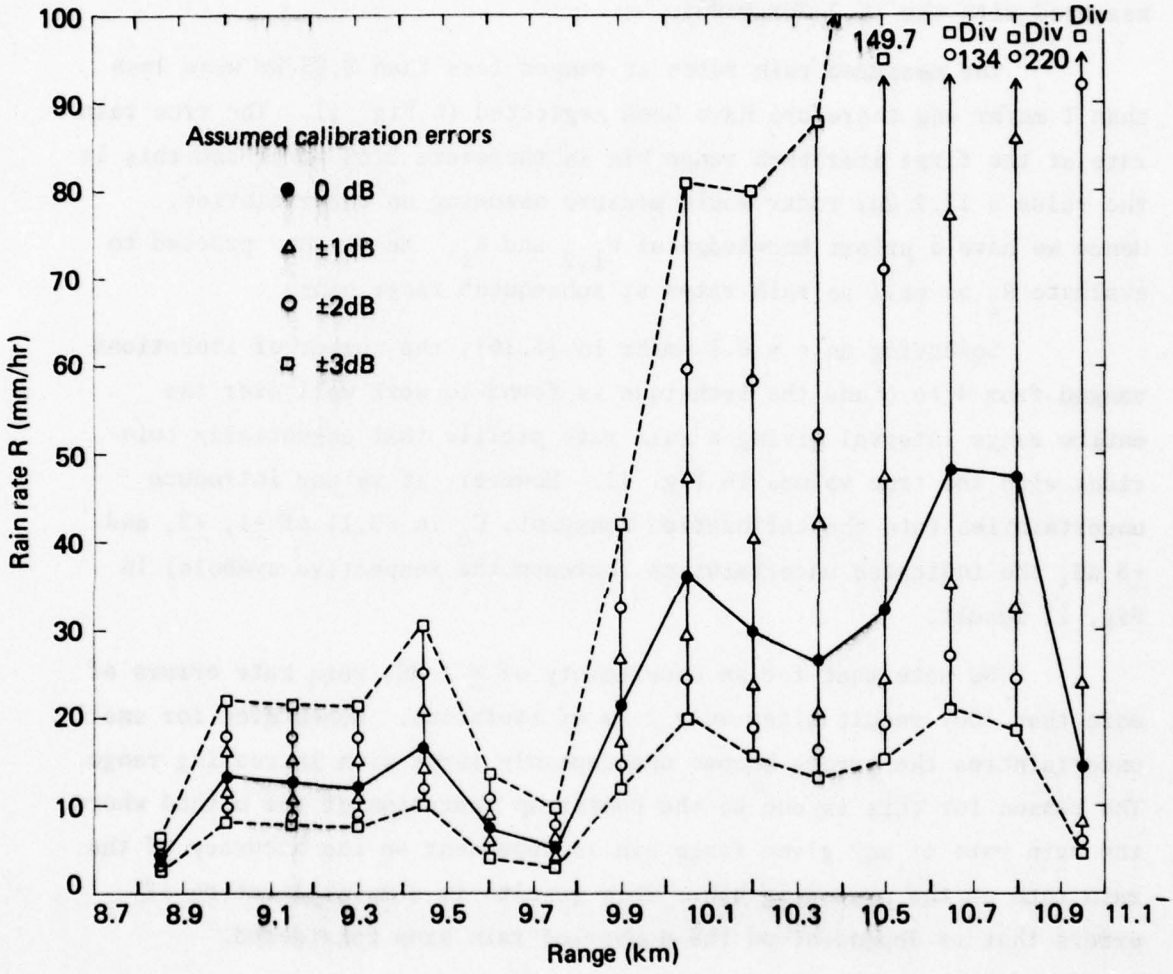

Figure 11. Segment of rain rate profile (solid line) as measured at Wallops Island, Va., on July 10, 1976, at 19:52:20 GMT at 60° azimuth and 20° elevation with an S-band radar. Other points represent apparent measured rain rates for given calibration errors using a 15.7 GHz radar and iteration method.

by a 15.7 GHz radar. This is achieved by computing individually the true values of $U_{j,j+1}$ given by (3.8) and $V_{j,j+1}$ given by (3.13). Hence the computed values of $W_{j,j+1}$ are considered true and the same as would be measured with the 15.7 GHz radar.

The measured rain rates at ranges less than 8.85 km were less than 1 mm/hr and therefore have been neglected in Fig. 11. The true rain rate at the first iteration range bin is therefore 3.65 mm/hr and this is the value a 15.7 GHz radar would measure assuming no uncertainties. Hence we have a priori knowledge of $W_{1,2}$ and R_1. We may now proceed to evaluate R_2 as well as rain rates at subsequent range bins.

Selecting an ε = 0.1 mm/hr in (3.16), the number of iterations ranged from 4 to 6 and the technique is found to work well over the entire range interval giving a rain rate profile that essentially coincides with the true values in Fig. 11. However, if we now introduce uncertainties into the calibration constant, C_o in (3.1) of ± 1, ± 2, and ± 3 dB, the indicated uncertainties (between the respective symbols) in Fig. 11 result.

We note that for an uncertainty of $\pm$ 1 dB, rain rate errors of more than 100% result after only 2 km of iteration. Hence even for small uncertainties the errors become unacceptably large with increasing range. The reason for this is due to the bootstrap operation of the method where the rain rate at any given range bin is dependent on the accuracy of the rain rate at the preceding bin. This results in a multiplication of errors that is dependent on the number of rain bins considered.

3.2 Errors Arising by Neglecting Attenuation

It is of interest to compare the results in Fig. 11 with those for the case in which attenuation is entirely neglected at 15.7 GHz.

The so-called true rain rate for the j^{th} bin may be obtained from (3.4) and is,

$$R_j = \left(\frac{r_j^2 \, P(r_j)}{C_o \, a'} \right)^{\frac{1}{b'}} 10^{+\frac{0.2}{b'} \int_o^{r_j} \alpha [R(r)]^{\beta} \, dr} \tag{3.22}$$

The "apparent" rain rate neglecting attenuation is,

$$R_{ja} = \left(\frac{r_j^2 \, P(r_j)}{C_o \, a'} \right)^{\frac{1}{b'}} \tag{3.23}$$

Comparing the apparent and true rain rates we observe,

$$R_{ja} = R_j \, 10^{-\frac{0.2}{b'} \int_o^{r_j} \alpha [R(r)]^{\beta} \, dr} \tag{3.24}$$

which may alternately be expressed by,

$$R_{ja} = R_j \, 10^{-\frac{0.2}{b'} \sum_{j=1}^{n-1} \int_{r_j}^{r_{j+1}} \alpha [R(r)]^{\beta} \, dr} \tag{3.25}$$

where n is the number of range bins considered.

Substituting the form (3.9) into the exponent of (3.25),

$$R_{ja} = R_j \, 10^{-\left[\frac{1}{10b'} \sum_{j=1}^{n-1} V_{j,j+1} \right]} \tag{3.26}$$

where $V_{j,j+1}$ is given by (3.13). The apparent rain rate as given by (3.26) is now a form ripe for computation.

In Fig. 12 are plotted both the true rain rate, R_j (solid line), as well as the apparent rain rate, R_{ja} (dashed line), given by (3.26). We observe that errors in excess of 100% result after only two kilometers for the case in which the influence of attenuation of the measured power is neglected. It should be noted that the above errors are in general even larger when calibration or measurement uncertainties are included.

3.3 Hitschfeld-Bordan Solution

A direct method for arriving at the true rain rate given rain attenuation has been described by Hitschfeld and Bordan [1954]. Using their methods, an equation of the form,

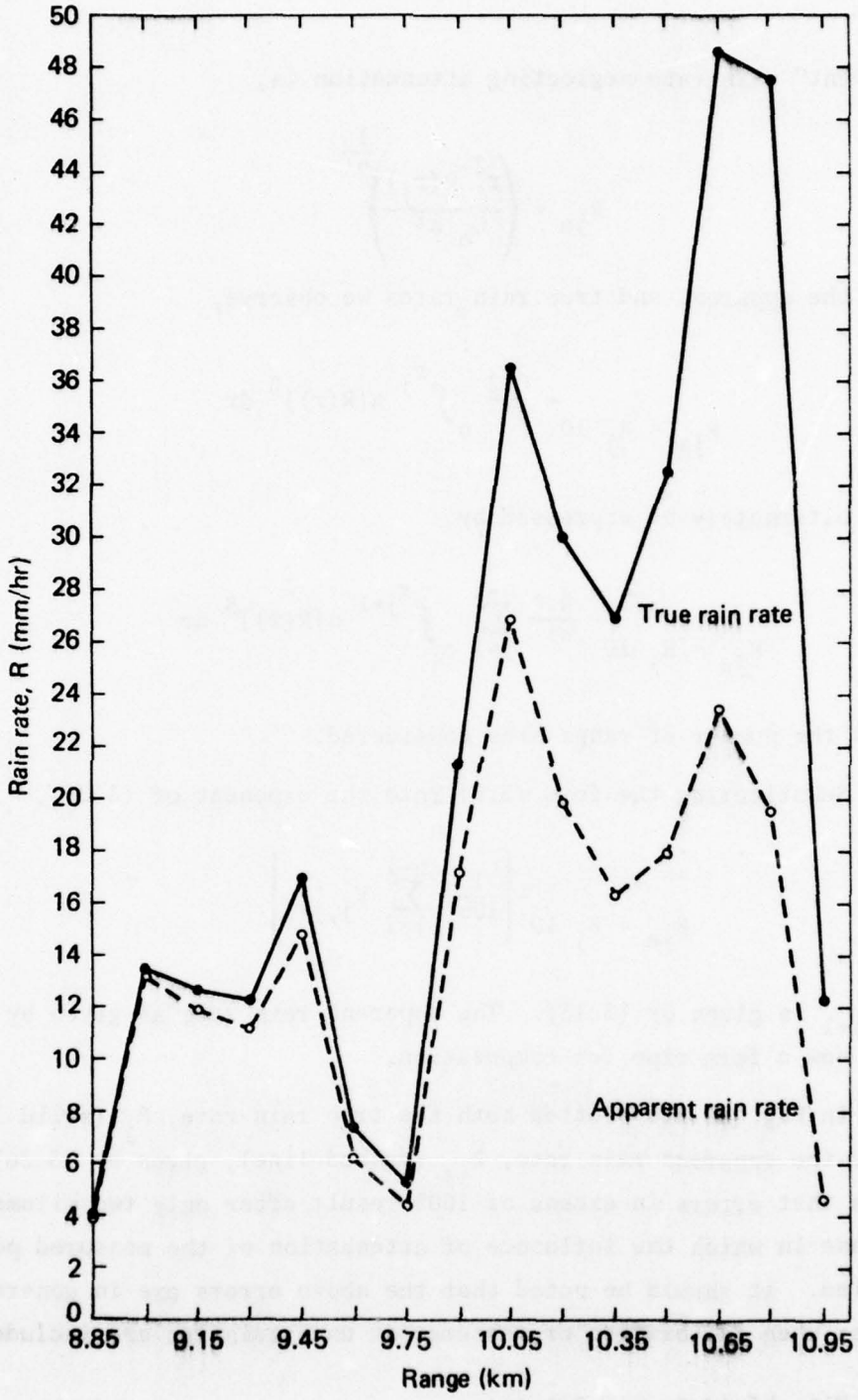

Figure 12. Measured true rain rate (solid line) and apparent rain rate (dashed line) arrived at by neglecting attenuation with a 15.7 GHz radar.

$$\frac{dU}{dr} + \beta U f(r) + K \beta = 0 \tag{3.27}$$

where

$$U = R_j^{-\beta} \tag{3.28}$$

$$f(r) = \frac{d}{dr} \log R_{ja} \tag{3.29}$$

$$K = \frac{0.2\ \alpha}{b'} \ln 10 \tag{3.30}$$

and where the true rain rate, R_j, is given by (3.22) and the apparent rain rate, R_{ja}, is defined by (3.23). The solution to (3.27) is given by,

$$R_j(r) = \frac{R_{ja}(r)}{\left\{1 - K \beta \int_o^r R_{ja}^{\beta} (v) d\, v\right\}^{1/\beta}} \tag{3.31}$$

Hence given the power received from rain scattering at each range, r_j [i.e., $P(r_j)$], R_{ja} as given by (3.23) may be calculated and the true rain rate, $R_j(r)$, given by (3.31) is established.

The expression (3.31) is exact assuming the empirical relations (3.2) and (3.3) are correct. However, the solution suffers from the same difficulty as the previously described iteration method; namely, a small uncertainty in, for example, the calibration constant results in unacceptably large errors in $R_j(r)$. As a matter of fact the two methods may be shown to be equivalent and the errors in $R_j(r)$ are the same as those using the iteration methods for the same uncertainties.

4.0 CHARACTERISTICS OF CLOUD PROPERTIES USING A RADAR AT K_u-BAND

We examine here the power scattered from cloud using a radar at 15.7 GHz and the ability of estimating the cloud liquid water content, M

(gm/m^3), from the received radar echoes. A knowledge of M allows for the computation of the attenuation coefficient and ultimately the integrated attenuation at other wavelengths. The radar parameters at 15.7 GHz used represent nominal values of a radar under design at RADC.

4.1 Attenuation Contributions from Atmospheric Gases

In using a radar at 15.7 GHz at shallow elevation angles, it is essential to establish the attenuation contribution due to atmospheric gases. In this section we evaluate this contribution using the theory of Van Vleck [1947, 1949] which is summarized by Bean and Dutton [1968]. The total attenuation coefficient is essentially due to the contributions of oxygen and water vapor. That is,

$$k_g = k(O_2) + k(H_2O) \tag{4.1}$$

The contribution due to O_2 is given by,

$$k(O_2) = \frac{0.34}{\lambda^2}\left(\frac{P}{1.01325}\right)\left(\frac{293}{T}\right)^2 \left\{ \frac{\Delta\nu_1}{\lambda^{-2} + (\Delta\nu_1)^2} + \frac{\Delta\nu_2}{(2 + \lambda^{-1})^2 + (\Delta r_2)^2} + \frac{\Delta\nu_2}{(2 - \lambda^{-1})^2 + \Delta\nu_2^2} \right\} \tag{4.2}$$

where λ is the wavelength in cm, P is the pressure in bars, and T is the temperature in °K. Also, $\Delta\nu_1$ and $\Delta\nu_2$ [cm^{-1}] are line width factors given by,

$$\Delta\nu_1 = 0.018\left(\frac{P}{1.01325}\right)\left(\frac{293}{T}\right)^{0.75} \quad [cm^{-1}] \tag{4.3}$$

$$\Delta\nu_2 = 0.049\left(\frac{P}{1.01325}\right)\left(\frac{300}{T}\right)^{0.75} \quad [cm^{-1}] \tag{4.4}$$

The contribution due to H_2O is comprised of two components; that arising from the absorption line at 1.35 cm $[k^{(1)}_{H_2O}]$ and that arising from the absorption bands above the 1.35 cm line $[k^{(2)}_{H_2O}]$. These contributions are given by,

$$k^{(1)}(H_2O) = \rho \frac{0.0318}{\lambda^2} \left(\frac{293}{T}\right)^{2.5} \exp\left(-\frac{644}{T}\right) \left\{ \frac{\Delta\nu_3}{(\lambda^{-1} - 0.74074)^2 + \Delta\nu_3^2} + \frac{\Delta\nu_3}{(\lambda^{-1} + 0.74074)^2 + \Delta\nu_3^2} \right\} \tag{4.5}$$

and

$$k^{(2)}(H_2O) = \rho \frac{0.05}{\lambda^2} \left(\frac{293}{T}\right) \left(\frac{P}{1.01325}\right) \left(\frac{318}{T}\right)^{0.5} [1 + .0046\ \rho]\Delta\nu_4 \tag{4.6}$$

where ρ is the water vapor density (gm/m^3), $\Delta\nu_3$ is the line width factor at 1.35 cm, and $\Delta\nu_4$ is the effective line width of the absorption bands above the 1.35 cm line. The line widths are given by,

$$\Delta\nu_3 = \Delta\nu_4 = 0.087 \left(\frac{P}{1.01325}\right) \left(\frac{318}{T}\right)^{0.5} (1 + .0046\ \rho) \tag{4.7}$$

In Fig. 13 are given curves describing the one way integrated path attenuation at 15.7 GHz due to atmospheric absorption as a function of range and path elevation. As a basis for comparison, a similar set of curves are given in Fig. 14 for f = 35 GHz. These curves were calculated using,

$$A_g = \int_o^r [k(O_2) + k^{(1)}(H_2O) + k^{(2)}(H_2O)]dr \tag{4.8}$$

where the component contributions in the integrand of (4.8) are given by (4.2), (4.5), and (4.6). Temperature and pressure-height profiles were

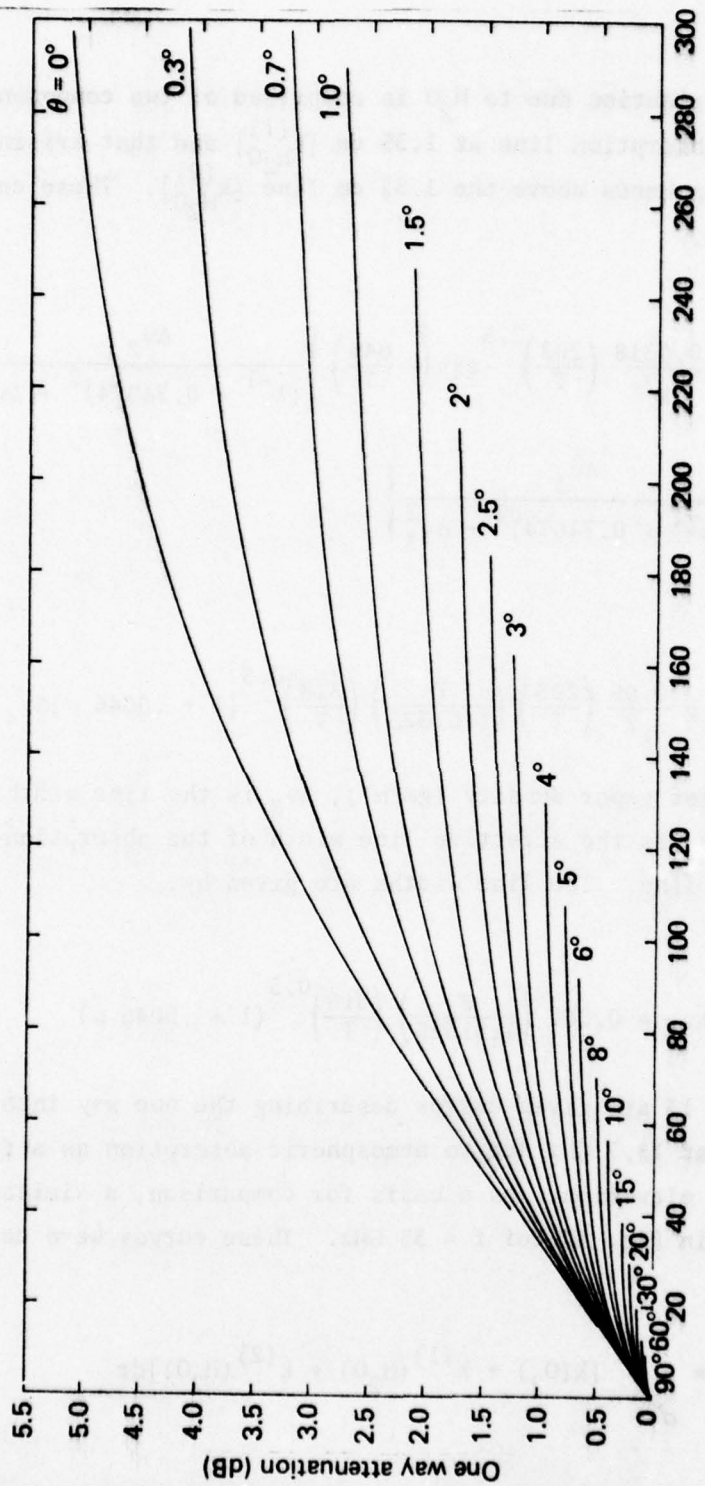

Figure 13. One way integrated path attenuation due to atmospheric O_2 and H_2O absorption as a function of range and elevation angle at f = 15.7 GHz. A ground humidity of ρ_o = 7.5 gm/m^3 is assumed.

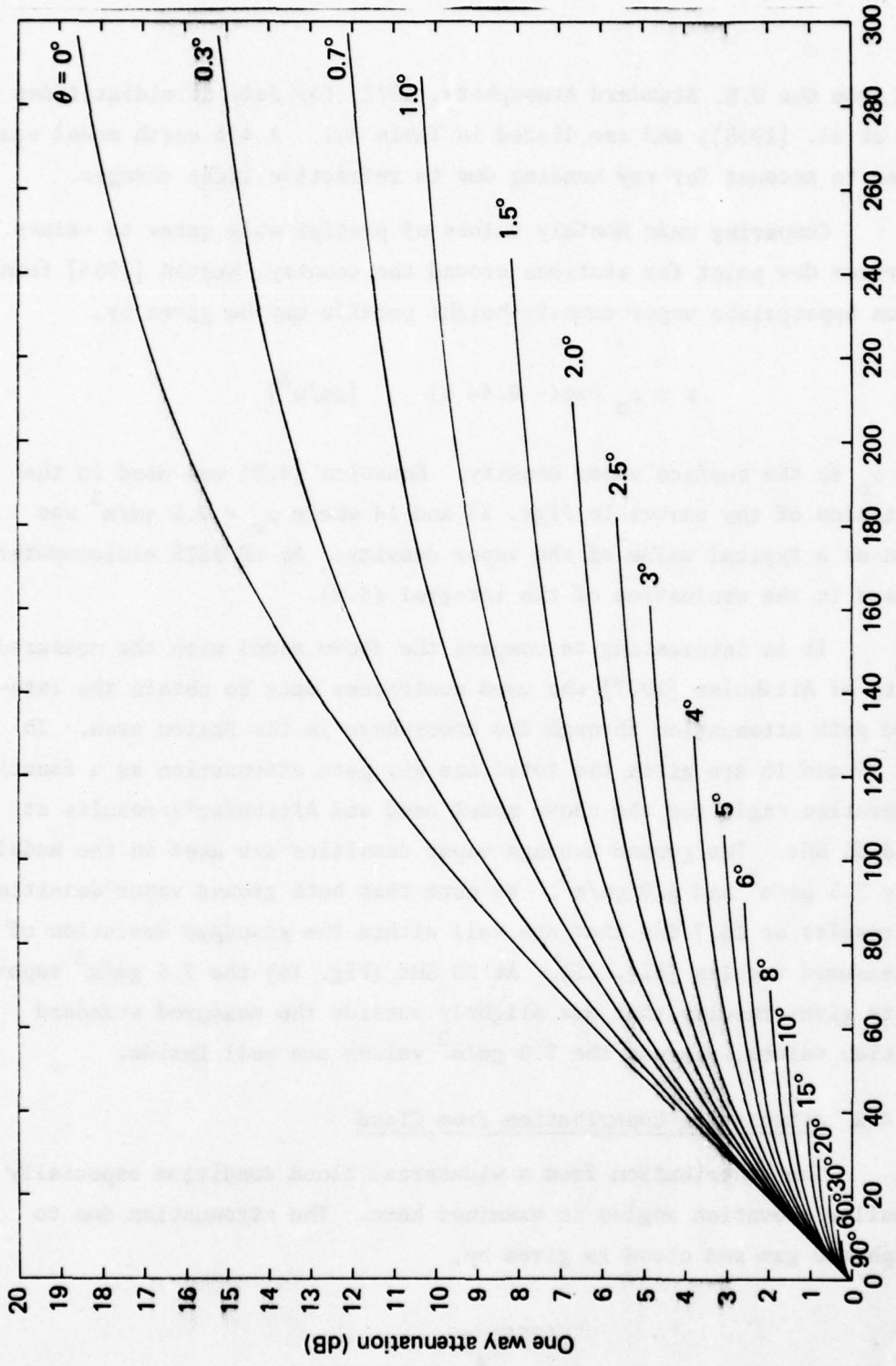

Figure 14. One way integrated path attenuation due to atmospheric O_2 and H_2O absorption as a function of range and elevation angle at f = 35 GHz. A ground humidity of 7.5 gm/m^3 is assumed.

taken from the U.S. Standard Atmosphere, 1972, for July at midlatitudes (Cole et al. [1965]) and are listed in Table 4.1. A 4/3 earth model was assumed to account for ray bending due to refractive index changes.

Comparing mean monthly values of precipitable water to values of surface dew point for stations around the country, Reitan [1963] found that an appropriate vapor density-height profile may be given by,

$$\rho = \rho_o \exp(-0.44\ h) \qquad [gm/m^3] \tag{4.9}$$

where ρ_o is the surface vapor density. Equation (4.9) was used in the computation of the curves in Figs. 13 and 14 where $\rho_o = 7.5\ gm/m^3$ was chosen as a typical value of the vapor density. An HP 9825 minicomputer was used in the evaluation of the integral (4.8).

It is interesting to compare the above model with the measured results of Altshuler [1977] who used suntracker data to obtain the integrated path attenuation through the atmosphere in the Boston area. In Figs. 15 and 16 are given the total one way path attenuation as a function of elevation angle for the above model used and Altshuler's results at 15 and 35 GHz. Two ground average vapor densities are used in the models; namely $7.5\ gm/m^3$ and $5.0\ gm/m^3$. We note that both ground vapor densities give results at 15.7 GHz that are well within the standard deviation of the measured results (Fig. 15). At 35 GHz (Fig. 16) the $7.5\ gm/m^3$ vapor density gives results that are slightly outside the measured standard deviation values, whereas the $5.0\ gm/m^3$ values are well inside.

4.2 Attenuation Contribution from Cloud

The contribution from a widespread cloud condition especially at shallow elevation angles is examined here. The attenuation due to atmospheric gas and cloud is given by,

$$A_g + A_c = \int_o^r (k_g + k_c)dr \tag{4.10}$$

Table 4.1

TEMPERATURE AND PRESSURE PROFILES FOR JULY AT MID LATITUDES.
From U.S. Standard Atmosphere, 1962 (Cole et al. [1965])

h(km)	T(°K)	P(atm)
0	294.15	1,01325
1	289.65	0,902198
2	285.15	0,801594
3	279.16	0,710433
4	273.17	0,628063
5	267.17	0,553615
6	261.19	0,486632
7	254.70	0,426404
8	248.22	0,372351
9	241.73	0,32402
10	235.25	0,28094

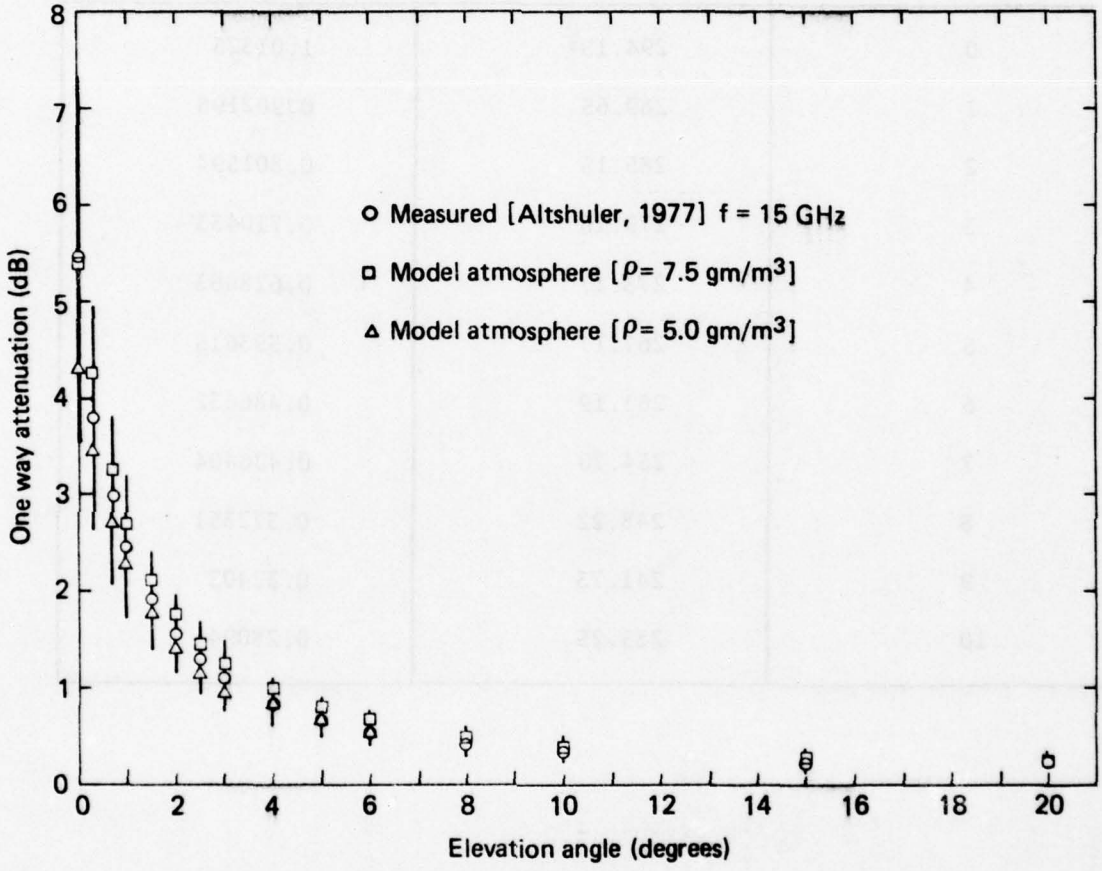

Figure 15. Measured one way atmospheric path attenuation by Altshuler [1977] as a function of elevation angle compared with model atmosphere attenuation at f = 15.7 GHz.

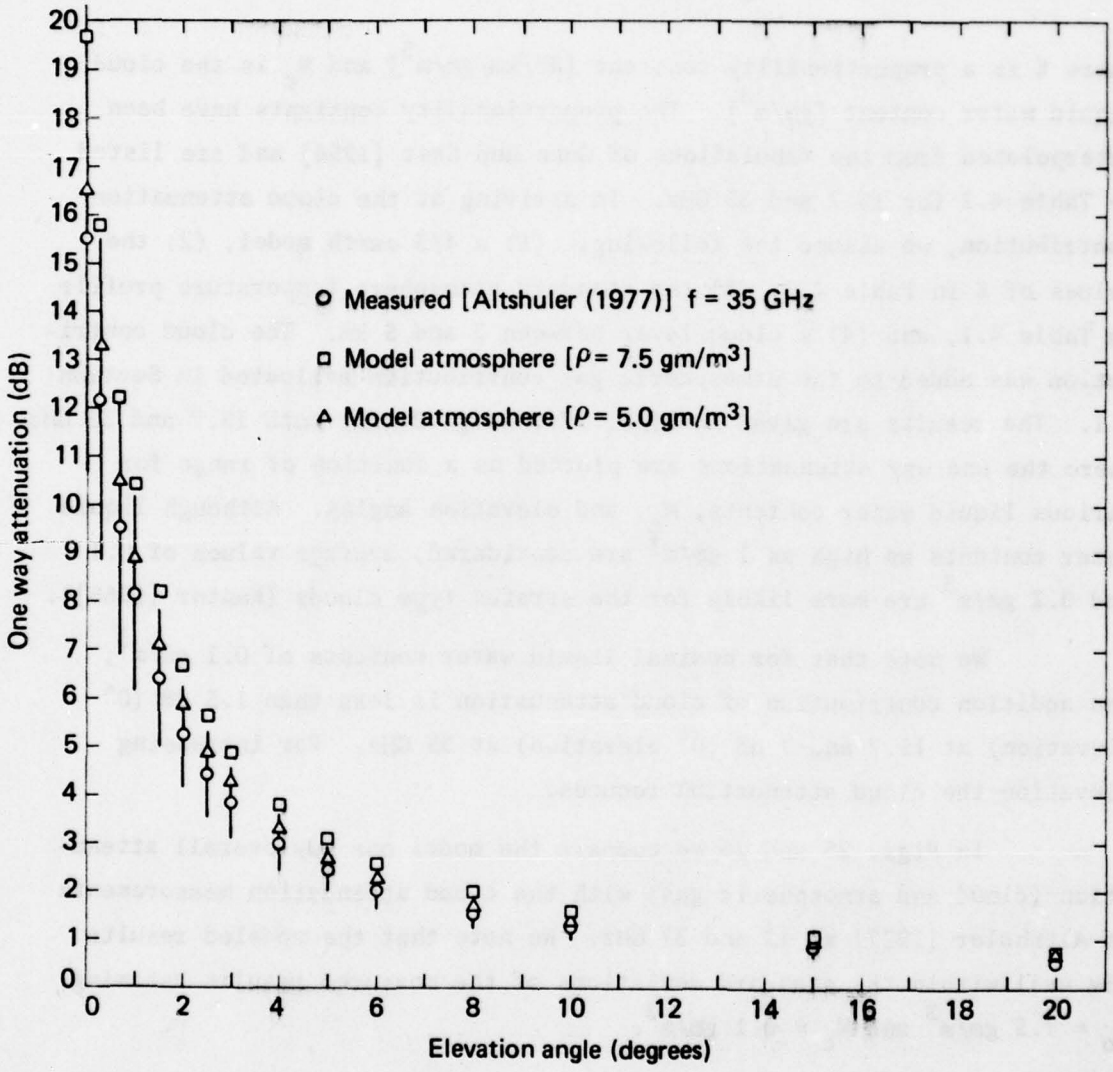

Figure 16. Measured one way atmospheric path attenuation by Altshuler [1977] as a function of elevation angle compared with model atmosphere attenuation at f = 35 GHz.

The attenuation coefficient due to cloud is given by,

$$k_c = K M_c \qquad [dB/km] \tag{4.11}$$

where K is a proportionality constant [$dB/km/gm/m^3$] and M_c is the cloud liquid water content [gm/m^3]. The proportionality constants have been interpolated from the tabulations of Gunn and East [1954] and are listed in Table 4.2 for 15.7 and 35 GHz. In arriving at the cloud attenuation contribution, we assume the following: (1) a 4/3 earth model, (2) the values of K in Table 4.2, (3) the standard atmosphere temperature profile in Table 4.1, and (4) a cloud layer between 3 and 5 km. The cloud contribution was added to the atmospheric gas contribution evaluated in section 4.1. The results are given in Figs. 17 through 24 for both 15.7 and 35 GHz where the one way attenuations are plotted as a function of range for various liquid water contents, M_c, and elevation angles. Although liquid water contents as high as 1 gm/m^3 are considered, average values of 0.1 and 0.2 gm/m^3 are more likely for the stratus type clouds (Kantor [1965]).

We note that for nominal liquid water contents of 0.1 gm/m^3, the addition contribution of cloud attenuation is less than 1.5 dB (0° elevation) at 15.7 and 7 dB (0° elevation) at 35 GHz. For increasing elevation the cloud attenuation reduces.

In Figs. 25 and 26 we compare the model one way overall attenuation (cloud and atmospheric gas) with the cloud attenuation measurements of Altshuler [1977] at 15 and 37 GHz. We note that the modeled results are well within the standard deviations of the measured results assuming $\rho_o = 7.5\ gm/m^3$ and $M_c = 0.1\ gm/m^3$.

4.3 Power Scattered from Cloud

We examine here the power scattered from cloud using a radar operating at 15.7 GHz. Starting with the radar equation (2.10), we assume the following radar parameters (suggested by RADC):

Table 4.2

INTERPOLATED VALUES OF k_c/M_c FROM GUNN AND EAST [1954]

Temperature °K	K(f = 15.7 GHz) (dB/km)/(gm/m^3)	K(f = 35 GHz) (dB/km)/(gm/m^3)
295	0.116	0.72
293	0.116	0.72
283	0.1605	0.74
273	0.237	1.05
265	0.303	1.35

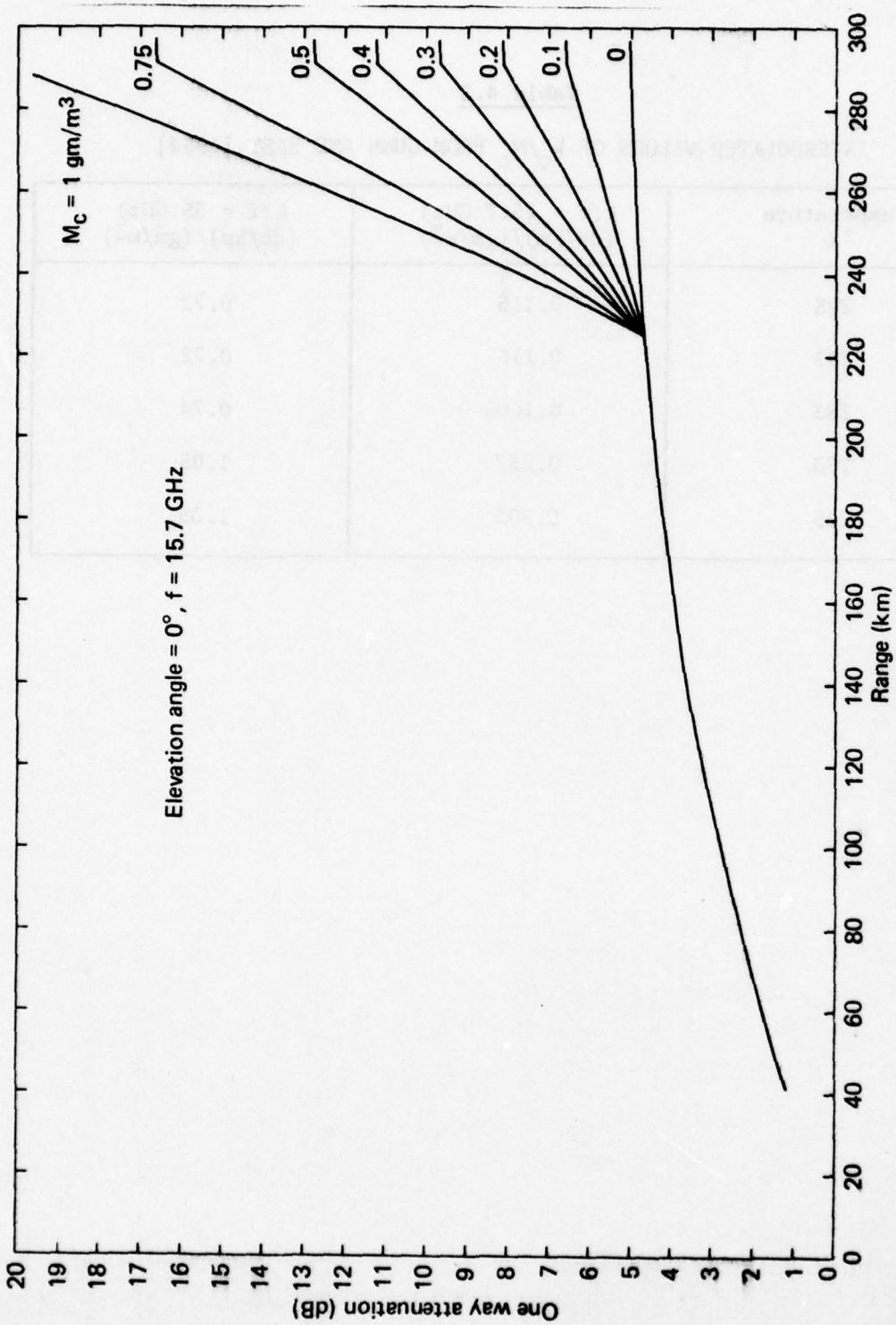

Figure 17. One way path attenuation as a function of range at f = 15.7 GHz, 0° elevation, for a given atmosphere and cloud model and variable cloud liquid water contents.

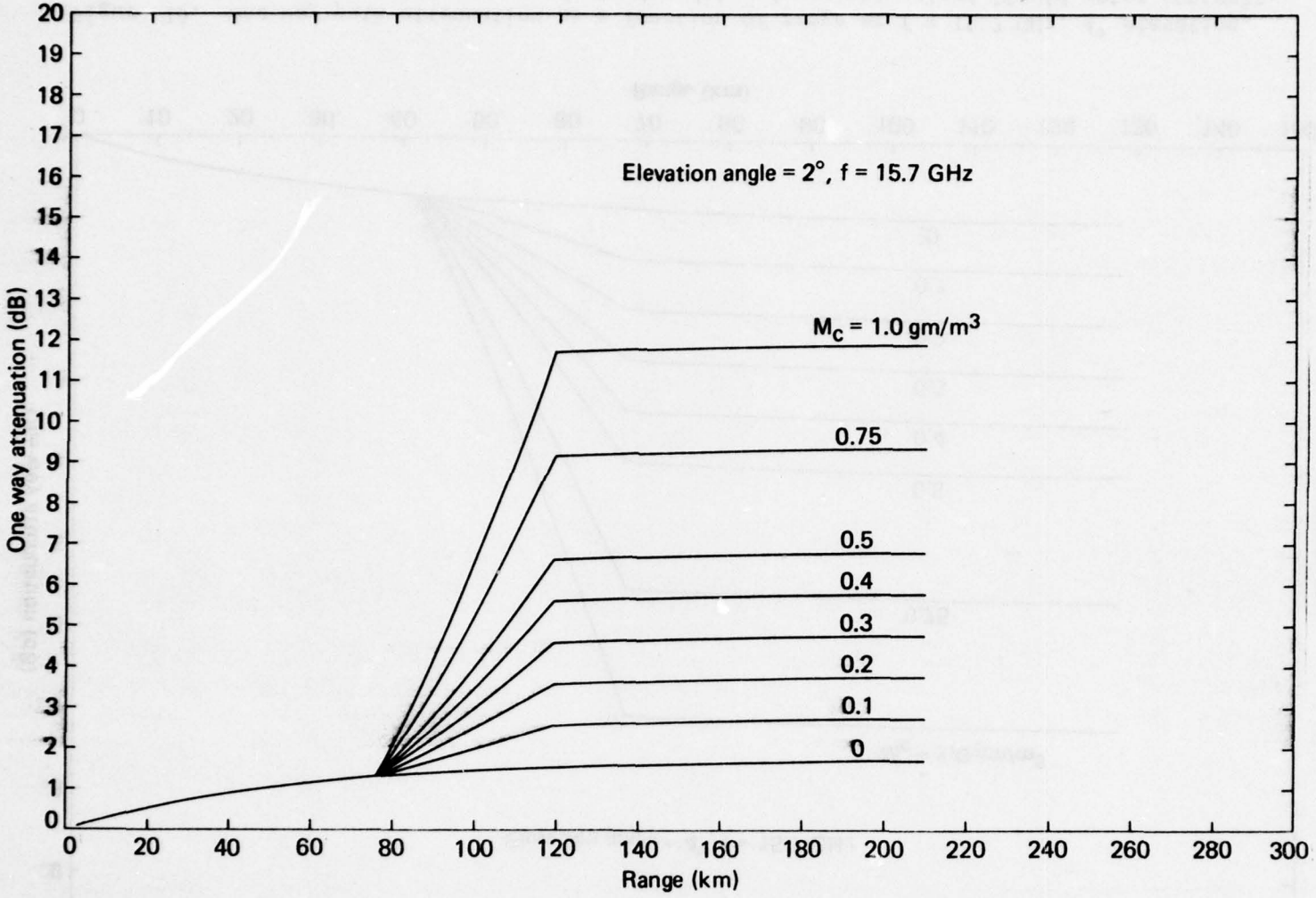

Figure 18. One way path attenuation as a function of range at f = 15.7 GHz, 2° elevation, for a given atmosphere and cloud model and variable cloud liquid water contents.

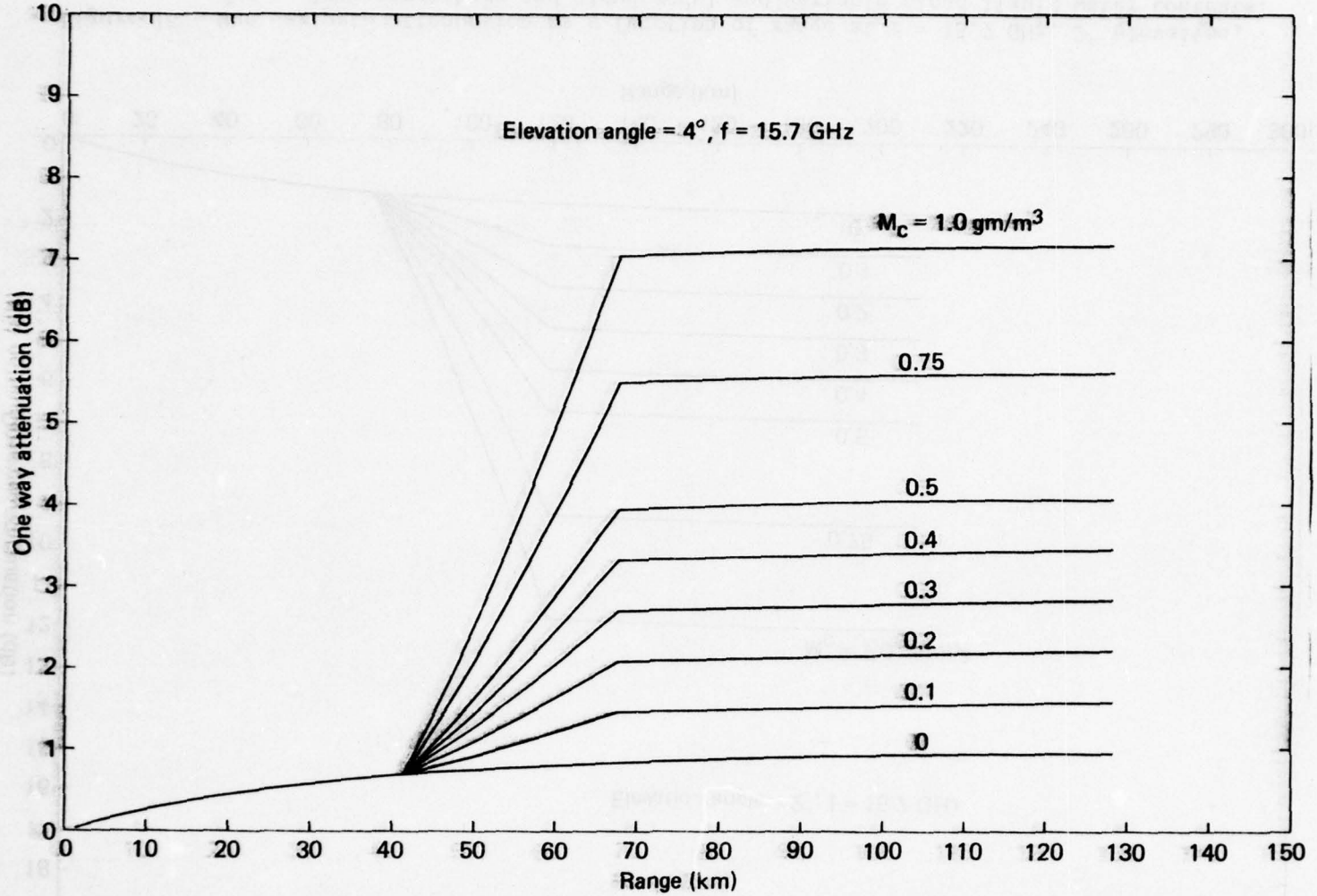

Figure 19. One way path attenuation as a function of range at f = 15.7 GHz, 4° elevation, for a given atmosphere and cloud model and variable cloud liquid water contents.

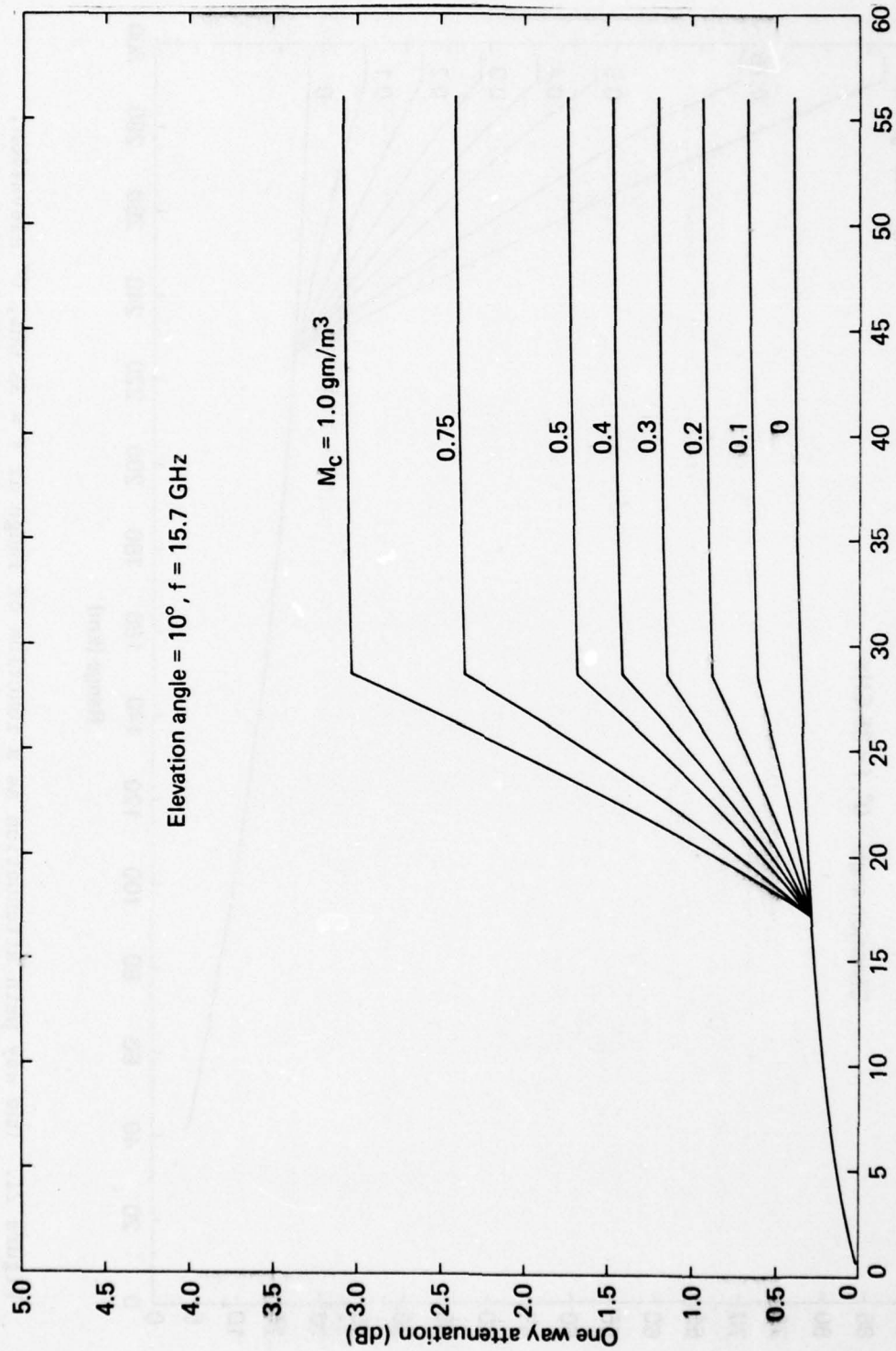

Figure 20. One way path attenuation as a function of range at f = 15.7 GHz, 10° elevation, for a given atmosphere and cloud model and variable cloud liquid water contents.

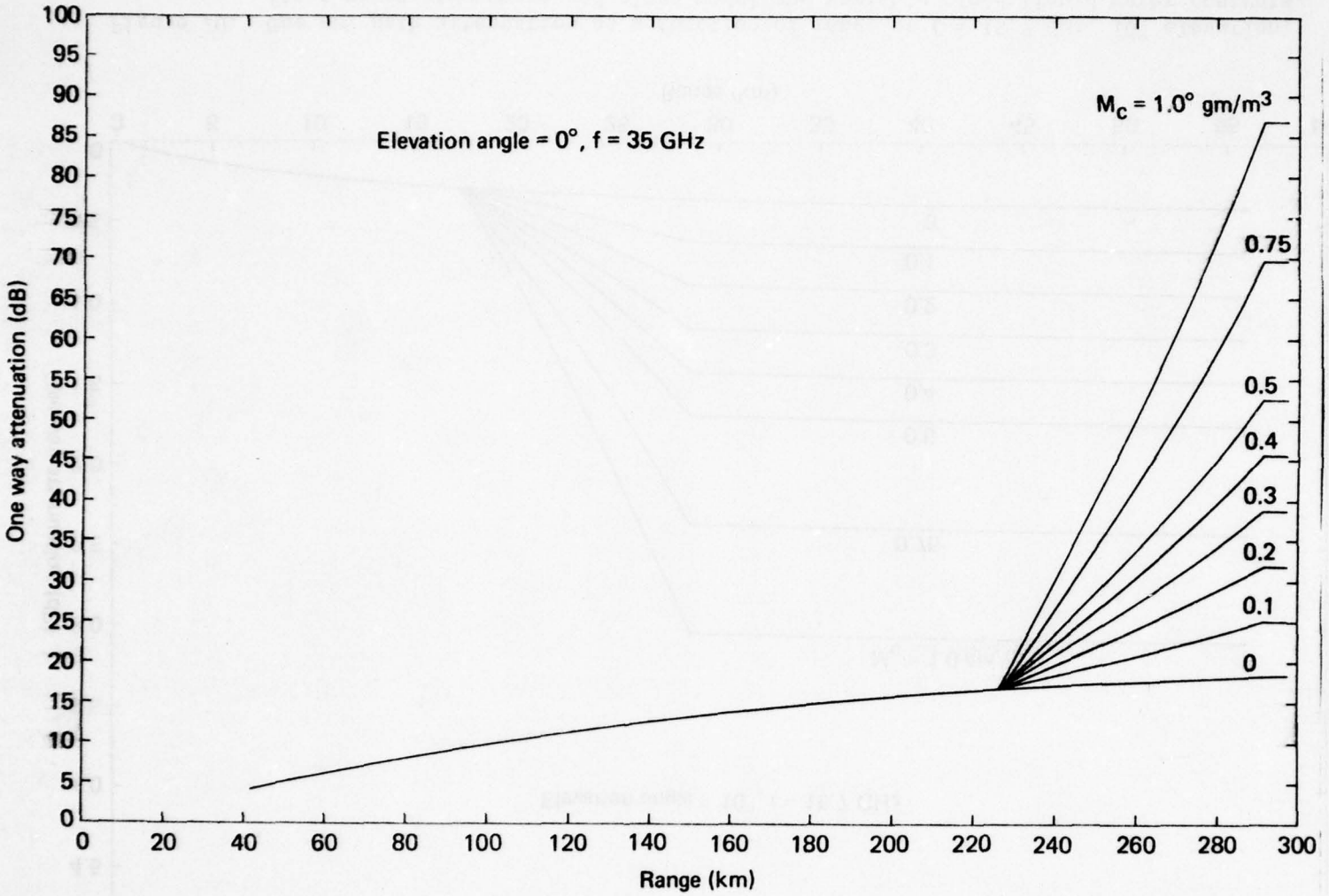

Figure 21. One way path attenuation as a function of range at f = 35 GHz, 0° elevation, for a given atmosphere and cloud model and variable cloud liquid water contents.

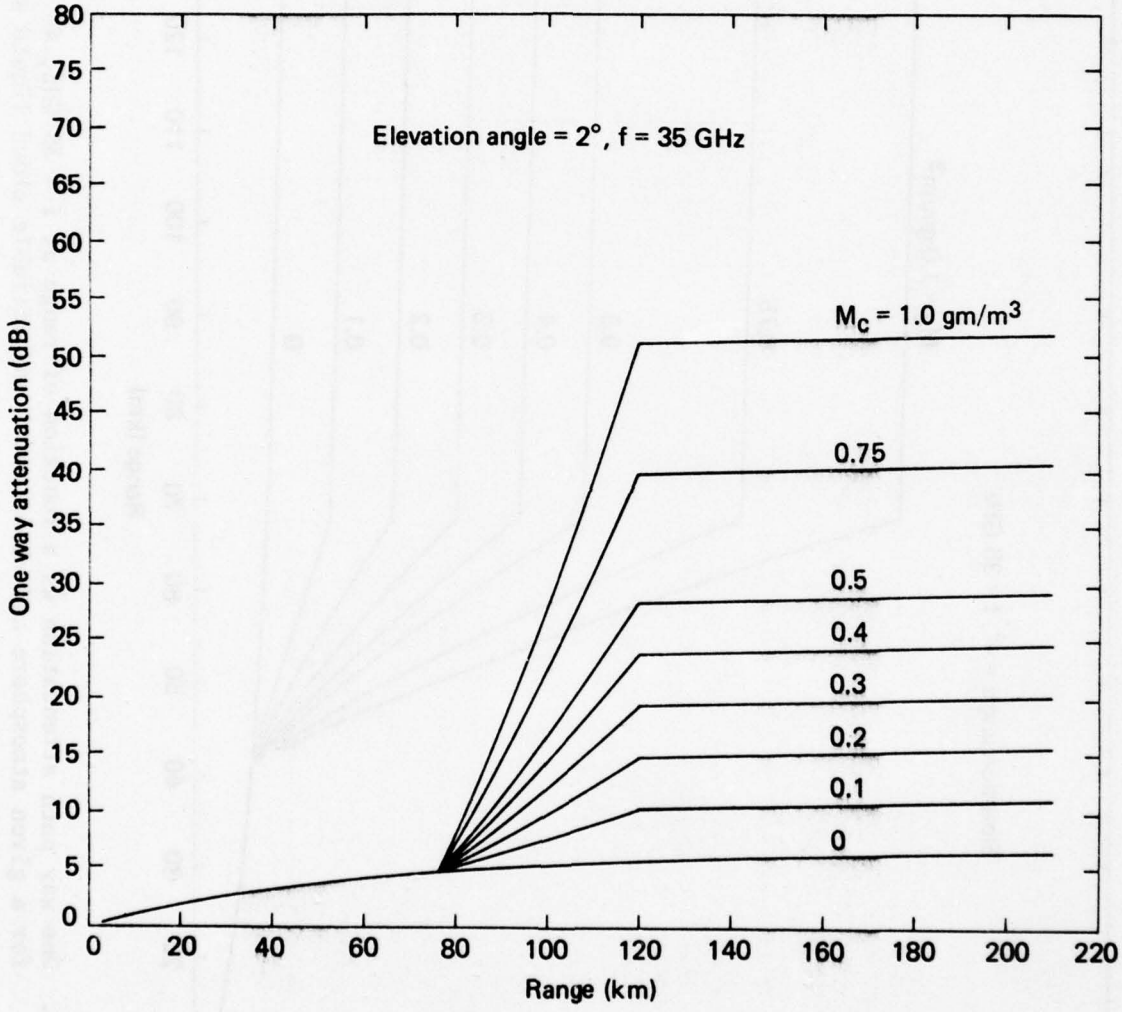

Figure 22. One way path attenuation as a function of range at f = 35 GHz, 2° elevation, for a given atmosphere and cloud model and variable cloud liquid water contents.

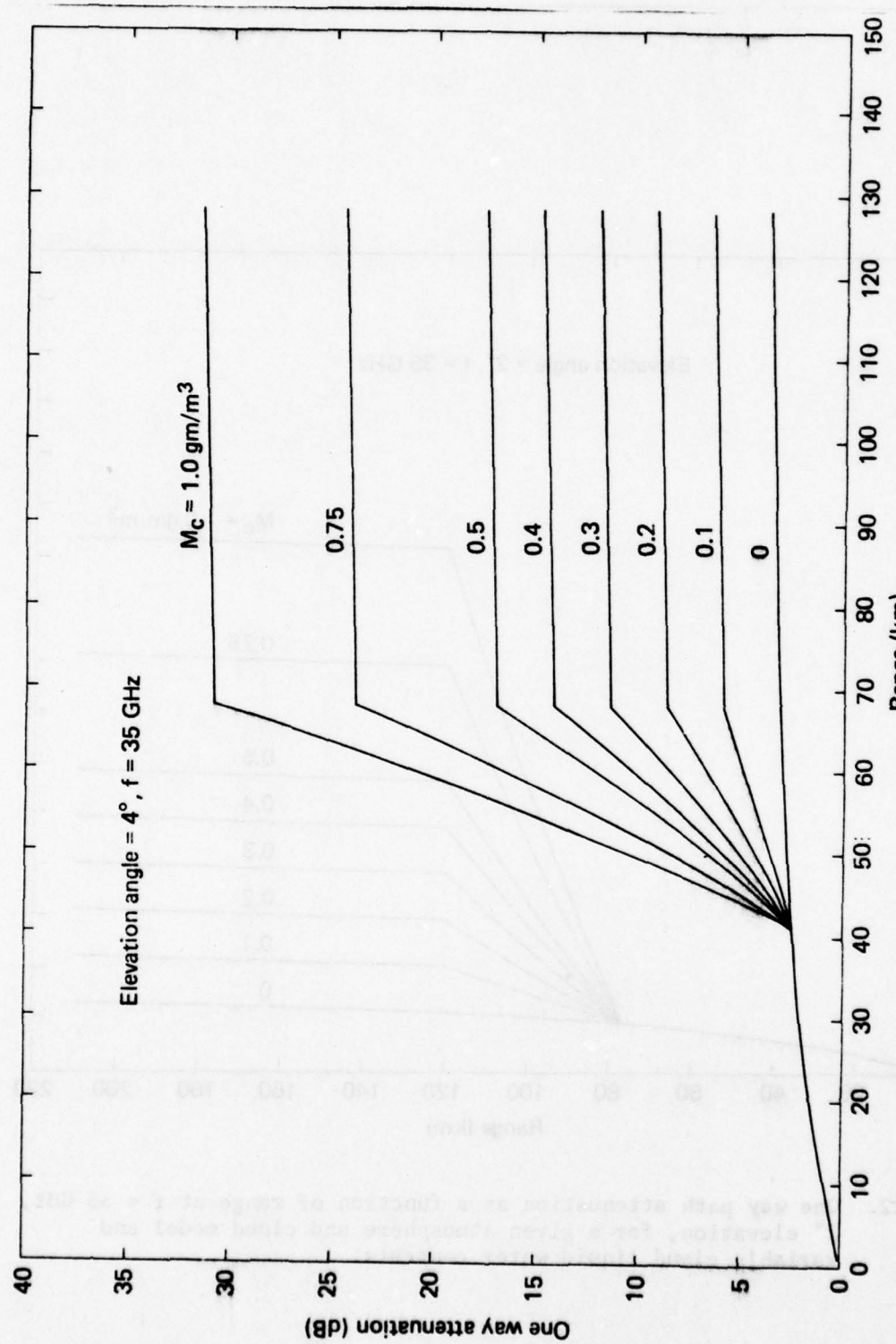

Figure 23. One way path attenuation as a function of range at f = 35 GHz, 4° elevation, for a given atmosphere and cloud model and variable cloud liquid water contents.

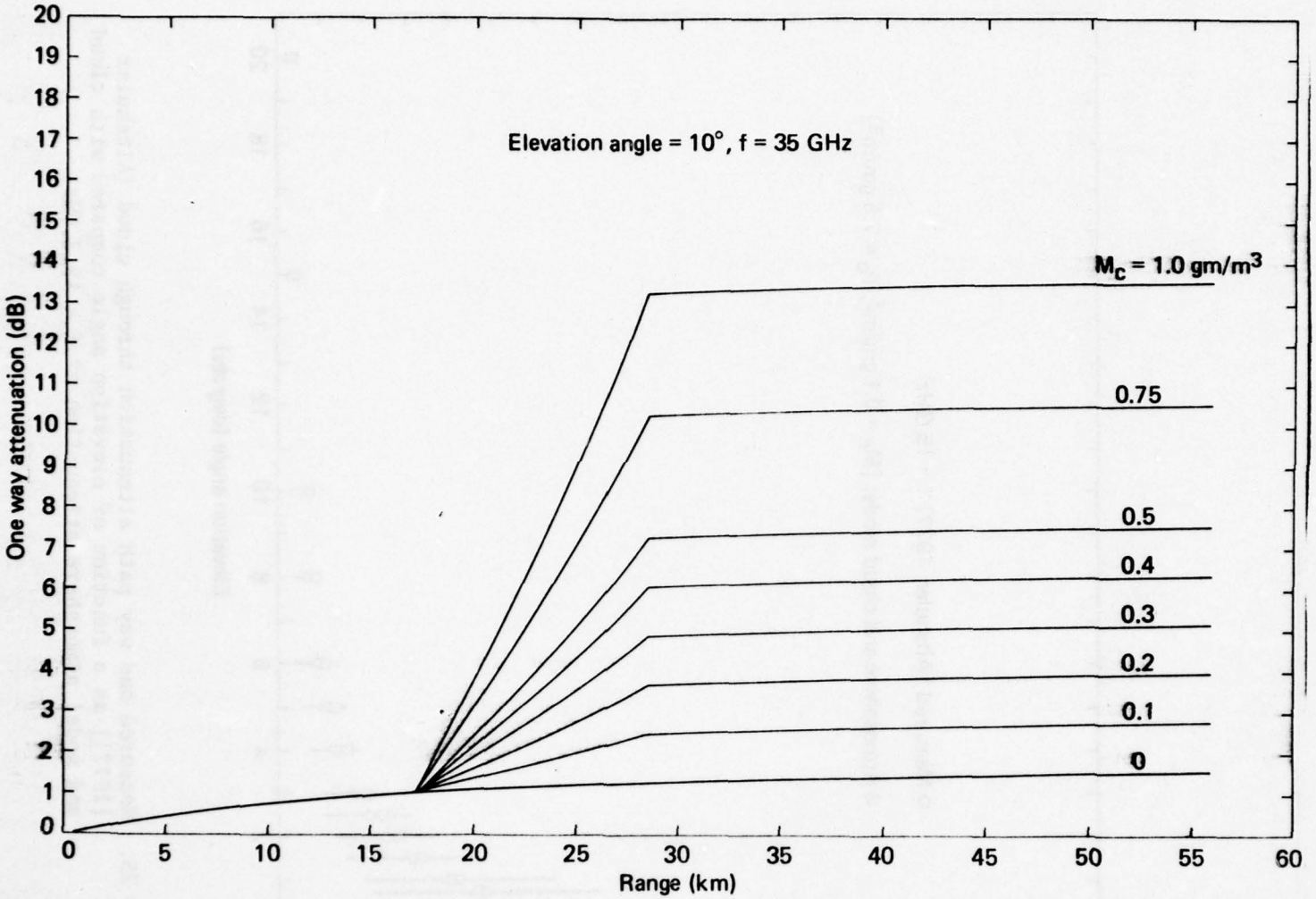

Figure 24. One way path attenuation as a function of range at f = 35 GHz, 10° elevation, for a given atmosphere and cloud model and variable cloud liquid water contents.

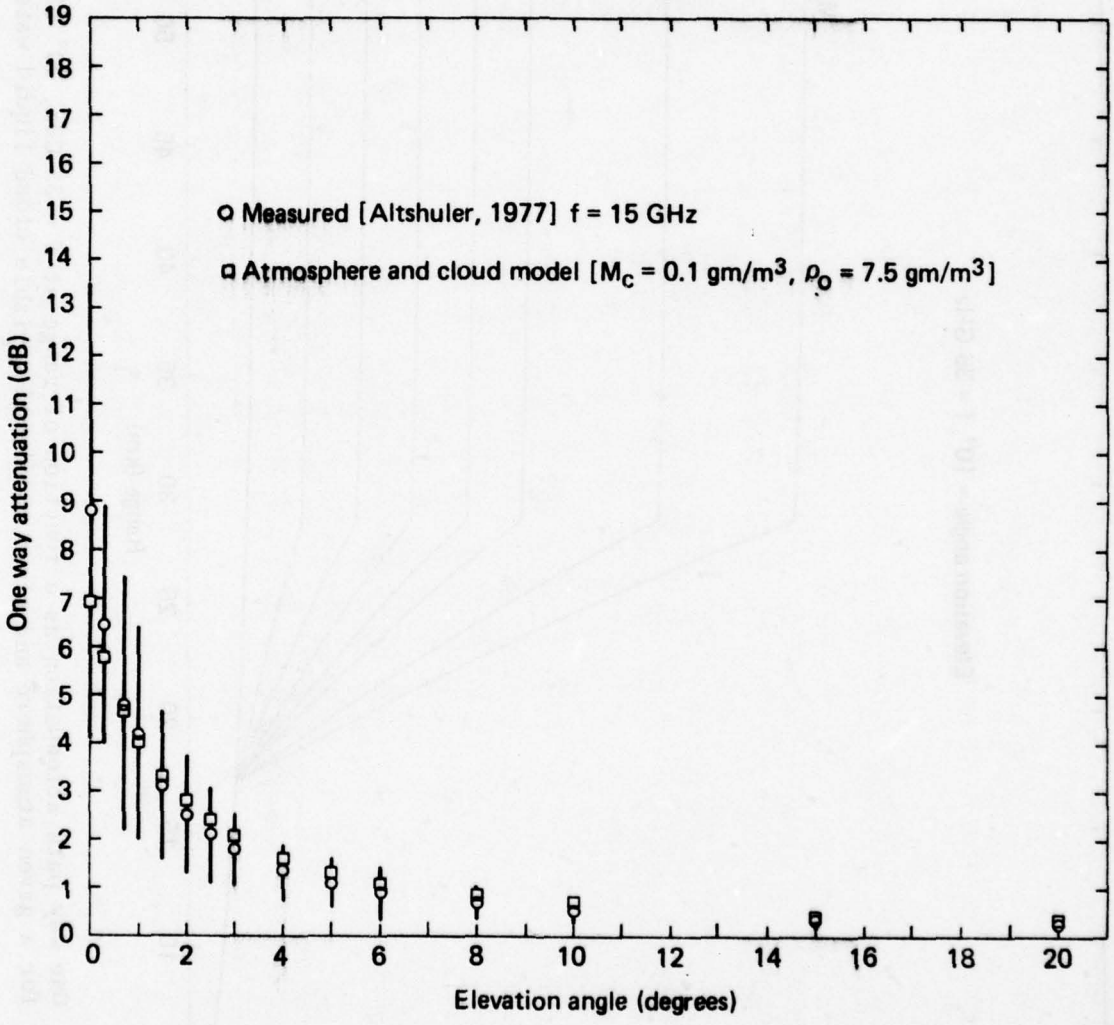

Figure 25. Measured one way path attenuation through cloud (Altshuler [1977]) as a function of elevation angle compared with cloud and model atmosphere attenuation at f = 15.7 GHz.

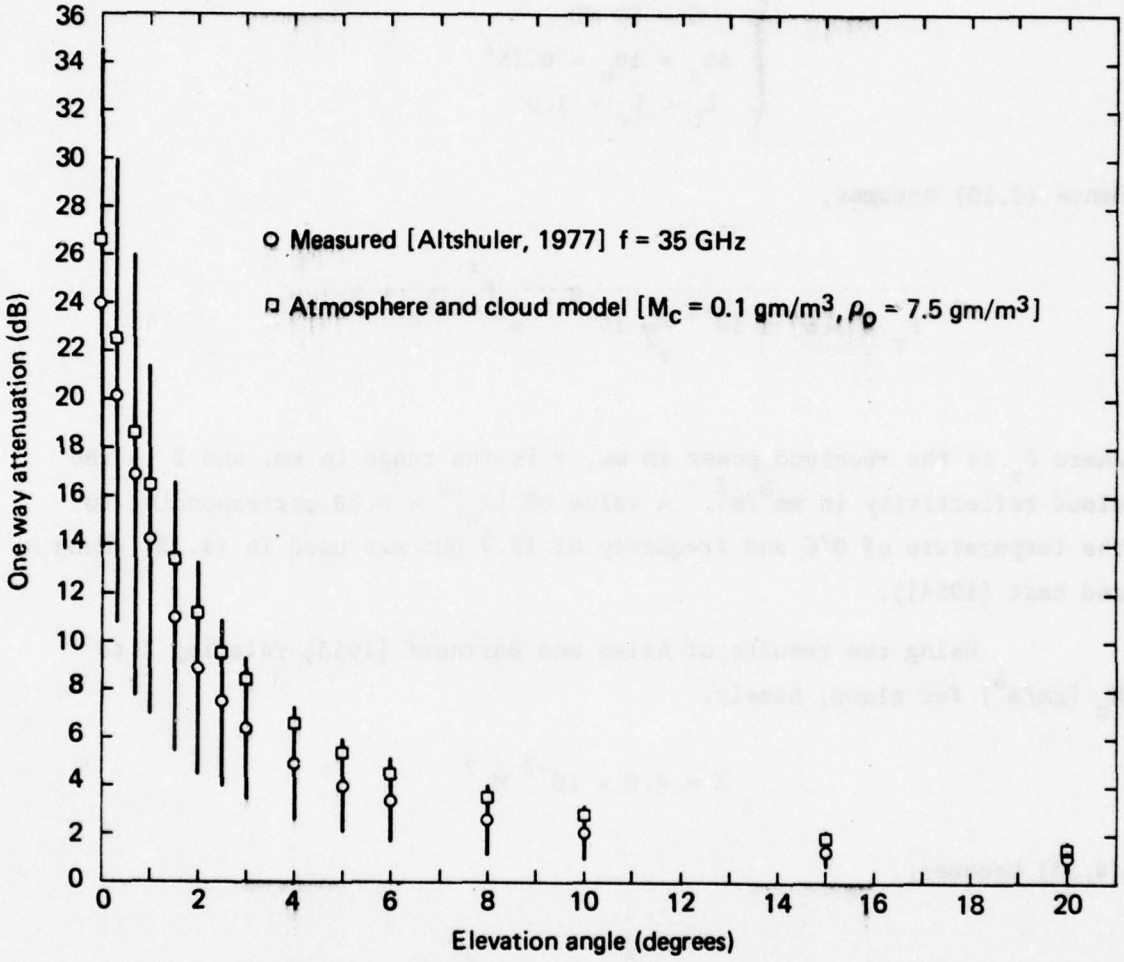

Figure 26. Measured one way path attenuation through cloud (Altshuler [1977]) as a function of elevation angle compared with cloud and model atmosphere attenuation at f = 35 GHz.

$$\begin{cases} \lambda = 1.91 \text{ cm} \\ P_t = 2 \times 10^3 \text{ watts} \\ \tau = .08 \ \mu\text{sec} \\ G = 60 \text{ dB} \\ \Delta\theta_e = \Delta\theta_h = 0.15^\circ \\ L_t = L_r = 1.0 \end{cases} \tag{4.12}$$

Hence (2.10) becomes,

$$P_r = 3.67 \times 10^{-8} \frac{Z}{r^2} 10^{-0.2 \int_o^r (k_g + k_c)dr} \tag{4.13}$$

where P_r is the received power in mw, r is the range in km, and Z is the cloud reflectivity in mm^6/m^3. A value of $|K_o|^2 = 0.92$ corresponding to the temperature of 0°C and frequency of 15.7 GHz was used in (4.13) (Gunn and East [1954]).

Using the results of Atlas and Bartnoff [1953] relating Z to M_c $[gm/m^3]$ for cloud; namely,

$$Z = 4.8 \times 10^{-2} M_c^2 \tag{4.14}$$

(4.13) becomes,

$$P_r = 1.76 \times 10^{-9} \frac{M_c^2}{r^2} 10^{-0.2 \int_o^r (k_g + k_c)dr} \tag{4.15}$$

Taking 10 Log_{10} of both sides of (4.15),

$$P_r(\text{dBm}) = -87.5 + 20 \text{ Log}_{10} M_c - 20 \text{ Log } r - 2 \int_o^r (k_g + k_c)dr \tag{4.16}$$

The received power as a function of range is plotted in Fig. 27 for various elevation angles and a cloud liquid water content of 0.2 gm/m^3. We note that for a receiver sensitivity of -145 dBm (suggested by RADC) cloud scatter can be detected at elevation angles equal to or greater than 2°. For M_c = 0.1 gm/m^3, all the curves shift down by 6 dB. For this latter case and for the same receiver sensitivity of -145 dBm, cloud at path angles greater than 4° are detectable.

It would thus appear that the 15.7 GHz radar with the given receiver sensitivity (-145 dBm) represents an excellent tool for measuring cloud liquid water content. At elevation angles greater than 2° and 4°, the two way total attenuation should be less than 6 and 4 dB (assuming the given cloud model and M_c = 0.2 gm/m^3) [Figs. 18 and 19]. The attenuation due to cloud itself is observed to be less than 4 and 2 dB.

4.4 Comparison of Scatter from Cloud Due to Refractive Index Variations

We examine here the possibility of confusion arising from scatter from irregularities of refractive index (i.e., clear air echoes). Under given assumptions of isotoropy, homogeneity, and eddy size dimensions, the reflectivity is given by (Tatarski [1964]),

$$\eta_{CA} = 39\, C_n^2\, \lambda^{-1/3} \qquad [m^{-1}] \tag{4.17}$$

where

C_n^2 = structure constant $[cm^{-2/3}]$
λ = wavelength [cm]

The reflectivity due to cloud scatter at f = 15.7 GHz corresponds to the Rayleigh expression,

$$\eta_{CL} = \left(\frac{\pi^5}{\lambda^4} |K_o|^2 Z\right) \times 10^{-10} \qquad [m^{-1}] \tag{4.18}$$

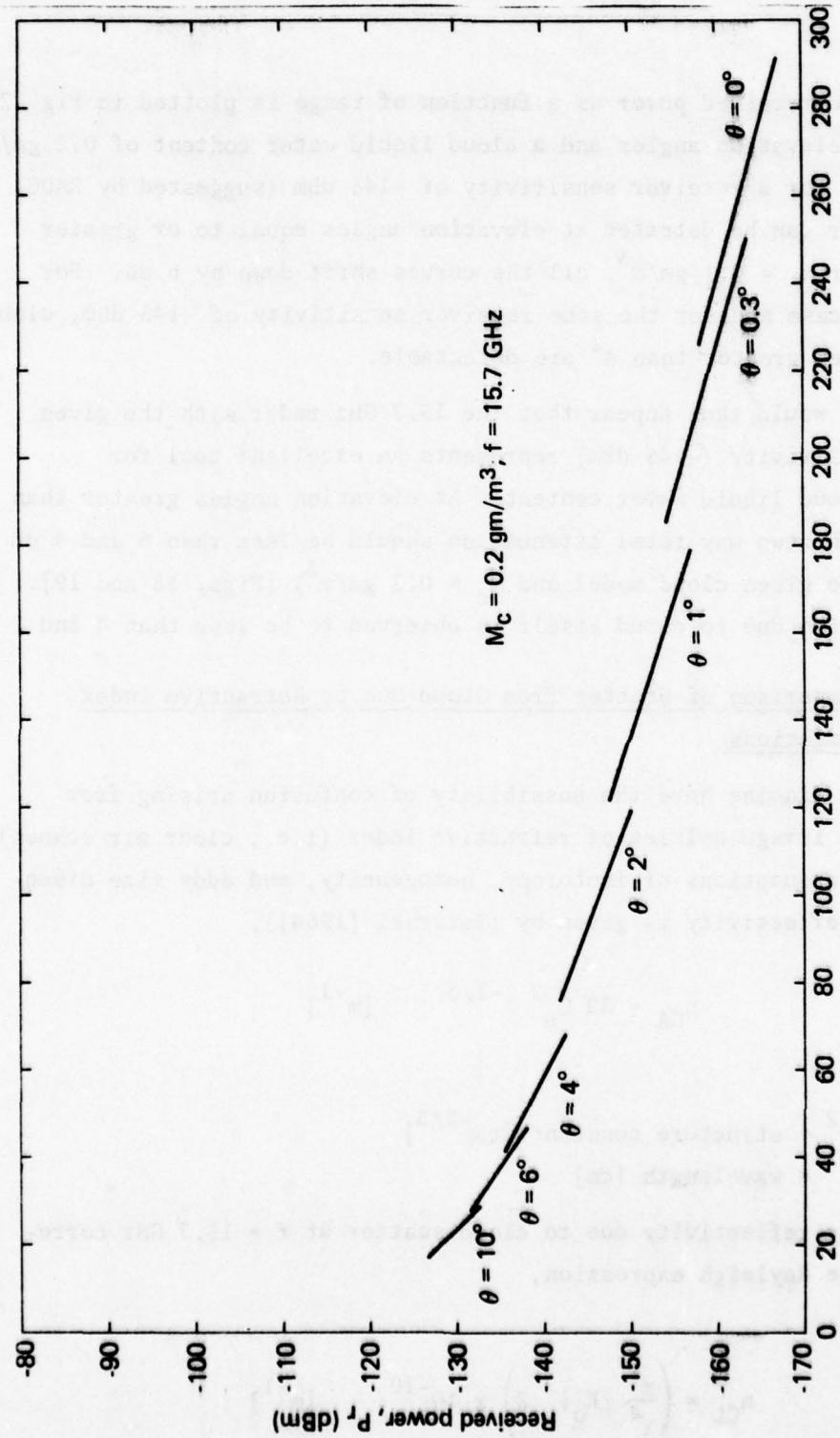

Figure 27. Received power from cloud scatter as a function of range for a given 15.7 GHz radar and cloud model at various elevation angles.

Injecting $|K_o|^2 = 0.92$ and (4.14) into (4.18) results in,

$$\eta_{CL} = 1.35 \times 10^{-9} M_c^2 \qquad [m^{-1}] \tag{4.19}$$

and dividing (4.19) by (4.17) gives,

$$\frac{\eta_{CL}}{\eta_{CA}} = 3.47 \times 10^{-11} \frac{M_c^2}{C_n^2 \lambda^{11/3}} \tag{4.20}$$

At f = 15.7 GHz (λ = 1.91 cm), (4.20) becomes,

$$\frac{\eta_{CL}}{\eta_{CA}} = 3.23 \times 10^{-12} \frac{M_c^2}{C_n^2} \tag{4.21}$$

In Fig. 28, the ratio (4.21) is plotted as a function of the structure constant for various values of M_c^2. We note that even for small values of M_c = 0.1 and 0.2 gm/m^3 and large values of $C_n^2 = 10^{-14}$ cm$^{-2/3}$ (Hardy and Katz [1969]) the reflectivity due to cloud exceeds that due to refractive index variations by a factor greater than 3 to 13, respectively. Hence little confusion should arise from the simultaneous existance of irregularities of refractive index imbedded in the cloud medium.

4.5 Extrapolation of Cloud Attenuation to Other Wavelengths

Assuming an estimate of the cloud liquid water content, M_c is arrived at using the 15.7 GHz radar, the cloud attenuation may be obtained at other wavelengths using,

$$k_c = K M_c \qquad [dB/km] \tag{4.22}$$

where K may be extracted from the plots of K versus frequency as given in Fig. 29 for various temperatures. The plots were taken from the data points of Gunn and East [1954].

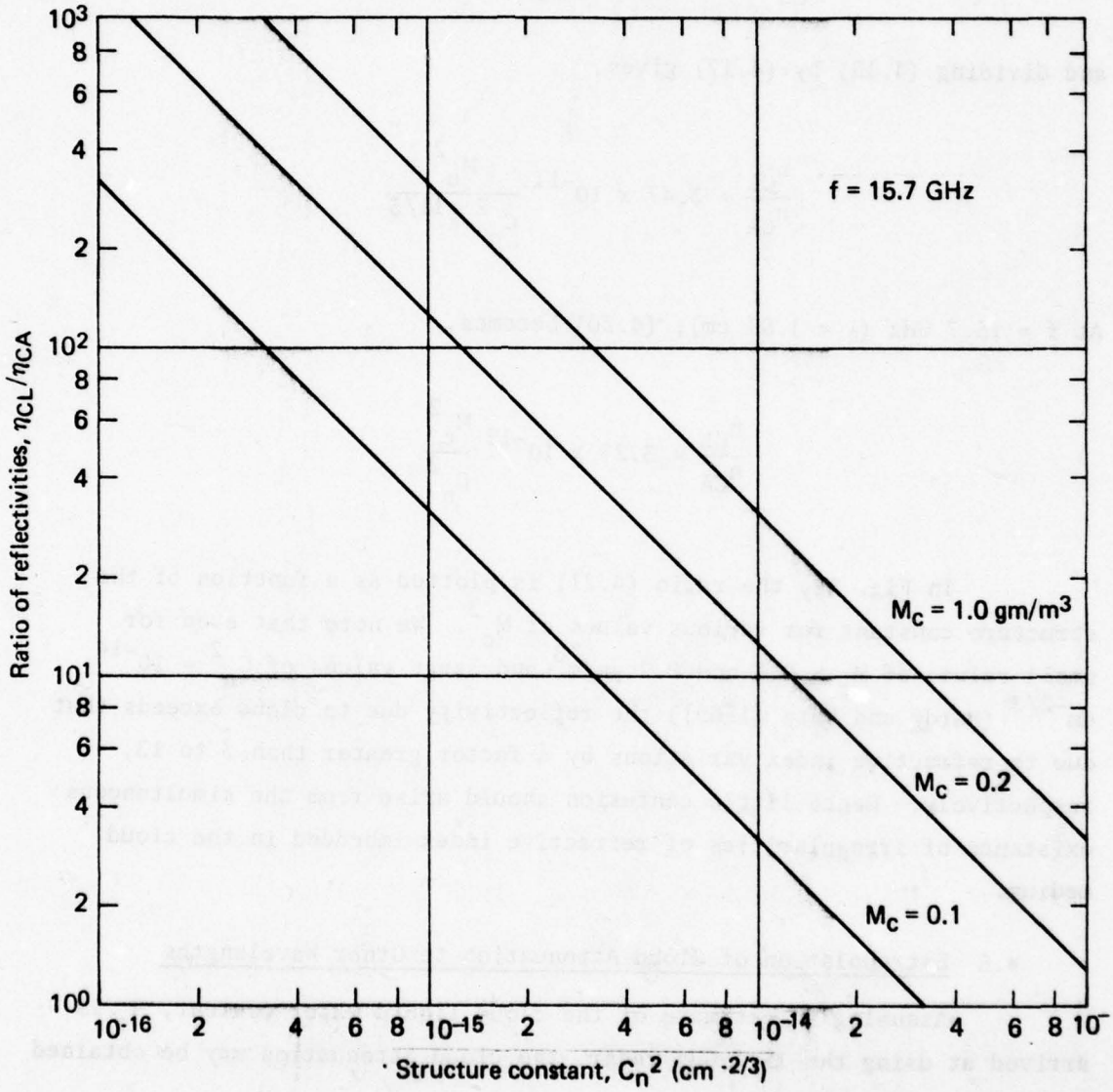

Figure 28. Ratio of cloud reflectivity to clear air irregularity reflectivity as a function of structure constant, C_n^2 and cloud liquid water content for f = 15.7 GHz.

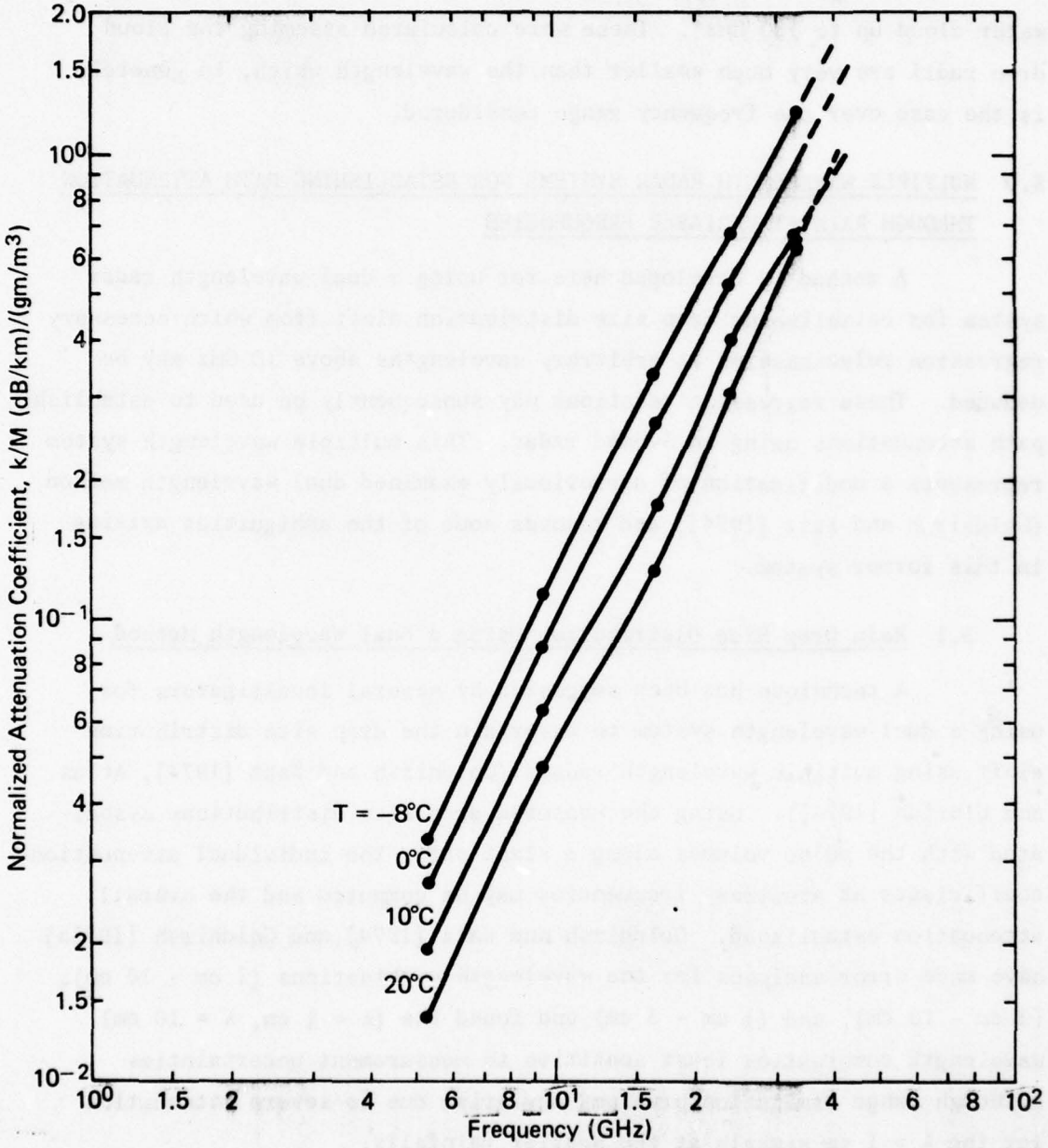

Figure 29. Normalized attenuation coefficient $K = k_c/M_c$ for water cloud as a function of frequency and temperature. (Data points taken from Gunn and East [1954].)

In Fig. 30 are plotted further theoretical values of K for water cloud up to 180 GHz*. These were calculated assuming the cloud drop radii are very much smaller than the wavelength which, in general, is the case over the frequency range considered.

5.0 MULTIPLE WAVELENGTH RADAR SYSTEMS FOR ESTABLISHING PATH ATTENUATION THROUGH RAIN AT VARIABLE FREQUENCIES

A method is developed here for using a dual wavelength radar system for establishing drop size distribution aloft from which necessary regression relationships at arbitrary wavelengths above 10 GHz may be deduced. These regression relations may subsequently be used to establish path attenuations using an S-band radar. This multiple wavelength system represents a modification of a previously examined dual wavelength method (Goldhirsh and Katz [1974]) and removes some of the ambiguities arising in this former system.

5.1 Rain Drop Size Distribution Using a Dual Wavelength Method

A technique has been suggested by several investigators for using a dual wavelength system to ascertain the drop size distribution aloft using multiple wavelength radars (Goldhirsh and Katz [1974], Atlas and Ulbrich [1974]). Using the measured drop size distributions associated with the pulse volumes along a slant path, the individual attenuation coefficients at arbitrary frequencies may be computed and the overall attenuation established. Goldhirsh and Katz [1974] and Goldhirsh [1975a] have made error analyses for the wavelength combinations (1 cm - 10 cm), (3 cm - 10 cm), and (1 cm - 3 cm) and found the (λ = 1 cm, λ = 10 cm) wavelength combination least sensitive to measurement uncertainties although range limitation problems may arise due to severe attenuation for the λ = 1 cm signals at the heavier rainfalls.

A distinct advantage of the dual wavelength technique is that no empirical relation of the form aZ^b needs to be assumed a priori. A

* Results are contained in CCIR Study Group Doc 2/181E, Doc. 5/161-E, 9 May 1977, Draft Report 234-3 (Rev. 76).

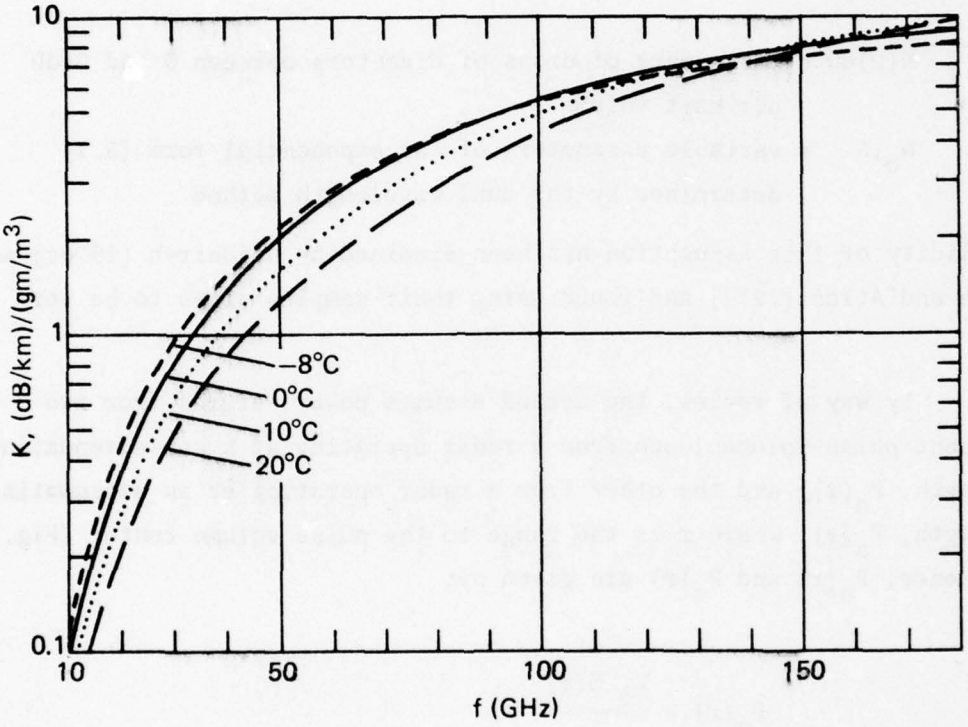

Figure 30. Theoretical values of $K = k_c/M_c$ for water cloud up to 180 GHz. These results are contained in CCIR Study Group Doc. 2/181-E, Doc. 5/161-E, 9 May 1977, Draft Report 234-3 (Rev. 76).

basic assumption in this method is that the drop size distribution possesses the general exponential form,

$$N(D)dD = N_o \exp(-\Lambda D)dD \tag{5.1}$$

where

$N(D)dD$ = the number of drops of diameters between D and D+dD per unit volume

N_o, Λ = variable parameters of the exponential form (5.1) determined by the dual wavelength method

The validity of this assumption has been examined by Goldhirsh [1976c] and Ulbrich and Atlas [1977] and found using their samples sizes to be very good.

By way of review, the method assumes power returns from two coincident pulse volumes; one from a radar operating at a non-attenuating wavelength, $P_o(r)$, and the other from a radar operating at an attenuating wavelength, $P_a(r)$, where r is the range to the pulse volume center (Fig. 31). Hence, $P_o(r)$ and $P_a(r)$ are given by,

$$P_o(r) = \frac{C_o Z(r)}{r^2} \tag{5.2}$$

$$P_a(r) = \frac{C_a \eta(r)}{r^2} 10^{-0.2 \int_o^r k\, dr} \tag{5.3}$$

where C_o and C_a are the appropriate radar constants, Z is the reflectivity factor, and η is the Mie reflectivity at the attenuating wavelength. We express the power return from the range, $r + \Delta$, in the same form as (5.3) and derive by straightforward methods the relation,

$$10 \log_{10}\left[\frac{r^2 P_a(r)}{(r+\Delta)^2 P_a(r+\Delta)}\right] = 10 \log_{10}\left[\frac{\eta(r)}{\eta(r+\Delta)}\right] + 2 \int_r^{r+\Delta} k\, dr \tag{5.4}$$

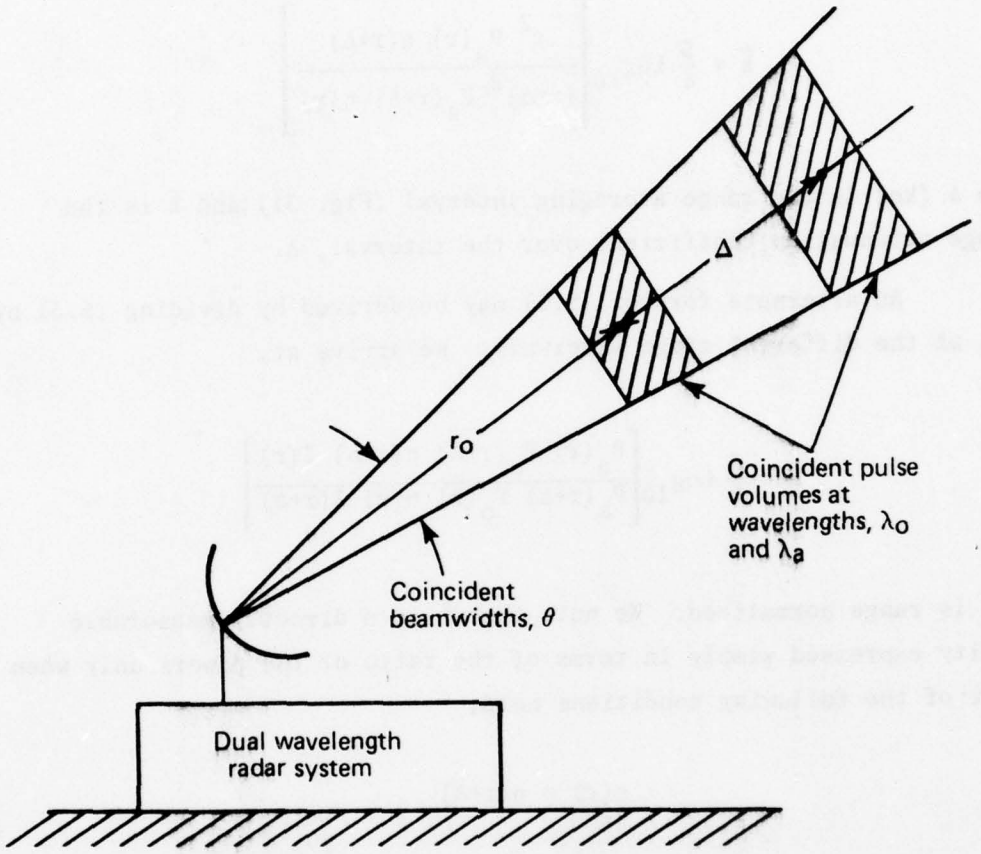

Figure 31. Geometrical configuration associated with the dual wavelength method for establishing drop size distributions.

from which,

$$\bar{k} = \frac{5}{\Delta} \text{Log}_{10}\left[\frac{r^2 P_a(r)\, \eta(r+\Delta)}{(r+\Delta)^2 P_a(r+\Delta)\, \eta(r)}\right] \tag{5.5}$$

where Δ [km] is the range averaging interval (Fig. 31) and $\bar{k}$ is the average attenuation coefficient over the interval, Δ.

An alternate form of (5.5) may be derived by dividing (5.3) by (5.2) at the different range intervals. We arrive at,

$$\bar{k} = \frac{5}{\Delta} \text{Log}_{10}\left[\frac{P_a(r)\, P_o(r+\Delta)\, \eta(r+\Delta)\, Z(r)}{P_a(r+\Delta)\, P_o(r)\, \eta(r)\, Z(r+\Delta)}\right] \tag{5.6}$$

which is range normalized. We note that $\bar{k}$ is a directly measurable quantity expressed simply in terms of the ratio of the powers only when either of the following conditions hold,

$$\eta(r) = \eta(r+\Delta) \tag{5.7}$$

or

$$\frac{\eta(r+\Delta)}{\eta(r)} \simeq \frac{Z(r+\Delta)}{Z(r)} \tag{5.8}$$

The equality (5.7) implies the rain is uniform at the range bins centered at r and r+Δ, although it may be non-uniform in the intervening bins. An examination of the validity of this equality at various wavelengths and rain rate combinations will be examined shortly.

Considering (5.2), the average reflectivity factor, $\bar{Z}$, over the range interval, Δ, is given by,

$$\bar{Z} = \frac{1}{C_o\, \Delta} \int_r^{r+\Delta} r^2 P_o(r)\, dr \tag{5.9}$$

The reflectivity factor, $\bar{Z}$, and attenuation coefficient, $\bar{k}$, may be expressed theoretically by,

$$\bar{Z} = N_o \int_{D_{min}}^{D_{max}} D^6 \exp(-\Lambda D) dD \tag{5.10}$$

$$\bar{k} = N_o \int_{D_{min}}^{D_{max}} C_{ext}(D) \exp(-\Lambda D) dD \tag{5.11}$$

where the exponential drop size distribution form given by (5.1) is assumed in the general forms, (2.28) and (2.29). In the above equations, D_{min}, D_{max} are minimum and maximum drop size diameters of the distribution (e.g., .03 and 0.5 cm, respectively).

If the conditions (5.7) or (5.8) are valid, $\bar{Z}$ and $\bar{k}$ in (5.10) and (5.11) are radar measurable quantities and those equations have the unknowns N_o and Λ which may be solved numerically. Hence an equivalent exponential distribution having associated with it a unique pair of values, (N_o, Λ) may be established for the interval, Δ. The attenuation coefficient, k_i, at any other wavelength may be calculated from (5.11) for each interval, Δ_i, and the integrated one way attenuation obtained using,

$$A = \sum_{i=1}^{n} \bar{k}_i \Delta_i \tag{5.12}$$

where n represents the total number of path intervals, Δ.

5.1.1 Errors Due to Inhomogeneous Rain Rates

We examine here the error in $\bar{k}$ due to inhomogeneous rain rates along the path. This error arises when (5.8) is assumed in (5.6) and $\bar{k}$

is expressed simply in terms of a ratio of received powers. In Fig. 32, the Mie reflectivity [m^{-1}] is plotted as a function of rain rate for X-band (10 GHz), K_u-band (15.7 GHz), and K_a-band (35 GHz). These curves were deduced from Haddock [1956] who assumed a Laws and Parsons distribution. Also plotted is the Rayleigh reflectivity at 3 GHz as a function of rain rate arrived at using (2.9) and $Z = 200\ R^{1.6}$.

Using the reflectivity results in Fig. 32, the attenuation coefficient error defined as,

$$\delta\bar{k} = \frac{5}{\Delta} \text{Log}_{10}\left[\frac{\eta(r+\Delta)\ Z(r)}{\eta(r)\ Z(r+\Delta)}\right] \tag{5.13}$$

is tabulated in the form $2\Delta\ \delta\bar{k}$ in Table 5.1 for various rain rate combinations at r and $r+\Delta$. Also tabulated are the values of $\bar{k}$ averaged over the indicated rain rates for the various frequencies. In arriving at these averages, the attenuation coefficient versus rain rate relations were obtained by interpolating the tabulations of Medhurst [1965]. These results are plotted in Fig. 33. In the averaging process, an exponential variation of rain rate with range over the interval, Δ, was assumed. In Table 5.2 are tabulated the corresponding percentage errors, $\delta\bar{k}/\bar{k} \times 100$, for the various rain rate intervals and frequency combinations. In these tabulations it is assumed $2\Delta = 1$ km. For other intervals Δ, the indicated error values should be divided by 2Δ. For example, for $\Delta = 0.15$ km, the errors in estimating $\bar{k}$ (from Table 5.2) in the rain rate interval 40 to 80 mm/hr is 97.9%, 56.9%, and 51.6% for the X-S, K_u-S, and K_a-S band cases, respectively (i.e., $\frac{1}{2\Delta} = 3.33$ times the corresponding values in Table 5.2). We note that although the attenuation errors $\delta\bar{k}$ are smallest at X-band, the percentage errors are largest.

The above results hence give sound notions as to the magnitude of errors that may be introduced in $\bar{k}$ for the various wavelength combinations due to the assumption (5.8). These may translate into sizeable errors in the estimation of drop size distribution and ultimately in attenuation coefficient at other wavelengths (see, for example, Goldhirsh and Katz [1974] and Goldhirsh [1975]).

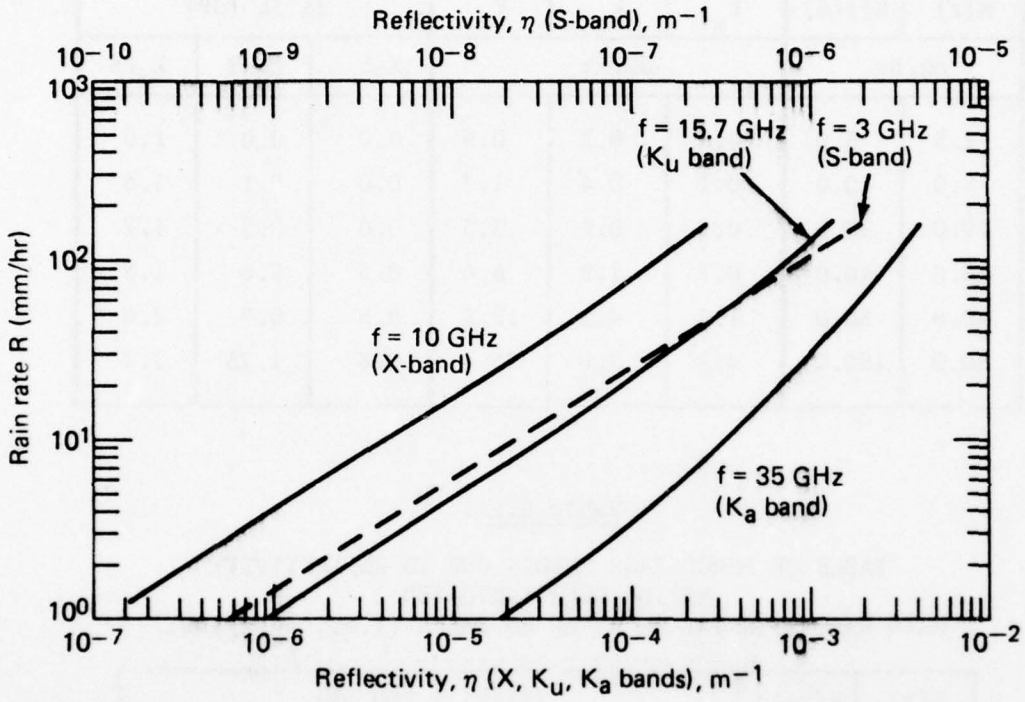

Figure 32. Mie reflectivity as a function of rain rate for X-band (10 GHz), K_u-band (15.7 GHz), and K_a-band (35 GHz) assuming a Laws and Parsons distribution. Also plotted is the S-band (3 GHz) Rayleigh reflectivity.

Table 5.1

TABLE OF VALUES OF $\bar{k}$ AVERAGED OVER THE INDICATED RAIN RATE INTERVALS AND ASSOCIATED REFLECTIVITY RATIO ERRORS, $2\Delta\ \delta\bar{k}$. (x = 10 GHz, u = 15.7 GHz, a = 35 GHz)

R(r)	R(r+Δ)	$\bar{k}_x$	$\bar{k}_u$	$\bar{k}_a$	$2\Delta\ \delta\bar{k}$ (dB)		
mm/hr		dB/km			X-S	K_u-S	K_a-S
2.5	5.0	0.0	0.2	0.9	0.0	0.0	1.0
5.0	10.0	0.1	0.4	1.7	0.0	0.1	1.6
10.0	20.0	0.3	0.9	3.3	0.0	0.5	1.7
20.0	40.0	0.7	1.9	6.6	0.3	0.6	1.8
40.0	80.0	1.7	4.1	12.9	0.5	0.7	2.0
80.0	160.0	4.2	9.0	25.4	0.8	1.25	2.4

Table 5.2

TABLE OF PERCENTAGE ERRORS DUE TO REFLECTIVITY RATIOS OVER INDICATED RAIN RATE INTERVAL ON A PER km BASIS (i.e., $\frac{\delta\bar{k}}{\bar{k}} \times 100$).

R(r)	R(r+Δ)	(δk/k) x 100 (%)		
mm/hr		X-S (10-3 GHz)	K_u-S (15.7-3 GHz)	K_a-S (35-3 GHz)
2.5	5	--	--	111.1
5	10	--	25.0	94.1
10	20	--	55.5	51.5
20	40	42.8	31.6	27.3
40	80	29.4	17.1	15.5
80	160	19.0	13.9	9.5

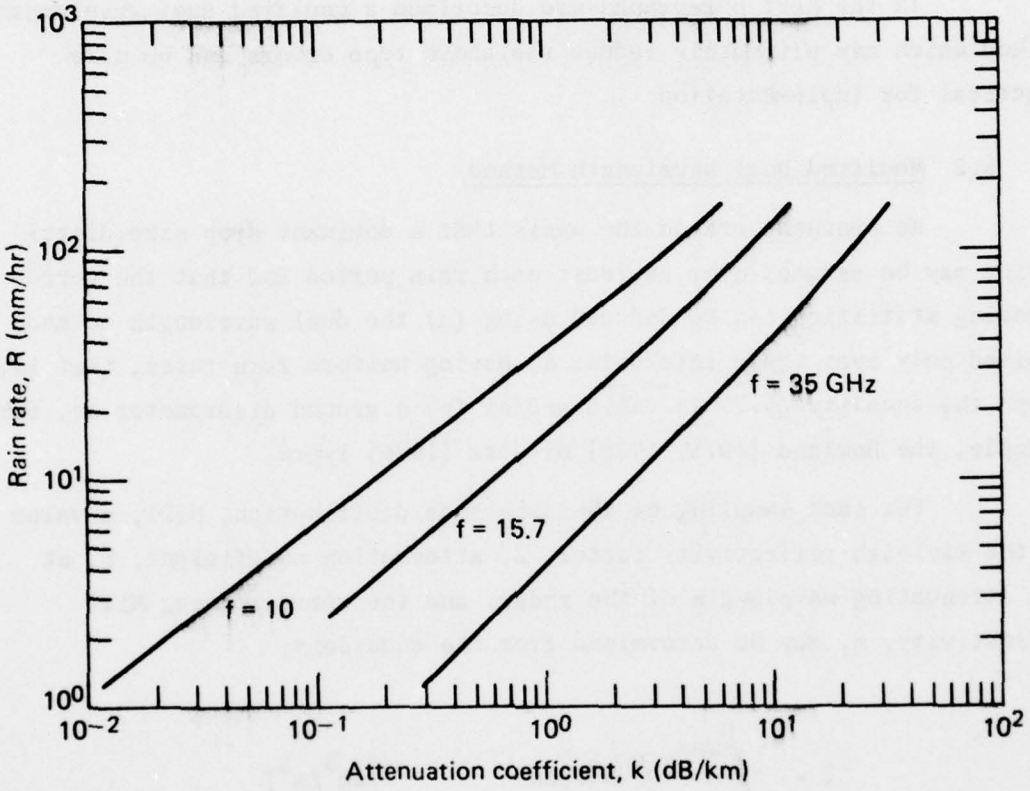

Figure 33. Attenuation coefficient as a function of rain rate for 10, 15.7, and 35 GHz assuming the Laws and Parsons drop size distribution. Curves were plotted by interpolating the tabulations of Medhurst [1965].

It may be noted that the errors due to the assumption (5.7) in presence of inhomogeneous rain rates have not been considered here as they are more severe than those arising from the assumption (5.8).

In the next paragraphs are described a modified dual wavelength method which may ultimately reduce the above type errors and be more practical for implementation.

5.2 Modified Dual Wavelength Method

We proceed here on the basis that a dominant drop size distribution may be assumed over at least each rain period and that the corresponding statistics can be deduced using (a) the dual wavelength method applied only over those intervals, Δ, having uniform rain rates; that is, where the equality (5.7) is valid and/or (b) a ground disdrometer as, for example, the Rowland [1975, 1976] or Joss [1976] types.

For each sampling of the drop size distribution, N(D), a value of the Rayleigh reflectivity factor, Z, attenuation coefficient, k, at the attenuating wavelength of the radar, and the corresponding Mie reflectivity, η, may be determined from the equations,

$$Z = \int_{D_{min}}^{D_{max}} D^6 \, N(D) dD \qquad [mm^6/m^3] \qquad (5.14)$$

$$k = \int_{D_{min}}^{D_{max}} C_{ext}(D) \, N(D) dD \qquad [dB/km] \qquad (5.15)$$

$$\eta = \int_{D_{min}}^{D_{max}} \sigma(D) \, N(D) dD \qquad [m^{-1}] \qquad (5.16)$$

where all of the above parameters have been previously defined except $\sigma(D)$ which represents the Mie scattering cross section [m^2] and is

dependent upon drop diameter, wavelength, and refractive index. This quantity has, for example, been tabulated by Stephens [1961] as a function of drop diameter for a series of wavelengths.

With k, Z, and η calculated for each drop size distribution, k-Z and η-Z scatter diagrams may be arrived at from which best fit regression relations of the form,

$$k = a\, Z^{b} \tag{5.17}$$

$$\eta = A\, Z^{B} \tag{5.18}$$

The next step in the modified dual wavelength method is to check (5.17) and (5.18) against the attenuating wavelength measurement (5.4) in all regions of rain including those intervals, Δ, where the rain is non-uniform. This may be referred to as the drop size distribution "truth" measurement phase of the method. Hence substituting (5.17) and (5.18) into (5.4) we obtain for the ratio of powers at the attenuating wavelength,

$$10\ \mathrm{Log}_{10}\left[\frac{r^2\, P_a(r)}{(r+\Delta)^2\, P_a(r+\Delta)}\right] = 10\ B\ \mathrm{Log}_{10}\left[\frac{Z(r)}{Z(r+\Delta)}\right] + 2a \int_{r}^{r+\Delta} Z^{b}\, dr \tag{5.19}$$

The right hand side (RHS) of (5.19) may be obtained from the S-band measurement of Z(r) and a straightforward calculation. The left hand side (LHS) is arrived at through a relative power measurement at the attenuating wavelength. Comparison of the LHS and RHS of (5.19) in both range and time enables one to check the validity of using (5.17) and (5.18) obtained from the original drop size distribution. It is, of course, not reasonable to expect a one-to-one check for all ranges and times. However, if a dominant drop size distribution does exist, then the check should at least show statistically good results. The LHS of (5.19) represents a relative measurement and therefore could be acquired

with good accuracy (e.g., 0.5 dB uncertainty). The RHS could be in error due to the variances associated with a, b, A, and B or due to the uncertainty in the measurement, Z, which requires an absolute calibration. In the event the RHS systematically underestimates or overestimates the LHS, the DSD may be adjusted such that the RHS produces a better check for the revised empirical parameters. A technique for taking out the uncertainty in k is described in Section 5.3.3.

Once confidence in the proper distribution is established through repeated checks using (5.19), only the S-band radar need be used and the reflectivity profile, Z(r), established. The attenuation at any other wavelength is merely,

$$A = \int_0^{\ell} a\, Z^b(r)\, dr \qquad [dB] \tag{5.20}$$

where a and b at other wavelengths are derived through scattergrams of k versus Z computed using the original (or corrected) drop size distribution data base.

In summary, the steps involved in using the modified dual wavelength method are:

(1) Measure the power scattered from rain at both S-band (3 GHz) and either K_u-band (15.7 GHz) or K_a-band (35 GHz) (the latter representing a preferable wavelength) using coincident beams.

(2) Over range intervals, Δ, only where the reflectivities are uniform, the dual wavelength method should be implemented and samples of N(D) acquired. If possible, ground measurements of DSD should also be obtained with disdrometers.

(3) Using the measured samples of DSD, Z, k, and η as given by (5.14), (5.15), and (5.16), respectively, should be calculated; k and η correspond to the attenuating wavelength of the radar.

(4) From the results of (3), scatter diagrams of log k and log η versus log Z may be plotted and best fit empirical relations (5.17) and (5.18) at the attenuating wavelength of the radar may be determined.

(5) The empirical parameters, a, b, and B and the S-band reflectivity levels Z(r) may now be injected in the RHS of (5.19) and checked against the relative power measurements of the attenuating wavelength radar [LHS of (5.19)] for all rain rate ranges.

(6) If the LHS under- or overestimates the RHS, equivalence of the two sides may be achieved by methods described in Section 5.3.3.

(7) With the RHS and LHS showing good statistical checks for a fixed calibration constant of the S-band radar, a dominant DSD is therefore established from which scatter diagrams of Log k versus Log Z may be obtained at other attenuating wavelengths where knowledge of the path attenuation is desired.

(8) Forming empirical relations of the form (5.17) from (7), appropriate parameters a and b may be determined at other wavelengths.

(9) The empirical parameters a and b may then be used in conjunction with the S-band reflectivity factor measurements, Z, to obtain the integrated path attenuation as given by (5.20) for other wavelengths.

5.2.1 Pertinent Parameters at 15.7 and 35 GHz.

In this section are provided the necessary data to implement the modified dual wavelength method at either the frequencies of 15.7 or 35 GHz. In Fig. 34 are plotted k/N_o versus Λ at these frequencies obtained through the numerical integration of the integral,

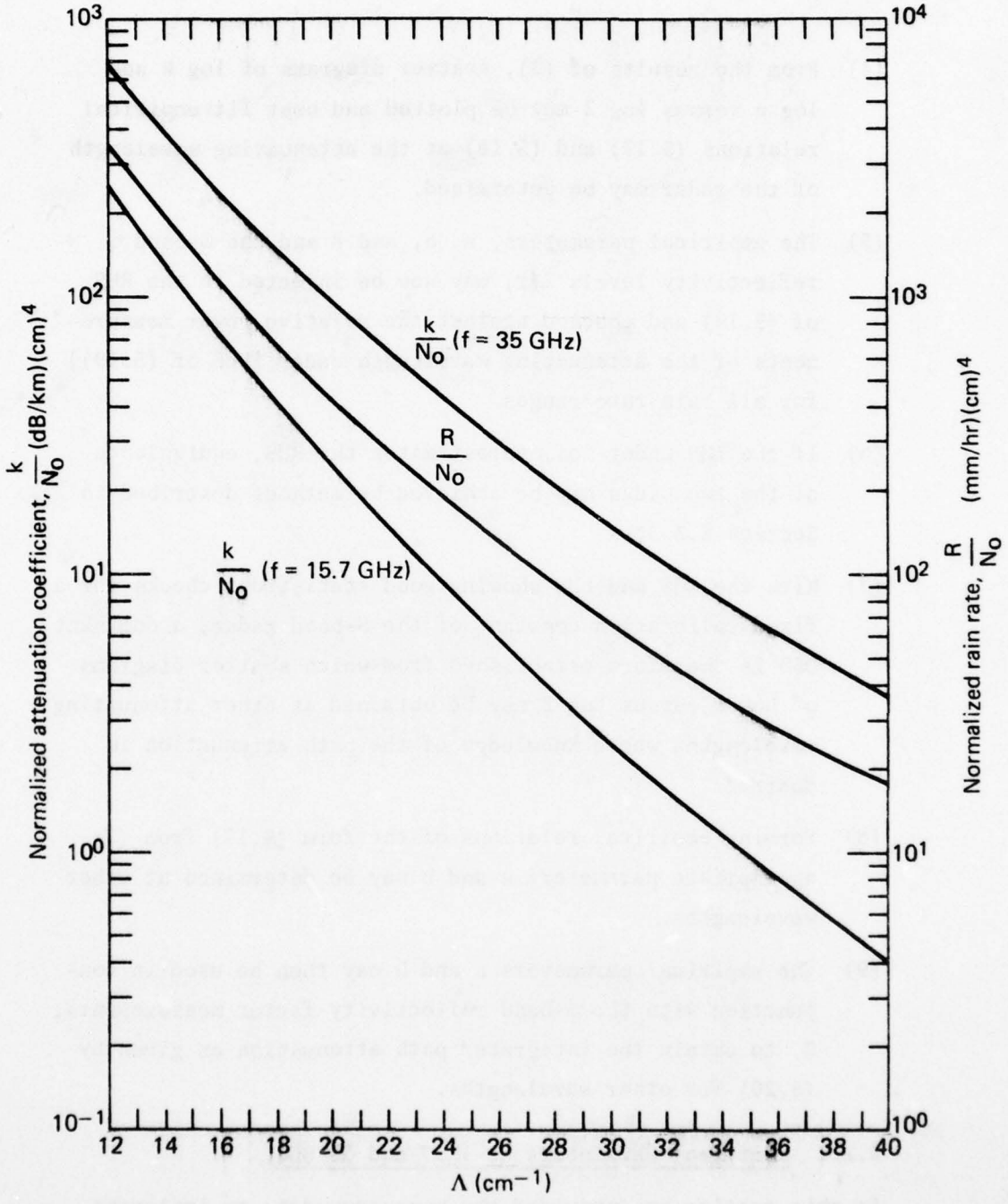

Figure 34. Normalized attenuation coefficients at 15.7 and 35 GHz plotted as a function of Λ. Normalized rain rate also plotted as a function of Λ.

$$\frac{\bar{k}}{N_o} = \int_{D_{min}}^{D_{max}} C_{ext}(D)\, \exp(-\Lambda D)\, dD \qquad [dB/km]cm^4 \tag{5.21}$$

where

$$D_{max} = 0.5 \text{ cm}$$
$$D_{min} = 0.03 \text{ cm} \tag{5.22}$$

and the values of C_{ext} are obtained by interpolating the tabulations in Medhurst [1965]. The resulting tabulations of C_{ext} vs D are given in Table 5.3. We note that the units of N_o are cm^{-4}.

The indicated minimum and maximum diameters in (5.22) were used as these were found to bound the drop diameters of most rain rates (Goldhirsh [1976c]). Also plotted in Fig. 34 is the normalized rain rate R/N_o $[(mm/hr)cm^4]$ as a function of Λ. This curve was obtained through the numerical integration of,

$$\frac{R}{N_o} = 1.885 \times 10^6 \int_{D_{min}}^{D_{max}} v(D)\, D^3 \exp(-\Lambda D)\, dD \qquad [mm/hr](cm^4) \tag{5.23}$$

where v(D) is the drop terminal velocity (m/sec) and D is expressed in cm. The tabulated data given in Table 5.4 was used in the numerical integration of (5.23).

In Fig. 35 are plotted the normalized Mie reflectivity η/N_o $(m^{-1})(cm^4)$ at 15.7 and 35 GHz. These curves were obtained through the numerical integration of,

$$\frac{\eta}{N_o} = 10^2 \int_{D_{min}}^{D_{max}} \sigma(D)\, \exp(-\Lambda D)\, dD \qquad (m^{-1})(cm^4) \tag{5.24}$$

AD-A055 397 JOHNS HOPKINS UNIV LAUREL MD APPLIED PHYSICS LAB F/G 17/9
ANALYSIS OF SINGLE AND MULTIPLE WAVELENGTH RADAR SYSTEMS FOR ES--ETC(U)
MAR 78 J GOLDHIRSH MIPR-FY7620-77-00026
UNCLASSIFIED APL/JHU-S1R77U-036 RADC-TR-78-60 NL

2 OF 2
ADA
055397

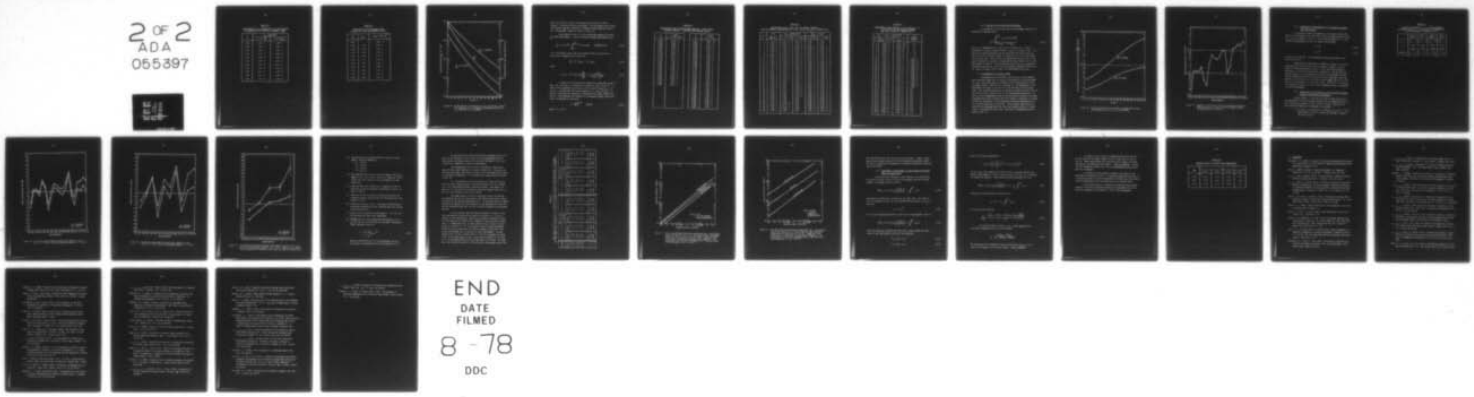

END
DATE
FILMED
8-78
DDC

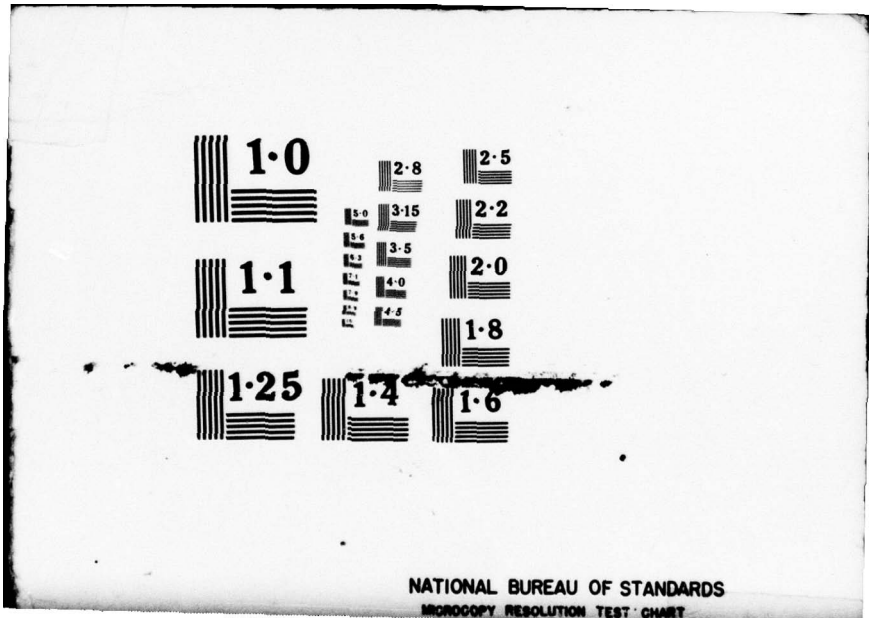
1·0
1·1
1·25
2·8
3·15
3·5
4·0
4·5
5·0
2·5
2·2
2·0
1·8
1·4
1·6
NATIONAL BUREAU OF STANDARDS
MICROCOPY RESOLUTION TEST CHART

Table 5.3

TABULATIONS OF C_{ext} [(dB/km)cm^3] vs D [cm] OBTAINED BY INTERPOLATING THE RESULTS OF MEDHURST [1965].

D cm	C_{ext} (dB/km)cm^3	
	f = 15.7 GHz	f = 35 GHz
0.03	8.90 + 0	1.89 + 1
0.05	1.05 + 1	6.65 + 1
0.10	1.60 + 2	1.54 + 3
0.15	1.33 + 3	9.03 + 3
0.20	6.83 + 3	2.49 + 4
0.25	1.99 + 4	5.06 + 4
0.30	3.23 + 4	8.61 + 4
0.35	5.25 + 4	1.23 + 5
0.40	8.11 + 4	1.58 + 5
0.45	1.21 + 5	1.86 + 5
0.50	1.71 + 5	2.36 + 5

Table 5.4

TABULATIONS OF THE INTEGRAND FACTOR
OF RAIN RATE TAKEN FROM MEDHURST [1965].

D cm	v m/sec	$1.885 \times 10^6 \, v \, D^3$
0.03		1.60 + 2
0.05	2.06	4.85 + 2
0.10	4.03	7.60 + 3
0.15	5.40	3.44 + 4
0.20	6.49	9.79 + 4
0.25	7.41	2.18 + 5
0.30	8.06	4.10 + 5
0.35	8.53	6.89 + 5
0.40	8.83	1.07 + 6
0.45	9.00	1.55 + 6
0.50	9.09	2.14 + 6

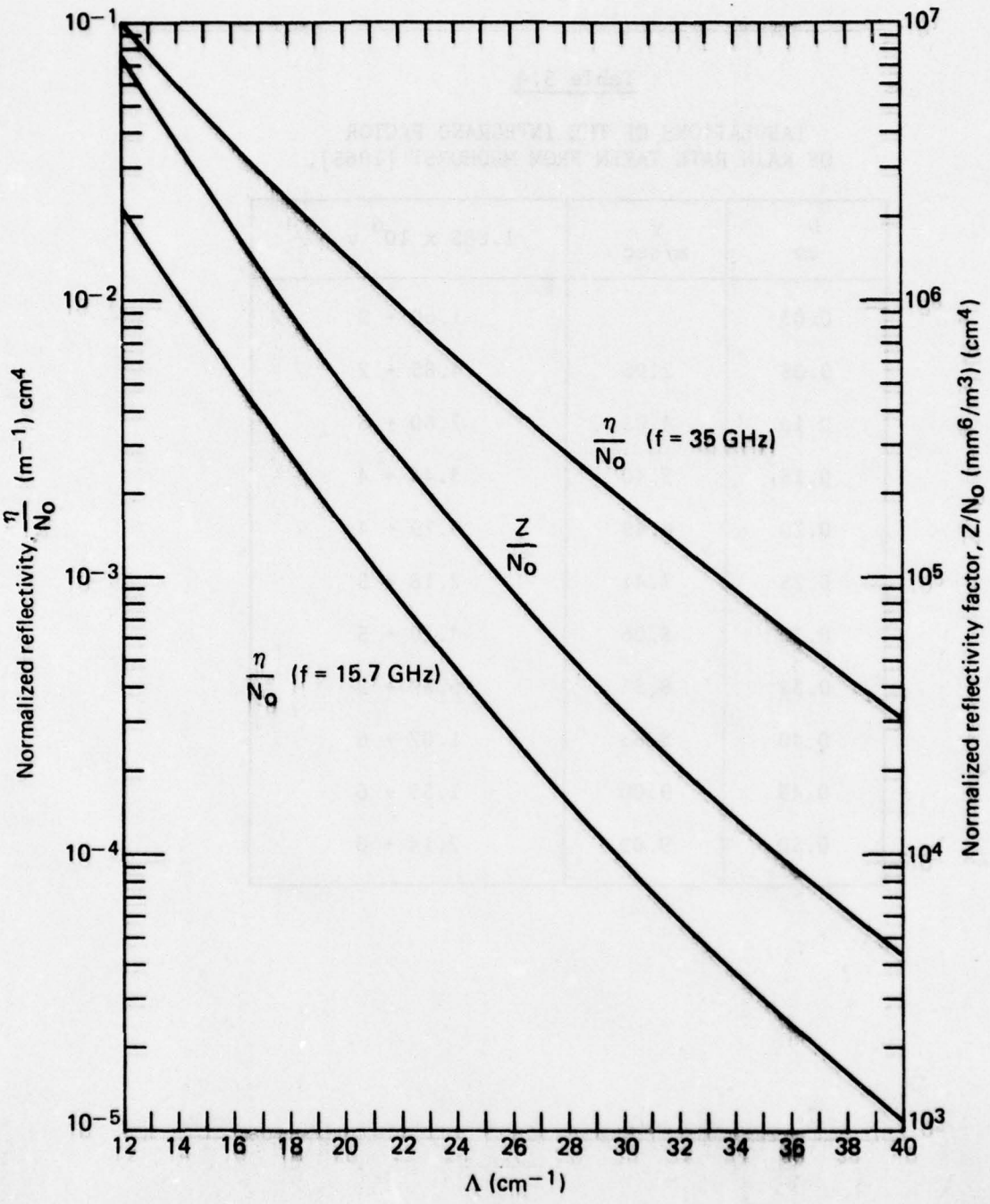

Figure 35. Normalized Mie reflectivities at 15.7 and 35 GHz plotted as a function of Λ. Normalized reflectivity factor, Z, as a function of Λ also shown.

where $\sigma(D)$ [cm^2] is the Mie scattering cross section of a drop of diameter, D [cm] for the given wavelength. The scattering cross sections were obtained from the tabulation of Stephens [1961] with the values at 15.7 interpolated. These are listed in Table 5.5.

Also plotted in Fig. 35 is the normalized reflectivity factor $\frac{Z}{N_o}$ $(mm^6/m^3)cm^4$ versus Λ. This was obtained through the integration of,

$$\frac{Z}{N_o} = (1 \times 10^{12}) \int_{D_{min}}^{D_{max}} D^6 \exp(-\Lambda D) dD \qquad [(mm^6/m^3)(cm^4)] \tag{5.25}$$

It is interesting to note that the righthand side of (5.25) may be analytically integrated and is given by,

$$\frac{Z}{N_o} = f(\Lambda, D_{max}) - f(\Lambda, D_{min}) \tag{5.26}$$

where,

$$f(\Lambda, D) = 10^{12} \exp(-\Lambda D) \sum_{p=0}^{6} (-1)^p \frac{6!\, D^{6-p}}{(6-p)!\, (-\Lambda)^{p+1}} \tag{5.27}$$

In Table 5.6 are tabulated the numerically calculated values of R/N_o, k/N_o, and η/N_o as a function of Λ plotted in Figs. 34 and 35. In Table 5.7 are tabulated Z/N_o versus Λ for the cases in which D_{max} = 0.5 cm and ∞. We note that this latter quantity (i.e., Z/N_o for $D_{max} = \infty$) which is often used for simplicity overestimates the actual reflectivity factor. Also tabulated for reference is the Marshall-Palmer [1948] rain rate as a function of Λ given by,

$$R = \left(\frac{41}{\Lambda}\right)^{4.76} \qquad [mm/hr] \tag{5.28}$$

where Λ is in cm^{-1}.

Table 5.5

TABULATIONS OF MIE SCATTERING CROSS SECTION, σ [cm^2] VERSUS RAINDROP DIAMETER, D, OBTAINED FROM STEPHENS [1961].

D cm	$\sigma(cm^2)$ f = 15.7 GHz
0.024	1.44 - 8
0.037	5.45 - 8
0.043	1.06 - 7
0.049	2.06 - 7
0.061	7.81 - 7
0.073	2.31 - 6
0.091	1.13 - 5
0.109	3.33 - 5
0.122	6.12 - 5
0.134	1.07 - 4
0.152	2.27 - 4
0.170	4.56 - 4
0.182	7.19 - 4
0.201	1.44 - 3
0.213	2.30 - 3
0.231	4.56 - 3
0.243	6.95 - 3
0.255	1.02 - 2
0.274	1.68 - 2
0.304	3.32 - 2
0.334	5.72 - 2
0.365	9.04 - 2
0.395	1.36 - 2
0.426	1.96 - 1
0.456	2.74 - 1
0.486	3.67 - 1

D cm	$\sigma(cm^2)$ f = 35 GHz
0.011	8.80 - 10
0.016	1.00 - 8
0.022	5.61 - 8
0.027	2.14 - 7
0.033	6.36 - 7
0.041	2.42 - 6
0.049	7.21 - 6
0.055	1.35 - 5
0.060	2.40 - 5
0.068	5.19 - 5
0.077	1.04 - 4
0.082	1.59 - 4
0.090	2.89 - 4
0.096	4.23 - 4
0.104	7.31 - 4
0.109	1.04 - 3
0.115	1.46 - 3
0.123	2.38 - 3
0.137	5.04 - 3
0.151	9.71 - 3
0.164	1.70 - 2
0.178	2.73 - 2
0.192	4.07 - 2
0.205	5.66 - 2
0.219	7.45 - 2
0.232	9.32 - 2
0.246	1.11 - 1
0.260	1.28 - 1
0.274	1.42 - 1
0.287	1.52 - 1
0.301	1.58 - 1
0.328	1.54 - 1
0.356	1.32 - 1
0.383	9.64 - 2
0.411	5.64 - 2
0.438	2.59 - 2
0.465	2.01 - 2
0.493	4.83 - 2

Table 5.6

TABULATIONS OF R/N_o, k/N_o, AND η/N_o VERSUS Λ OBTAINED FROM THE NUMERICAL INTEGRATIONS OF (5.23), (5.21), AND (5.24), RESPECTIVELY.

Λ $(cm)^{-1}$	R/N_o $(\frac{mm}{hr})(cm)^4$	k/N_o, $(dB/km)(cm)^4$		η/N_o, $(m^{-1})cm^4$	
		f = 15.7 GHz	f = 35 GHz	f = 15.7 GHz	f = 35 GHz
1	1.74 + 5	1.34 + 4	2.61 + 4	1.68	2.22
2	1.16 + 5	9.01 + 3	1.79 + 4	1.11	1.64
3	7.89 + 4	6.09 + 3	1.24 + 4	7.31 - 1	1.22
4	5.38 + 4	4.14 + 3	8.66 + 4	4.85 - 1	9.06 - 1
5	3.70 + 4	2.84 + 3	6.10 + 3	3.23 - 1	6.78 - 1
6	2.56 + 4	1.95 + 3	4.34 + 3	2.16 - 1	5.10 - 1
7	1.79 + 4	1.36 + 3	3.11 + 3	1.45 - 1	3.85 - 1
8	1.26 + 4	9.53 + 2	2.25 + 3	9.85 - 2	2.93 - 1
9	9.00 + 3	6.73 + 2	1.65 + 3	6.71 - 2	2.24 - 1
10	6.49 + 3	4.79 + 2	1.21 + 3	4.60 - 2	1.71 - 1
11	4.71 + 3	3.44 + 2	9.04 + 2	3.16 - 2	1.31 - 1
12	3.46 + 3	2.49 + 2	6.79 + 2	2.20 - 2	1.02 - 1
13	2.58 + 3	1.83 + 2	5.16 + 2	1.54 - 2	7.89 - 2
14	1.94 + 3	1.34 + 2	3.95 + 2	1.08 - 2	6.15 - 2
15	1.46 + 3	9.94 + 1	3.05 + 2	7.63 - 3	4.81 - 2
16	1.13 + 3	7.44 + 1	2.39 + 2	5.44 - 3	3.78 - 2
17	8.71 + 2	5.60 + 1	1.88 + 2	3.90 - 3	2.98 - 2
18	6.81 + 2	4.26 + 1	1.49 + 2	2.81 - 3	2.36 - 2
19	5.39 + 2	3.26 + 1	1.19 + 2	2.05 - 3	1.88 - 2
20	4.29 + 2	2.51 + 1	9.54 + 1	1.50 - 3	1.49 - 2
21	3.45 + 2	1.95 + 1	7.73 + 1	1.11 - 3	1.20 - 2
22	2.80 + 2	1.51 + 1	6.30 + 1	8.21 - 4	9.60 - 3
23	2.29 + 2	1.19 + 1	5.16 + 1	6.14 - 4	7.73 - 3
24	1.89 + 2	9.39	4.26 + 1	4.61 - 4	6.25 - 3
25	1.56 + 2	7.45	3.54 + 1	3.49 - 4	5.08 - 3
26	1.30 + 2	5.94	2.95 + 1	2.66 - 4	4.13 - 3
27	1.09 + 2	4.76	2.48 + 1	2.04 - 4	3.36 - 3
28	9.23 + 1	3.84	2.09 + 1	1.58 - 4	2.76 - 3
29	7.83 + 1	3.10	1.76 + 1	1.22 - 4	2.26 - 3
30	6.69 + 1	2.53	1.50 + 1	9.54 - 5	1.86 - 3
31	5.73 + 1	2.06	1.29 + 1	7.49 - 5	1.54 - 3
32	4.94 + 1	1.69	1.10 + 1	5.93 - 5	1.28 - 3
33	4.28 + 1	1.40	9.45	4.70 - 5	1.06 - 3
34	3.71 + 1	1.16	8.16	3.76 - 5	8.86 - 4
35	3.24 + 1	9.60 - 1	7.06	3.03 - 5	7.41 - 4
36	2.84 + 1	8.05 - 1	6.14	2.44 - 5	6.21 - 4
37	2.49 + 1	6.73 - 1	5.35	1.99 - 5	5.23 - 4
38	2.19 + 1	5.66 - 1	4.69	1.63 - 5	4.40 - 4
39	1.94 + 1	4.80 - 1	4.10	1.34 - 5	3.71 - 4
40	1.73 + 1	4.08 - 1	3.61	1.10 - 5	3.15 - 4

Table 5.7

TABULATIONS OF Z/N_o FOR D_{max} = 0.5 cm AND $D_{max} = \infty$. ALSO PLOTTED ARE THE MARSHALL-PALMER RAIN RATES [1948] AS A FUNCTION OF Λ.

Λ cm^{-1}	Z/N_o - $(mm^6/m^3)cm^4$		R (M-P) (mm)/hr
	D_{max} = 0.5 cm	$D_{max} = \infty$	
1	7.24 + 8	7.20 + 14	----
2	4.68 + 8	5.62 + 12	----
3	3.05 + 8	3.29 + 11	----
4	1.99 + 8	4.39 + 10	----
5	1.31 + 8	9.22 + 9	----
6	8.62 + 7	2.57 + 9	----
7	5.71 + 7	8.74 + 8	----
8	3.79 + 7	3.43 + 8	----
9	2.54 + 7	1.50 + 8	----
10	1.71 + 7	7.20 + 7	8.26 + 2
11	1.16 + 7	3.69 + 7	5.25 + 2
12	7.83 + 6	2.01 + 7	3.47 + 2
13	5.43 + 6	1.15 + 7	2.37 + 2
14	3.76 + 6	6.83 + 6	1.66 + 2
15	2.62 + 6	4.21 + 6	1.20 + 2
16	1.84 + 6	2.68 + 6	8.82 + 1
17	1.31 + 6	1.75 + 6	6.61 + 1
18	9.33 + 5	1.18 + 6	5.03 + 1
19	6.73 + 5	8.05 + 5	3.89 + 1
20	4.89 + 5	5.63 + 5	3.05 + 1
21	3.59 + 5	4.00 + 5	2.42 + 1
22	2.66 + 5	2.89 + 5	1.94 + 1
23	1.99 + 5	2.12 + 5	1.57 + 1
24	1.50 + 5	1.57 + 5	1.28 + 1
25	1.14 + 5	1.18 + 5	1.05 + 1
26	8.73 + 4	8.96 + 4	8.7
27	6.75 + 4	6.88 + 4	7.3
28	5.26 + 4	5.34 + 4	6.1
29	4.13 + 4	4.17 + 4	5.2
30	3.27 + 4	3.29 + 4	4.4
31	2.60 + 4	2.62 + 4	3.8
32	2.09 + 4	2.10 + 4	3.3
33	1.68 + 4	1.69 + 4	2.8
34	1.37 + 4	1.37 + 4	2.4
35	1.12 + 4	1.12 + 4	2.1
36	9.18 + 3	9.18 + 3	1.9
37	7.58 + 3	7.58 + 3	1.6
38	6.29 + 3	6.29 + 3	1.4
39	5.24 + 3	5.24 + 3	1.3
40	4.39 + 3	4.39 + 3	1.1

5.2.2 Solving for the Drop Size Distribution

In solving for N_o and Λ using the dual wavelength method, it is convenient to use the ratio,

$$\frac{k}{Z} = \frac{\int_{D_{min}}^{D_{max}} C_{ext}(D)\, \exp(-\Lambda D)\, dD}{f(\Lambda, D_{max}) - f(\Lambda, D_{min})} \tag{5.29}$$

since it is independent of N_o and is only a function of Λ. Hence a measurement of k and Z uniquely defines a value of Λ, using (5.29). The above ratios may be obtained from the tabulations of k/N_o and Z/N_o in Tables 5.6 and 5.7 and are plotted in Figure 36 for f = 15.7 and 35 GHz as a function of Λ. With Λ known, the appropriate value of k/N_o or Z/N_o may be obtained (by exponential interpolation) from Tables 5.6 or 5.7 or from Figures 34 and 35. The corresponding value of N_o is calculated by dividing the normalized values into the respective measured values (k or Z). Hence, the pair k and Z enable the determination of N_o and Λ.

5.3 Error Analysis at K_a and K_u Bands

We examine here uncertainties that may arise in the modified dual wavelength method due to realistic uncertainties in the measurement of k and Z from which empirical parameters are obtained using the dual wavelength method. Specifically, we assume a $\pm$ 2 dB uncertainty in the measurement of Z and a $\pm$ 25% error in k for both the 15.7 and 35 GHz cases. With these uncertainties, we examine the degree of sensitivity of the RHS of (5.19) to these errors at the corresponding frequencies. It will in fact be demonstrated that the uncertainties at 35 GHz is far more pronounced that at 15.7 GHz and that this enables a correction to be made in both the calibration of the attenuating wavelength measurements and the resulting drop size distribution. The previously used measured Z profile from which empirical rain rates were deduced in Fig. 11 (solid curve) is used here as a test case. The partial Z profile measured is given in Fig. 37.

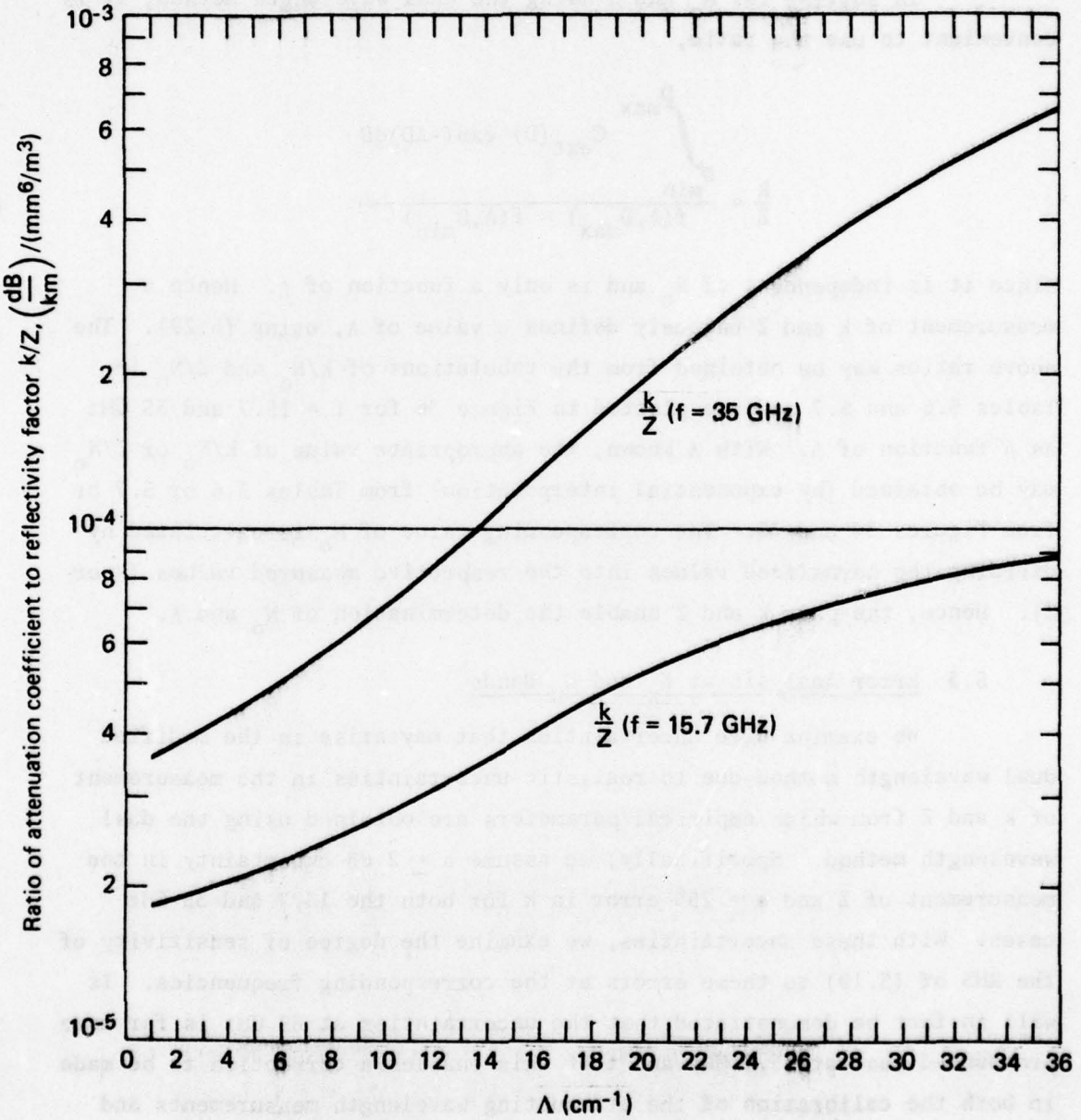

Figure 36. Ratio of attenuation coefficient to reflectivity factor as a function of Λ for f = 15.7 and 35 GHz.

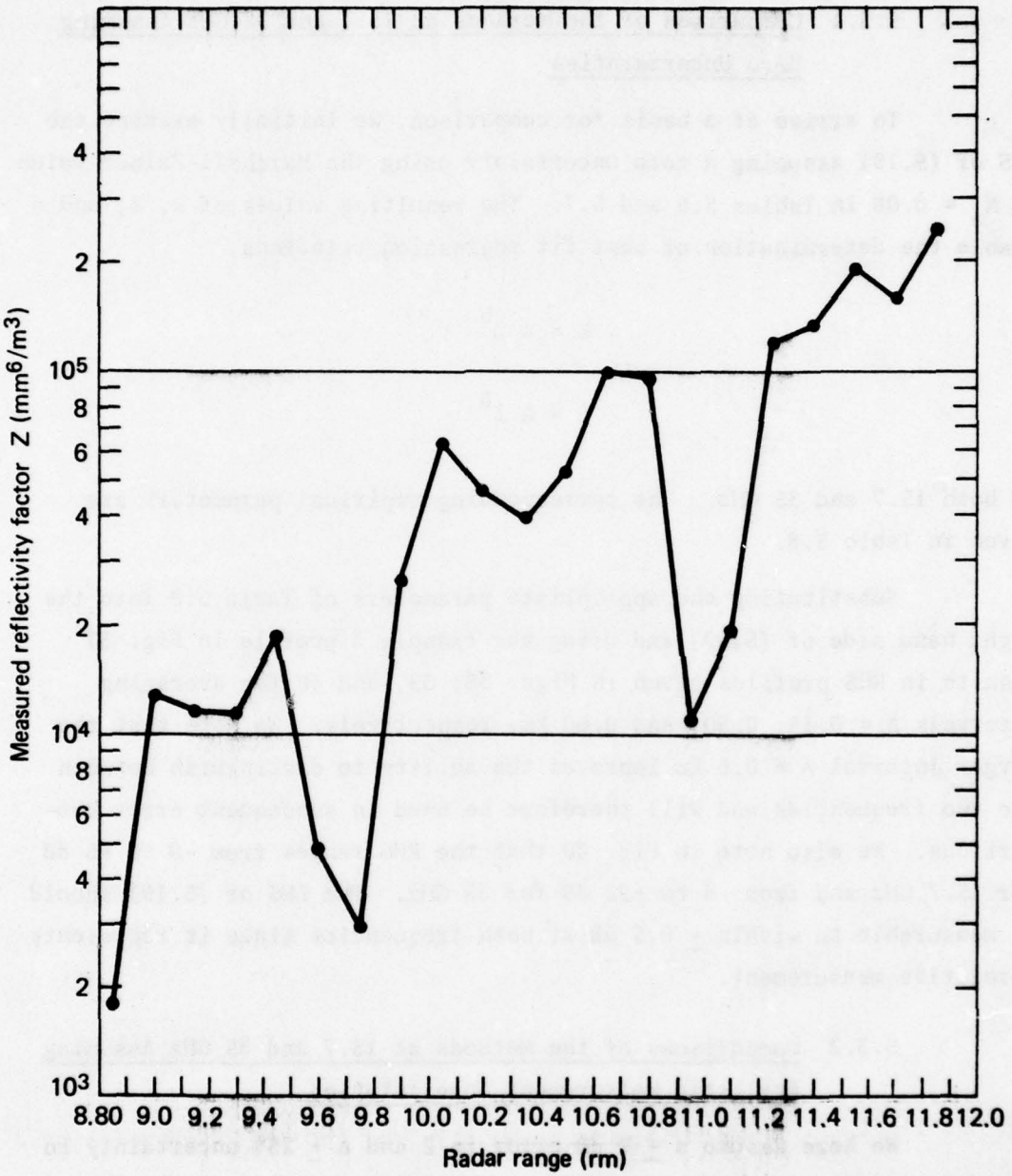

Figure 37. Segment of reflectivity profile as measured at Wallops Island, Virginia, on July 10, 1976 at 19:52:20 GMT at 60° azimuth and 20° elevation.

5.3.1 Comparison of the Methods at 15.7 and 35 GHz Assuming Zero Uncertainties

To arrive at a basis for comparison, we initially examine the RHS of (5.19) assuming a zero uncertainty using the Marshall-Palmer value of $N_o = 0.08$ in Tables 5.6 and 5.7. The resulting values of k, Z, and η enable the determination of best fit regression relations,

$$k = a\, Z^b \tag{5.30}$$

$$\eta = A\, Z^B \tag{5.31}$$

at both 15.7 and 35 GHz. The corresponding empirical parameters are given in Table 5.8.

Substituting the appropriate parameters of Table 5.8 into the right hand side of (5.19) and using the example Z profile in Fig. 37 results in RHS profiles given in Figs. 38, 39, and 40 for averaging intervals $\Delta = 0.15$, 0.30, and 0.60 km, respectively. We note that the larger interval $\Delta = 0.6$ km improves the ability to distinguish between the two frequencies and will therefore be used in subsequent error comparisons. We also note in Fig. 40 that the RHS ranges from -9 to +5 dB for 15.7 GHz and from -4 to +22 dB for 35 GHz. The LHS of (5.19) should be measurable to within $\pm$ 0.5 dB at both frequencies since it represents a relative measurement.

5.3.2 Comparisons of the Methods at 15.7 and 35 GHz Assuming Realistic Measurement Uncertainties

We here assume a $\pm$ 2 dB error in Z and a $\pm$ 25% uncertainty in the measurement of k and with these uncertainties re-examine the RHS of (5.19) using the Z profile of Fig. 37 and $\Delta = 0.6$ km. The method in which this error analysis is performed is as follows:

(1) k_o and Z_o is calculated as a function of Λ_o for $N_o = 0.08$ using Tables 5.6 and 5.7; where the subscript o implies the "true values".

Table 5.8

REGRESSION PARAMETERS a, A, b, B OVER INDICATED RAIN RATE INTERVALS, R. COEFFICIENT OF DETERMINATION, r^2, GIVES MEASURE OF GOODNESS OF FIT.

	k(15.7) (dB/km)	η(15.7) (m^{-1})	k(35) (dB/km)	η(35) (m^{-1})
a, A	3.25 - 4	3.47 - 9	5.48 - 3	4.43 - 7
b, B	0.835	0.986	0.685	0.745
r^2	0.99998	0.99980	0.99999	0.99903
R(mm/hr)	10 - 206	10 - 206	5 - 120	5 - 120

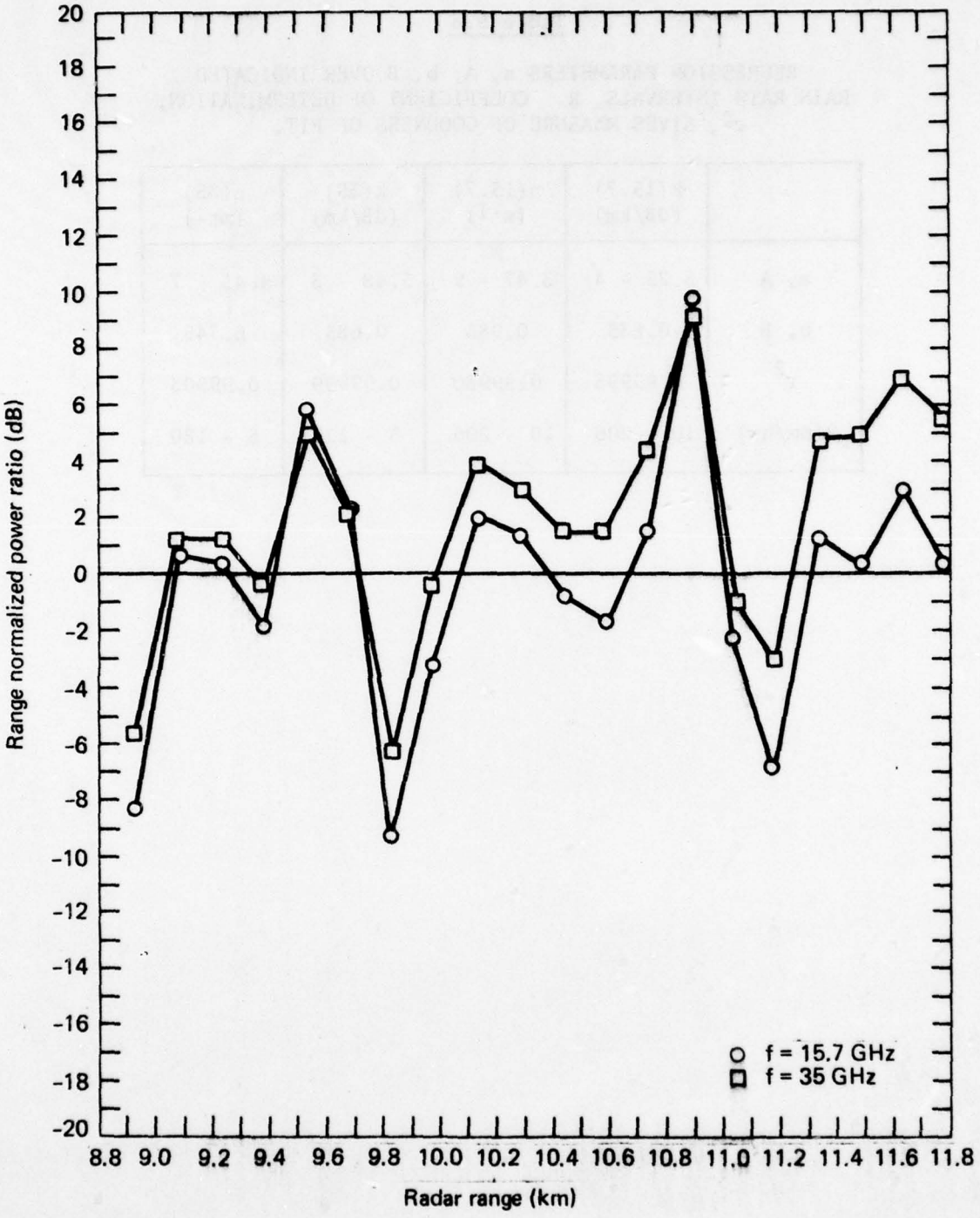

Figure 38. Calculated range normalized power ratio [RHS of (5.19)] for f = 15.7 and 35 GHz and averaging interval, Δ = 0.15 km.

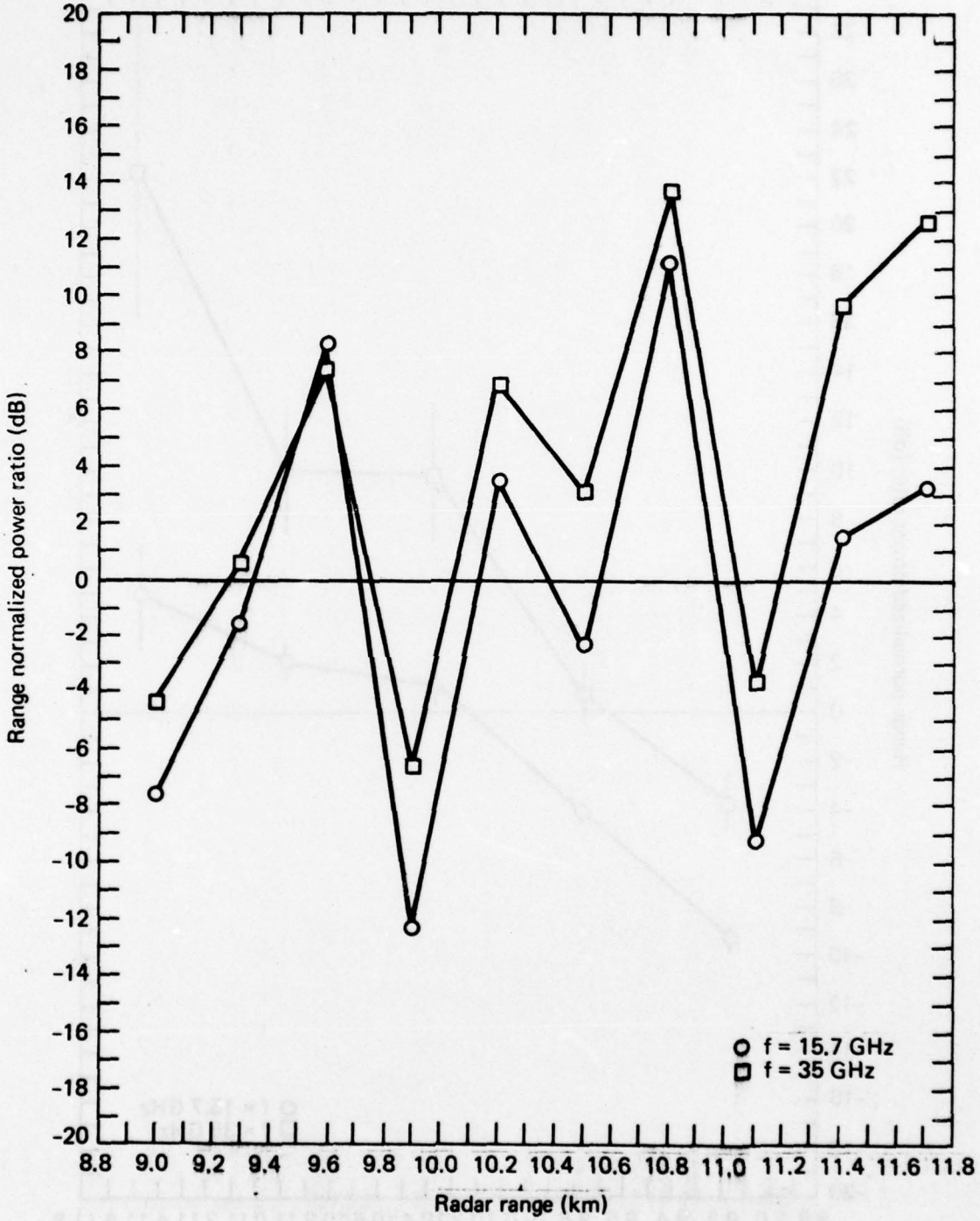

Figure 39. Calculated range normalized power ratio [RHS of (5.19)] for f = 15.7 and 35 GHz and averaging interval, Δ = 0.3 km.

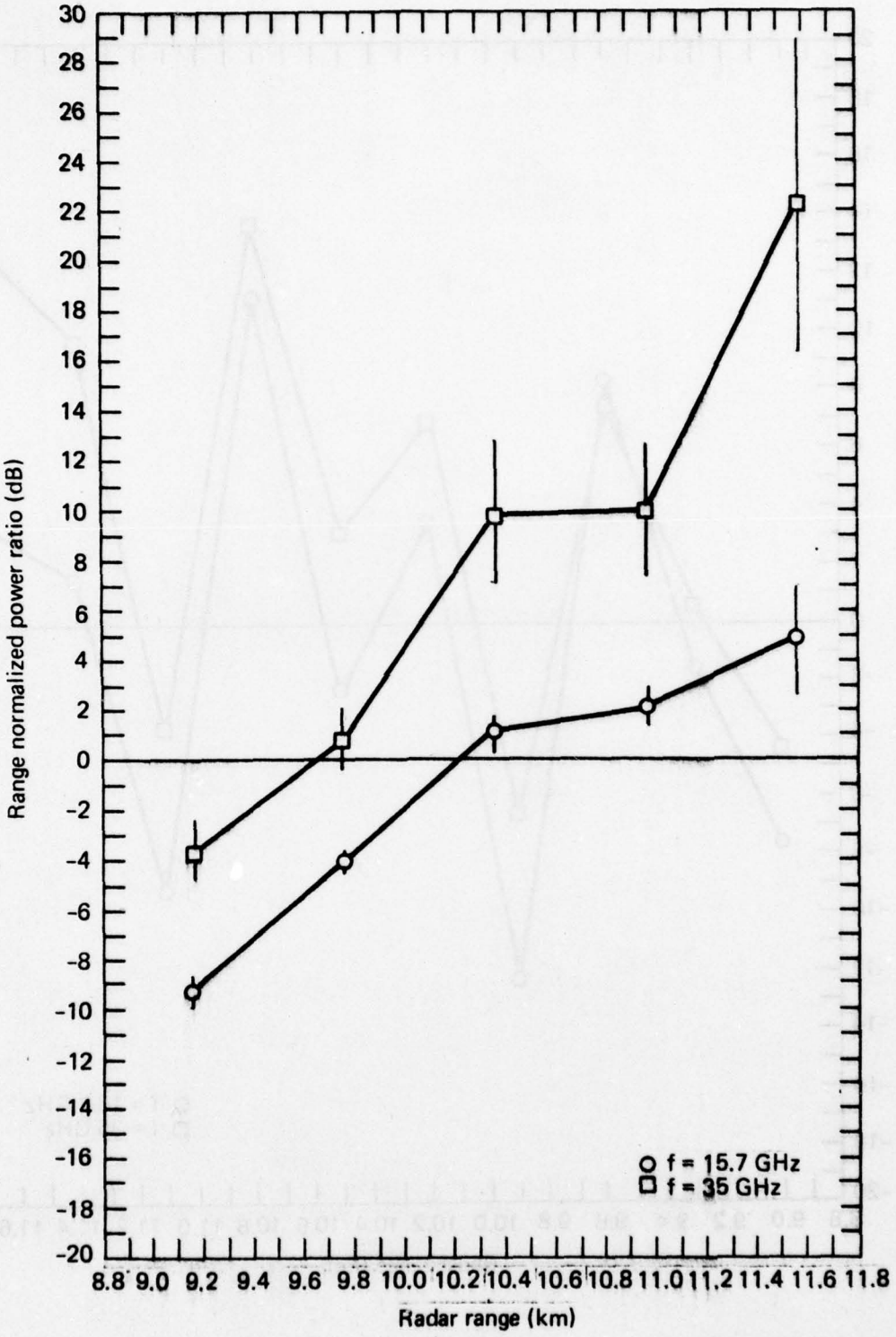

Figure 40. Calculated range normalized power ratio [RHS of (5.19)] for f = 15.7 and 35 GHz and averaging interval, Δ = 0.6 km. Vertical lines depict extreme uncertainties assuming a $\pm$25% error in k and $\pm$2 dB error in Z.

(2) For each value of Λ_o error values of k and Z are calculated. These are defined as

$$k+ = 1.25\ k_o$$
$$k- = 0.75\ k_o$$
$$Z+ = 1.58\ Z_o$$
$$Z- = 0.63\ Z_o$$

(3) Four combinations of ratios, k/Z are computed for each Λ_o; namely, k+/Z+, k-/Z+, k+/Z-, and k-/Z-. Using the curves of Fig. 36, error values of Λ may be computed for each error ratio.

(4) Using the four error values for Λ, normalized values of k/N_o and Z/N_o may be obtained using Tables 5.6 and 5.7 or Figs. 34 and 35.

(5) Four error values of N_o may be obtained by dividing the normalized values, k/N_o and Z/N_o into the respective error values of k and Z.

(6) Using the four pairs of N_o, Λ calculated corresponding to each error combination, we may calculate four error values of the reflectivity, η.

(7) Best fit error regression relationships $\eta = A\ Z^B$ may thus be calculated for each error combination.

(8) Modified best fit error regression relationships of $k_o = a_o\ Z_o^{b_o}$ may also be calculated for each error combination. This is generally given by,

$$k = \frac{(1 + \delta_k)}{(1 + \delta_Z)^{b_o}}\ a_o\ Z^{b_o} \qquad (5.32)$$

where δ_k (uncertainties in k) for the present case are $\pm$ 0.25 and δ_Z (uncertainties in Z) are +0.58 and -0.37.

We note from (5.32) that uncertainties in measured values of Z and k do not influence b but do alter a (to be demonstrated shortly). Substituting the revised values of a and B into the RHS of (5.19), new values may be computed for each error combination.

The corresponding error values of the RHS as a function of range for each error combination is given in Table 5.9. Also given are the zero error cases (subscript o) as well as the calculated error values of the empirical parameters. The extreme error values are shown plotted in Fig. 40.

It is interesting to note from Table 5.9 or Fig. 40 that the RHS of (5.19) is less sensitive to the given errors at f = 15.7 whereas at f = 35, significantly greater sensitivity exists. For example, we note that at 11.55 km the uncertainties about the nominal values are $\pm$ 2 dB at f = 15.7 GHz and -6 to +7 dB at 35 GHz.

The larger errors in the K_a-S band case in Fig. 40 represent an advantage over the K_u-S band case in that these can be used to reduce the errors in the original measurement in k. In the next section we demonstrate how an analysis of the differences in the measured left hand side and the calculated right hand side may be used to improve the measurement accuracy.

In utilizing the dual wavelength procedures to arrive at drop size distributions from which the empirical relation $k = a Z^b$ may be deduced at other wavelengths, significantly smaller errors may be shown to arise using the K_a-S band case as compared to the K_u-S band configuration. To demonstrate this, we show plotted in Fig. 41 worst case predicted k-Z curves at f = 15.7 GHz predicted using the dual wavelength method for the K_a-S band case (35-3 GHz) assuming a $\pm$25% error in the K_a-band measurement and a $\pm$2 dB error in the Z measurement. The percentage error in k for Z values below $Z = 10^5$ are in general well below $\pm$ 40%. On the other hand, in Fig. 42 are shown a similar set of curves at f = 35 GHz predicted from the K_u-S band case (15.7-3 GHz). The upper error case results in errors in k of more than a few hundred percent and

Table 5.9

ERROR VALUES OF RHS OF (5.19) AS A FUNCTION OF RANGE FOR EACH ERROR COMBINATION. ALSO SHOWN ARE ZERO ERROR CASES (SUBSCRIPT o) AS WELL AS CALCULATED VALUES OF PERTINENT EMPIRICAL PARAMETERS.

Range	RHS of (5.19) f = 35 GHz					RHS of (5.19) f = 15.7 GHz				
km	k+/Z+	k-/Z+	k+/Z-	k-/Z-	k_o/Z_o	k+/Z+	k-/Z+	k+/Z-	k-/Z-	k_o/Z_o
9.15	-2.4	-3.5	-3.5	-4.7	-3.8	-8.7	-8.9	-9.9	-9.6	-9.15
9.75	2.1	0.2	1.5	-0.4	0.7	-3.7	-4.2	-4.3	-4.5	-4.1
10.35	12.8	7.3	12.6	7.1	9.9	2.0	0.45	1.7	0.3	1.15
10.95	12.6	7.4	12.6	7.4	10.0	2.9	1.4	2.8	2.2	2.1
11.55	28.4	17.1	28.9	16.3	22.2	6.85	2.9	6.3	2.6	4.75
a	5.00 - 3	3.00 - 3	9.39 - 3	5.63 - 3	5.48 - 3	2.78 - 4	1.67 - 4	5.94 - 4	3.56 - 4	3.25 - 4
B	0.701	0.624	0.815	0.747	0.745	0.962	0.941	1.078	1.008	0.986
b	0.685	0.685	0.685	0.685	0.685	0.825	0.825	0.825	0.825	0.825

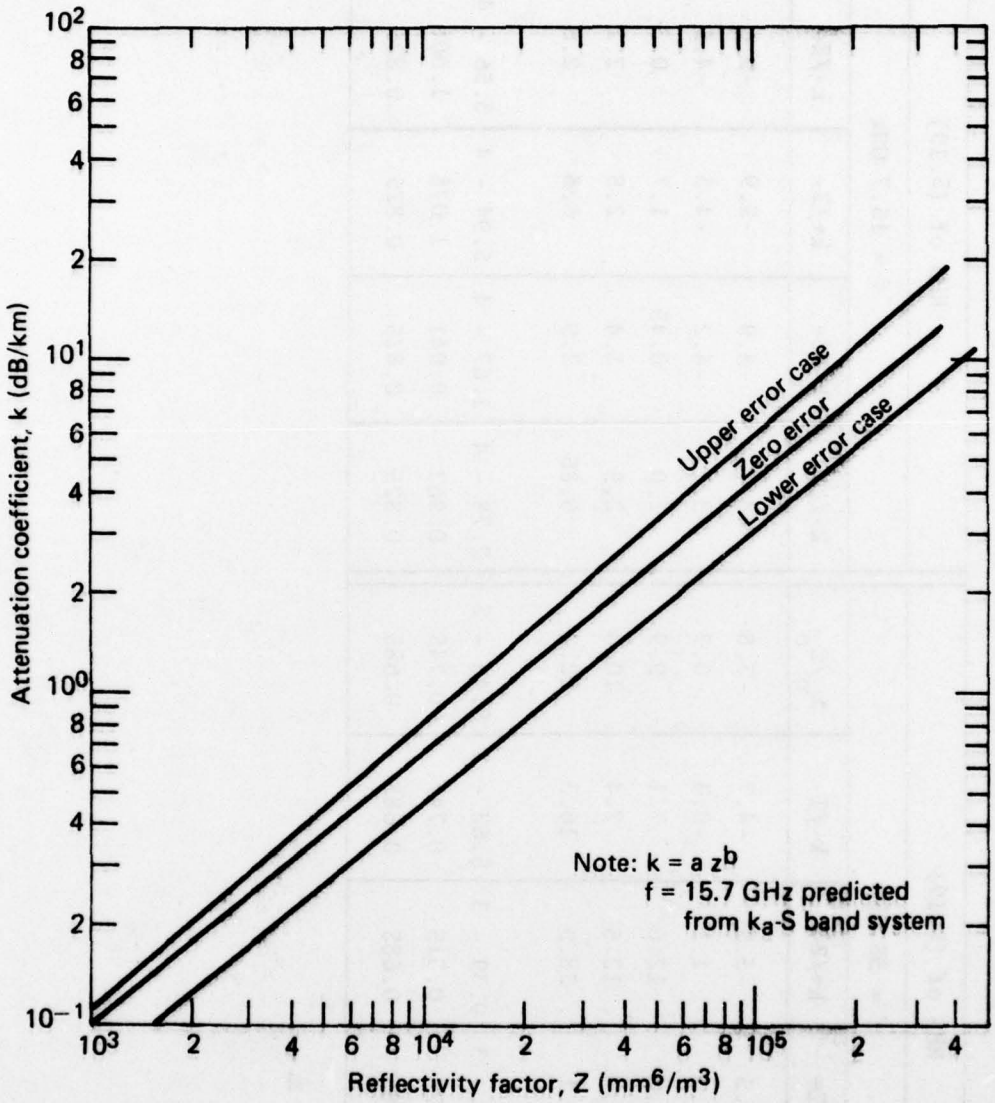

Figure 41. Best fit predicted attenuation coefficient (k) - reflectivity factor (Z) curves for f = 15.7 GHz using the dual wavelength method for the K_a-S band case (35-3 GHz). Upper and lower error curves correspond to extreme errors assuming ± 2 dB uncertainty in Z and $\pm 25\%$ uncertainty in k. The zero error case corresponds to $N_o = .08$ cm^{-4}.

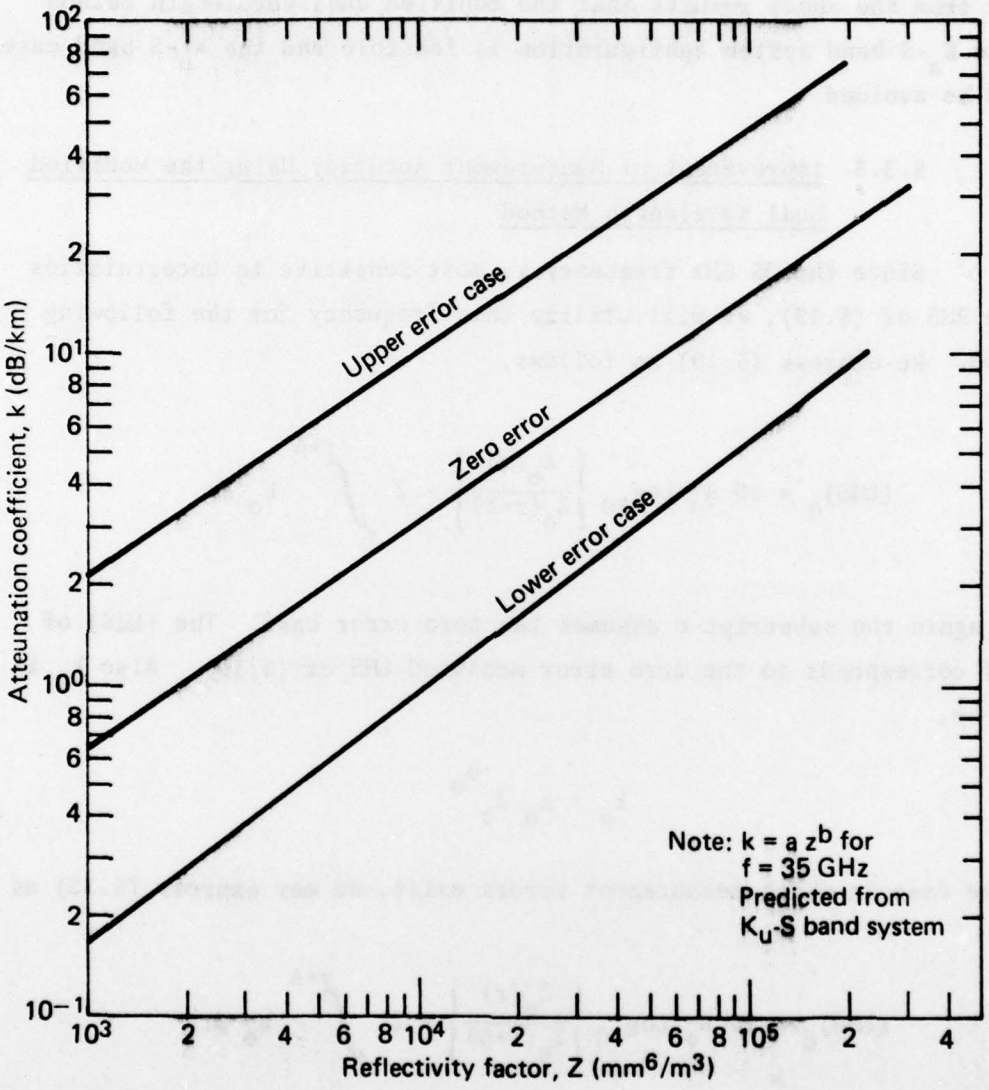

Figure 42. Best fit predicted attenuation coefficient (k) - reflectivity factor (Z) curves for f = 35 GHz using the dual wavelength method for K_u-S band case (15.7-3 GHz). Upper and lower error curves correspond to extreme errors assuming $\pm$ 2 dB uncertainty in Z and $\pm$25% uncertainty in k. The zero error case corresponds to $\bar{N_o}$ = .08 cm^{-4}.

more than 60% for the lower error case for any fixed Z. Hence it would appear from the above results that the modified dual wavelength method for the K_a-S band system configuration is feasible and the K_u-S band case should be avoided.

5.3.3 Improvement of Measurement Accuracy Using the Modified Dual Wavelength Method

Since the 35 GHz frequency is most sensitive to uncertainties of the RHS of (5.19), we will utilize this frequency for the following example. Re-express (5.19) as follows,

$$(LHS)_o = 10\, B_o\, \text{Log}_{10} \left\{ \frac{Z_o(r)}{Z_o(r+\Delta)} \right\} + 2 \int_r^{r+\Delta} k_o\, dr \tag{5.33}$$

where again the subscript o assumes the zero error case. The (LHS) of (5.33) corresponds to the zero error measured LHS of (5.19). Also k_o is given by,

$$k_o = a_o\, Z_o^{\,b_o} \tag{5.34}$$

For the case in which measurement errors exist, we may express (5.33) as

$$(LHS)_e = 10\, B_e\, \text{Log}_{10} \left\{ \frac{Z_e(r)}{Z_e(r+\Delta)} \right\} + 2 \int_r^{r+\Delta} k_e\, dr \tag{5.35}$$

where the subscript e denotes the error case. We may relate the error values to the true values Z_o and k_o by the relations,

$$Z_e = Z_o(1 + \delta_Z) \tag{5.36}$$

$$k_e = k_o(1 + \delta_k) \tag{5.37}$$

Hence (5.34) may be expressed by,

$$k_e = a_o \frac{(1 + \delta_k)}{(1 + \delta_Z)^b} Z_e^{b_o} \simeq (1 + \delta_k)\, a_o\, Z_o^{b_o} \tag{5.38}$$

We note that if the regression relation (5.34) is obtained through independent measurements of k and Z, only the error in k (i.e., δ_k), influences the regression relation. Substituting the above relations in (5.35),

$$(LHS)_e = 10\, B_e\, \text{Log}_{10} \left\{ \frac{Z_o(r)}{Z_o(r+\Delta)} \right\} + 2(1 + \delta_k) \int_r^{r+\Delta} k_o\, dr \tag{5.39}$$

Defining the calculated error attenuation by,

$$A_e = 2(1 + \delta_k) \int_r^{r+\Delta} k_o\, dr \tag{5.40}$$

we may derive the relation,

$$\frac{\delta_k}{1+\delta_k} = \frac{(LHS)_e - (LHS)_o + 10(B_o - B_e)\, \text{Log}_{10} \frac{Z_o(r)}{Z_o(r+\Delta)}}{A_e} \tag{5.41}$$

We note from Table 5.9 that $B_e \simeq B_o$. Hence neglecting the associated difference term in (5.41) we obtain,

$$\delta_k \simeq \frac{[(LHS)_e - (LHS)_o]}{A_e - [(LHS)_e - (LHS)_o]} \tag{5.42}$$

The neglecting of the difference term associated with $(B_o - B_e)$ is only valid in the higher Z levels where $[(LHS)_e - (LHS)_o]$ dominates.

In Table 5.10 are listed the computed errors (5.42) for the various cases of the nominal ranges of 10.35, 10.95, and 11.55 km in Fig. 40. These latter ranges were selected as the Z levels are higher resulting in the difference term $[(LHS)_e - (LHS)_o]$ dominating. We note that the originally assumed error in δ_k is approximately predicted and may thus be removed.

Of course, the above analysis assumes a zero error in the measurement of the LHS of (5.19). As mentioned previously since this is a relative quantity, it should be measurable to within $\pm$ 0.5 dB and only a minor perturbation of the calculated value of δ_k should result.

With the error due to k reduced, the drop size distributions obtained via the dual wavelength method may be recomputed and used to establish regression relationships $k = aZ^b$ at other wavelengths.

Table 5.10

COMPUTED ERRORS FOR VARIOUS ERROR COMBINATIONS.

r (km)	δ_k			
	k+/Z+	k-/Z+	k+/Z-	k-/Z-
10.35	+0.26	-0.23	+0.23	-0.24
10.95	+0.25	-0.24	+0.25	-0.24
11.55	+0.25	-0.22	+0.28	-0.24

6.0 REFERENCES

Altshuler, E. E. [1977], "A Review of Slant-Path attenuation Measurements at 15 and 35 GHz", 1977 GTE Satellite Communications Symposium, GTE Laboratories, January 25-26.

Atlas, D. [1964], "Advances in Radar Meteorology", In 'Advances in Geophysics', Vol. 10, pp 318-478. Academic Press, New York.

_____ and S. Bartnoff [1953], "Cloud Visibility, Radar Reflectivity and Drop Size Distributions", J. Meteor., Vol. 10, p 143.

_____ and C. W. Ulbrich [1974], "The Physical Basis for Attenuation-Rainfall Relationships and the Measurement of Rainfall Parameters by Combined Attenuation and Radar Methods", Journal De Recherches Atmospheriques, Colloque De L'IUCRM, Vol. VIII, Janvier-Juin, pp 275-298.

Austin, P. M. and M. R. Shaffner [1970], "Computations and Experiments Relevant to Digital Processing of Weather Radar Echoes", Proc. 14th Radar Meteor. Conf., Boston, Mass., AMS, pp 375-380.

Battan, L. J. [1973], "Radar Observation of the Atmosphere", University of Chicago Press, Chicago, Ill.

Bean, B. R. and E. J. Dutton [1968], "Radar Meteorology", Dover Publications, Inc., New York, p 270.

Blake, L. V. [1969,1970], "A Guide to Basic Pulse-Radar Maximum-Range Calculations", Naval Res. Lab., Report 5868, Dec. 1962 (Reprinted with revisions, Dec. 1963), Second Edition, Part 1, Naval Res. Report 6930, 1969 and Part 2, 1970.

Cole, A. E., A. Court, and A. J. Kantor [1965], "Model Atmospheres", in Handbook of Geophysics and Space Environments, Scientific Editor, S. L. Valley, Air Force Cambridge Research Laboratory, McGraw-Hill Book Co., New York, p 2-13.

Donaldson, R. J. and R. T. Tear [1963], "Distortions in Reflectivity Patterns by Antenna Side Lobes", Proc. 10th Radar Meteor. Conf., Boston, Mass., AMS, pp 108-115.

_____ [1964a], "A Demonstration of Antenna Beam Errors in Radar Reflectivity Patterns", J. Appl. Meteor., October, pp 611-623.

_____ [1964b], "Improvement in Accuracy of Thunderstorm Echo Top Measurements", Proc. 11th Radar Meteor. Conf., Boston, Mass., AMS, pp 228-291

Goldhirsh, J. [1975a], "Improved Error Analysis in Estimation of Raindrop Spectra, Rain Rate, and Liquid Water Content Using Multiple Wavelength Radars", IEEE Trans. on Antennas and Propagation, September, pp 718-720.

_____ [1975b], "Prediction Methods for Rain Attenuation Statistics at Variable Path Angles and Carrier Frequencies Between 13 and 100 GHz", IEEE Trans. on Antennas and Propagation, Vol. AP-23, No. 6, 786-791, November.

_____ [1976a], "Attenuation of Propagation Through Rain for an Earth-Satellite Path Correlated with Predicted Values Using Radar", IEEE Trans. on Antennas and Propagation, Vol. AP-24, No. 6, pp 800-806.

_____ [1976b], "Path Attenuation Statistics Influenced by Orientation of Rain Cells", IEEE Trans. on Antennas and Propagation, Vol. AP-24, No. 6, pp 792-799.

_____ [1976c], "Validity of the Exponential Drop-Size Distribution Assumption in Determining Rain Rate and Liquid Water Content Using Dual Wavelength Radars", APL/JHU Tech. memo F1E76U-007, April.

_____ and I. Katz [1974], "Estimation of Raindrop Size Distribution Using Multiple Wavelength Radar Systems", Radio Science, Vol. 9, No. 4, April, pp 439-446.

_____ and F. L. Robison [1975], "Attenuation and Space Diversity Statistics Calculated from Radar Reflectivity Data of Rain", IEEE Trans. on Antennas and Propagation, Vol. AP-23, No. 2, pp 221-227, March.

Gunn, K. L. S. and T. W. R. East [1954], "The Microwave Properties of Precipitation Particles", Q. J. Roy. Meteor. Soc., Vol. 80, pp 522-545.

Haddock, F. T. [1956], "Scattering and Attenuation of Microwave Radiation Through Rain", Naval Res. Lab. Report, Washington, D. C., pp 15-21.

Hardy, K. R. and I. Katz [1969], "Probing the Clear Atmosphere with High Power, High Resolution Radars", Proc. IEEE, Vol. 57, No. 4, April, pp 468-480.

Hitschfeld, W. and J. Bordan [1954], "Errors Inherent in the Radar Measurement of Rainfall at Attenuating Wavelengths", J. Meteor., Vol. 11, pp 58-67.

Hodge, D. B. [1976], "Radar Studies of Rain Attenuation and Diversity Gain", McGill University Stormy Weather Group Scientific Report, MW-87, Montreal, Quebec, Canada.

Inkster, D. R. and R. R. Rogers [1974], "More Radar-Derived Statistics on Slant-Path Attenuation at 10 GHz", Journal De Recherches Atmospherques, Colloque De L'IUCRM, Vol. VIII, Janvier-Juin, pp 421-428.

Joss, J., J. C. Thams, and A. Waldvogel [1968], "The Variation of Rain Drop Size Distribution in Locarno", in Proc. Int. Conf. on Cloud Physics, Toronto, Ont., Canada, August 26-30.

_____ and A. Waldvogel [1967], "Ein Spektrograph fur Niederschlagstrapher mit Automaticher Auswertung", Pure and Appl. Geophys., Vol. 68, pp 240-246.

Kantor, A. J. [1965], "Section 5.3 of 'Precipitation, Cloud and Aerosols', from Handbook of Geophysics and Space Environments", S. L. Valley, Scientific Editor, Air Force Cambridge Research Laboratories, McGraw-Hill Book Co., New York, pp 5-19.

Katz, I. [1976], "A Rain Cell Model", Proc. 17th Conf. on Radar Meteor., Seattle, Wash., Oct 26-29, AMS, 45 Beacon St., Boston, Mass. 02108.

Laws, J. O. and D. A. Parsons [1943], "The Relation of Raindrop Size to Intensity", Trans. Amer. Geophys. Union, Vol. 22, pp 709-721.

Marshall, J. S. and W. Hitschfeld [1965], "Interpretation of the Fluctuating Echo from Randomly Distributed Scatterers" Part 1", Canadian J. Physics., Vol. 31, pp 962-964.

_____ and W. McK. Palmer [1948], "The Distribution of Raindrops With Size", J. Meteor., Vol. 5, pp 165-166.

McCormick, K. S. [1972], "A Comparison of Precipitation Attenuation and Radar Backscatter Along Earth-Satellite Paths", IEEE Trans. on Antennas and Propagation, Vol. AP-20, No. 6, pp 747-755.

Medhurst, R. G. [1965], "Rainfall Attenuation of Centimeter Waves: Comparison of Theory and Measurement", IEEE Trans. on Antennas and Propagation, Vol. AP-13, pp 550-564.

Olsen, R. L., D. V. Rovers, and D. B. Hodge [1977], "The aR^b Relation in the Calculation of Rain Attenuation", to be published in a future issue of IEEE Trans. Antennas and Propagation.

Probert-Jones, J. R. [1962], "The Radar Equation in Meteorology", Quart. J. Roy. Meteor. Soc., Vol. 88, pp 485-495.

Reitan, C. H. [1963], "Surface Dew Point and Water Vapor Aloft", J. Appl. Phys., Vol. 2, pp 776-779.

Rogers, R. R. [1971], "The Effect of Variable Target Reflectivity on Weather Radar Measurements", Quart. J. Roy. Meteor. Soc., Vol. 97, pp 154-167.

_____ [1972], "Radar Derived Statistics on Slant-Path Attenuation at 10 GHz", Radio Science, Vol. 7, No. 6, pp 631-643.

Rogers, D. V. and R. L. Olsen [1977], "Tables of Scattering Functions for Propagation in Rain at Frequencies Between 1 and 1000 GHz", CRC Report in preparation, Communications Research Centre, Department of Communications, Ottawa, Canada.

Rowland, J. R. [1976], "Comparison of Two Different Raindrop Disdrometers", Proc. 17th Conf. on Radar Meteor., October 26-29, Seattle, Wash., pp 398-405.

_____, L. W. Bennett, and R. E. Miller [1975], "Description of the APL Disdrometer-Raingage System", APL Tech. memo F1E75U-026, September.

Setzer, D. E. [1970], "Computed Transmission Through Rain at Microwave and Visible Frequencies", B.S.T.J., Vol. 49, pp 1873-1892.

Skolnik, M. I.; Editor, Radar Handbook [1970] (Chapter 2, L. V. Blake), McGraw-Hill Book Co., New York.

Smith, P. L. [1966], "Interpretation of the Fluctuating Echo from Randomly Distributed Scatterers" Part 3, 12th Conf. on Radar Meteor., Norman, Oklahoma, October 17-20.

Stephens, J. J. [1961], "Radar Cross-Sections for Water and Ice Spheres", J. Meteor., Vol. 18, pp 348-359.

Strickland, J. I. [1972], "Simultaneous Direct, Radiometric and Radar Measurements of Precipitation Attenuation at 15.3 GHz", Earth-Satellite Propagation Above 10 GHz, Papers from the 1972 Spring URSI Session on Experiments Utilizing the ATS-5 Satellite, Compiled by L. J. Ippolito, Goddard Space Flight Center, Greenbelt, Maryland, May.

_____ [1972], "Radar Measurements of Site-Diversity Improvement During Precipitation", Journal De Research Atmospheriques, Colloque De L'IUCRM, Vol. VIII, Janvier-Juin 1974, pp 451-464.

_____ [1974], "The Measurement of Slant Path Attenuation Using Radar, Radiometers, and Satellite Beacons", Journal De Recherches Atmospheriques, Colloque De L'IUCRM, Vol. VIII, Janvier-Juin, pp 347-358.

Tatarski, V. I. [1964], "Wave Propagation in a Turbulent Medium", New York, Mc-Graw Hill.

Ulbrich, C. W. and D. Atlas [1977], "A Method for Measuring Precipitation Parameters and Raindrop Size Distributions Using Radar Reflectivity and Optical Extinction", Proc. Int. Sym. of URSI, Commission F (Propagation in Non-Ionized Media), 28 April-6 May, La Baule, France, pp 219-230.

Van Vleck, J. H. [1947], "Absorption of Microwaves by Oxygen", Phys. Rev., Vol. 71, April, pp 413-424.

_____ [1949], "Absorption of Microwaves by Uncondensed Water Vapor", Phys. Rev., Vol. 71, April, pp 425-433.

Zawadzki, I. I. and R. R. Rogers [1972], "ADA: An Instrument for Measuring Attenuation Due to Rain Over Slant Paths", Radio Science, Vol. 7, pp 619-624.